THE CITY UNIVERSITY

SOLUTIONS OF CERTAIN BOUNDARY INTEGRAL EQUATIONS IN POTENTIAL THEORY

BY

SAROJ KUMAR LASKAR, M.Sc.

A Thesis Presented for the Degree of

Doctor of Philosophy

Department of Mathematics
The City University
London E.C.1.

December 1971

ABSTRACT

Certain Fredholm integral equations are studied which arise from boundary value problems of potential theory. It is shown how these may be solved numerically to a good approximation. The results are applied to the calculation of electrostatic capacities and to the computation of velocity potentials.

TABLE OF CONTENTS

TABLES

FIGURES

ACKNOWLEDGEMENTS

It gives me great pleasure to express my sincere thanks to my supervisor Professor M. A. Jaswon, for introducing me to this field, and for his helpful advice and guidance at all times.

I also wish to thank Professor V. E. Price, The City University, for helpful advice on the numerical analysis, and to Mr. M. M. Freestone, Department of Aeronautical Engineering, The City University, for several useful discussions.

I wish to thank Mr. L. T. G. Clarke, Manager of the Computer Unit, The City University, for helpful guidance on the writing of computer programs, and for placing his computing facilities at my disposal.

I am grateful to The British Council for paying my postgraduate tution fees at The City University. Finally, I am grateful to the Government of Assam, India, for the award of an Overseas Scholarship.

INTRODUCTION

This thesis deals with certain three-dimensional boundary value problems of potential theory. Such problems may be formulated in many different ways, both numerically and analytically. Here we use exclusively the method of boundary integral equations. The idea goes back nearly 100 years but was not systematically exploited until after 1955. One reason is that, generally speaking, the equations can only be solved numerically utilising fast digital computers which were not available before about 1955. In some cases the existence of the solution did not seem to be clearly established. Difficulties also arise from the presence of weakly singular kernels.

Part I of the thesis deals with the formulation of certain boundary integral equations arising in electrostatics and in potential fluid motion. As regards the determination of electrostatic capacity of conductors, we introduce simple sources on the boundary which generate a unit potential everywhere in the interior and on the boundary. This leads to a Fredholm integral equation of the first kind for the source density distribution on the boundary. We establish the existence and uniqueness of the solution of this equation, which does not seem to be readily available elsewhere. The electrostatic problem can alternatively be formulated by a normal derivative condition, leading to a Fredholm integral equation of the second kind for the source density distribution on the boundary. We have made a comparison between the two approaches, which seem to be interesting both on analytical and numerical grounds.

In Part I we also treat the velocity potential of potential fluid flows past various rigid obstacles, of shapes which can not be handled analytically. Two distinct formulations are studied. The first, due to A.M.O. Smith in U.S.A., represents the velocity potential as generated by a simple source distribution on the boundary. This source distribution satisfies a Fredholm integral equation of the second kind expressing a normal derivative condition on the boundary. The second formulation, due to M. A. Jaswon, utilises Green's formula on the boundary to determine the velocity potential directly. Here again we have made a comparison between the two approaches, which seems to be interesting both on numerical and analytical grounds.

Part II shows how to discretise the preceding equations. Our main problem here concerns the subdivision of a given surface into small intervals, i.e. sub-areas. Special complications arise when the boundary has sharp edges and corners. We also show how the presence of homogeneous equations affects the discretisation procedures.

In Part III we compute the electrostatic capacity of a cube. Our results lie within all known bounds. We also compute the capacity of circular discs of varying thicknesses. Our results converge to the exact known result for a thin circular disc.

In Part IV we compute the velocity potential for shapes of cylindrical symmetry, as well as for a thick delta wing. In all these cases we first work with a suitable test velocity potential. This is a necessary precaution against any errors which may arise in the discretisation procedures and in our computer programs. In this section we also deal with the thin delta wing problem discussed by Brown and Stewartson. The thin delta may be considered as a limiting case of a thick delta, but such an approach is not practicable numerically for reasons given in Chapter 18. Accordingly we attack the problem by analysing the velocity potential of a thick delta wing into symmetric and antisymmetric components. The symmetric part arise from the thickness effect, and the antisymmetric part accordingly solves the problem of a thin delta wing.

In the final Chapter we experiment with a method of successive approximations. In effect this amounts to obtaining an approximate analytical solution of a Fredholm integral equation of the second kind using a perturbation technique. Although it works very well for smooth boundaries, e.g. a sphere, it appears not to work well with boundaries having sharp edges and corners.

PART I

THE FORMULATION OF BOUNDARY INTEGRAL EQUATIONS IN POTENTIAL THEORY

CHAPTER I

PROPERTIES OF POTENTIALS GENERATED BY SIMPLE AND DOUBLE LAYERS

Simple Layer Potential

Let B_i denote a finite domain bounded by a smooth regular surface δB. The infinite region exterior to B_i is denoted by B_e. Let there be a surface distribution of simple sources on δB of density σ, which is a continuous function on δB and satisfies a Hölder condition[1] at every point on δB. This distribution generates a Newtonian potential at any point $\underset{\sim}{p}$ which is given by

$$V(\underset{\sim}{p}) = \int_{\delta B} \frac{\sigma(q)dq}{|\underset{\sim}{p}-\underset{\sim}{q}|} \;;\; \underset{\sim}{q}\in\delta B \;, \qquad \text{either} \quad \underset{\sim}{p}\in B_i \text{ or } \underset{\sim}{p}\in B_e \;, \tag{1}$$

where $\underset{\sim}{p}$ and $\underset{\sim}{q}$ are vector variables such that $\underset{\sim}{p}$ specifies a field point in B_i or in B_e and $\underset{\sim}{q}$ specifies a source point on δB; dq and $\sigma(\underset{\sim}{q})$ denote the area differential and source density, respectively, at the point $\underset{\sim}{q}$ on δB; $|\underset{\sim}{p} - \underset{\sim}{q}|$ denotes the distance from $\underset{\sim}{p}$ to $\underset{\sim}{q}$ (Fig. 1). The simple layer integral (1) remains continuous as $\underset{\sim}{p}$ crosses δB, and therefore on δB

$$V(\underset{\sim}{p}) = \int_{\delta B} \frac{\sigma(q)dq}{|\underset{\sim}{p}-\underset{\sim}{q}|} \;;\; \underset{\sim}{p},\, \underset{\sim}{q}\in\delta B \;. \tag{2}$$

Although V remains continuous at δB, its normal derivative is discontinuous. The interior normal derivative of V at a point $\underset{\sim}{p}$ of δB (Fig. 2) is given by (Kellogg)[1]

$$V_i^1(\underset{\sim}{p}) = -2\pi\sigma(\underset{\sim}{p}) + \int_{\delta B} \frac{\sigma(q)dq}{{}_i^1|\underset{\sim}{p}-\underset{\sim}{q}|} \;;\; \underset{\sim}{p},\, \underset{\sim}{q}\in\delta B \tag{3}$$

where ${}_i^1|\underset{\sim}{p} - \underset{\sim}{q}|^{-1}$ stands for the interior normal derivative of $|\underset{\sim}{p} - \underset{\sim}{q}|^{-1}$ at $\underset{\sim}{p}$ keeping $\underset{\sim}{q}$ fixed. The exterior normal derivative of V at $\underset{\sim}{p}$ on δB (Fig. 2) is given by

$$V_e^1(\underset{\sim}{p}) = -2\pi\sigma(\underset{\sim}{p}) + \int_{\delta B} \frac{\sigma(q)dq}{{}_e^1|\underset{\sim}{p}-\underset{\sim}{q}|} \;;\; \underset{\sim}{p},\, \underset{\sim}{q}\in\delta B \tag{4}$$

where ${}_e^{1}|\underset{\sim}{p} - \underset{\sim}{q}|^{-1}$ stands for the exterior normal derivative of $|\underset{\sim}{p} - \underset{\sim}{q}|^{-1}$ at $\underset{\sim}{p}$ keeping $\underset{\sim}{q}$ fixed. Bearing in mind (Fig. 2) that

$$ {}_i^{1}|\underset{\sim}{p}-\underset{\sim}{q}|^{-1} + {}_e^{1}|\underset{\sim}{p}-\underset{\sim}{q}|^{-1} = 0 \; ; \; \underset{\sim}{p}\in\delta B \quad , \tag{5}$$

We find

$$ V_i^1(\underset{\sim}{p}) + V_e^1(\underset{\sim}{p}) = -4\pi\sigma(\underset{\sim}{p}) \quad . \tag{6}$$

Further, $V(\underset{\sim}{p}) \to |\underset{\sim}{p}|^{-1} \int_{\delta B} \sigma(\underset{\sim}{q})dq \quad \text{as} \quad |\underset{\sim}{p}| \to \infty \quad .$

More precisely

$$ V(\underset{\sim}{p}) = |\underset{\sim}{p}|^{-1} \int_{\delta B} \sigma(\underset{\sim}{q})dq + 0|\underset{\sim}{p}|^{-2} $$

$$ = 0|\underset{\sim}{p}|^{-1} \quad \text{as} \quad |\underset{\sim}{p}| \to \infty \quad . $$

<u>Double Layer Potential</u>

Let there be a surface distribution of double layer sources on δB of density μ which is a piecewise continuous function at every point of δB. The potential W generated by this distribution is given by

$$ W_i(\underset{\sim}{p}) = \int_{\delta B} \frac{\mu(q)dq}{|\underset{\sim}{p}-\underset{\sim}{q}|_i^1} \; ; \quad \underset{\sim}{q}\in\delta B, \; \underset{\sim}{p}\in B_i \quad , \tag{7}$$

where ${}_i^{1}|\underset{\sim}{q} - \underset{\sim}{p}|^{-1}$ stands for the interior normal derivative of $|\underset{\sim}{p} - \underset{\sim}{q}|^{-1}$ at $\underset{\sim}{q}$ keeping $\underset{\sim}{p}$ fixed. Unlike the simple layer integral, the double layer integral is discontinuous at δB whereas its normal derivative is continuous.[1] If we approach a surface point $\underset{\sim}{p}$ from the interior, W_i jumps by an amount $- 2\pi\mu(\underset{\sim}{p})$. Let W represent a continuous function ϕ, in which case

$$ \phi(\underset{\sim}{p}) = W(\underset{\sim}{p}) \; ; \; \text{either } \underset{\sim}{p}\in B_i \text{ or } \underset{\sim}{p}\in B_e \quad . \tag{8}$$

when $\underset{\sim}{p}$ approaches δB along the normal at p to δB, either from the interior or from the exterior, if follows that

$$ \phi(\underset{\sim}{p}) = W(\underset{\sim}{p}) + 2\pi\mu(\underset{\sim}{p}) \; ; \quad \underset{\sim}{p}\in\delta B \quad . \tag{9}$$

The above sign conventions are those adopted by Jaswon (1963).[2] This convention has the advantage of ensuring that the interior and the exterior formulae carry the same signs i.e. (3) and (4) for the normal derivative expression and (8) and (9) for the double layer surface relations.

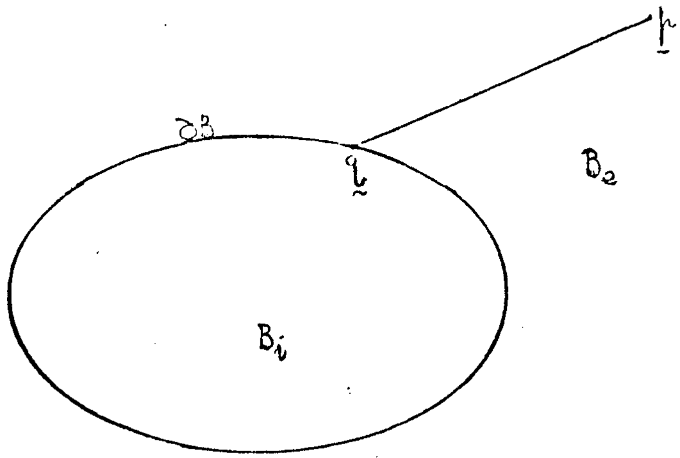
$\underset{\sim}{p}$
∂B
$\underset{\sim}{q}$
B_e
B_i

Fig. 1

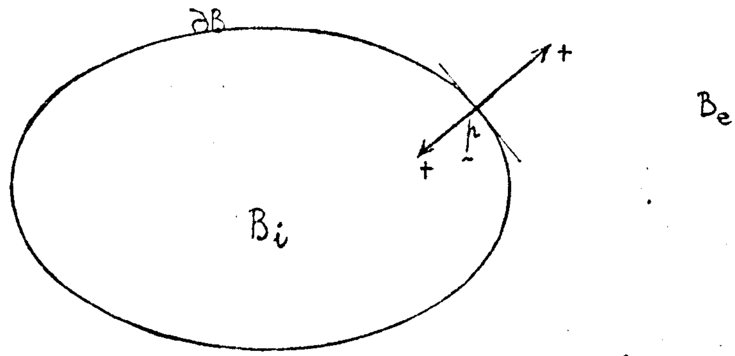
∂B
+
B_e
$\underset{\sim}{p}$
+
B_i

Fig. 2

Green's Formula

Since every Newtonian potential is a harmonic function, it follows that the potentials V and W are harmonic. Now the question arises whether an arbitrary harmonic function ϕ in B_i can be represented by potentials such as (1) or (7). According to Kellogg[1] if ϕ is given on δB (Dirichlet problem), it may be represented by (7). If ϕ_i', the interior normal derivative of ϕ, is given on δB (Neumann problem), it may be represented by (1). However a more general representation is provided by Green's formula. Given a harmonic function ϕ defined throughout B_i, which assumes values ϕ on δB and normal derivatives ϕ_i' on δB, Green's formula states that

$$\int_{\delta B} G(\underset{\sim}{p},\underset{\sim}{q})_i'\phi(\underset{\sim}{q})dq - \int_{\delta B} G(\underset{\sim}{p},\underset{\sim}{q})\phi_i'(\underset{\sim}{q})dq = \phi(\underset{\sim}{p});\ \underset{\sim}{q}\in\delta B,\ \underset{\sim}{p}\in B_i \tag{10}$$

where $G^{-1} = 4\pi|\underset{\sim}{p} - \underset{\sim}{q}|$ and $G(\underset{\sim}{p},\underset{\sim}{q})_i'$ represents the interior normal derivative of G at $\underset{\sim}{q}$ keeping $\underset{\sim}{p}$ fixed. When $\underset{\sim}{p}$ lies on δB, (10) becomes

$$\int_{\delta B} G(\underset{\sim}{p},\underset{\sim}{q})_i'\phi(\underset{\sim}{q})dq - \int_{\delta B} G(\underset{\sim}{p},\underset{\sim}{q})\phi_i'(\underset{\sim}{q})dq = \tfrac{1}{2}\phi(\underset{\sim}{p});\ \underset{\sim}{q},\underset{\sim}{p}\in\delta B \tag{11}$$

by virtue of the jump $-\frac{1}{2}\phi$ in the double layer integral

$$\int_{\delta B} G(\underset{\sim}{p},\underset{\sim}{q})_i'\phi(\underset{\sim}{q})dq\ .$$

This is Green's boundary formula for the interior harmonic ϕ. When $\underset{\sim}{p}$ lies in B_e, (10) becomes

$$\int_{\delta B} G(\underset{\sim}{p},\underset{\sim}{q})_i'\phi(\underset{\sim}{q})dq - \int_{\delta B} G(\underset{\sim}{p},\underset{\sim}{q})\phi_i'(\underset{\sim}{q})dq = 0;\ \underset{\sim}{p}\in B_e,\ \underset{\sim}{q}\in\delta B \tag{12}$$

by virtue of the further jump in the integral

$$\int_{\delta B} G(\underset{\sim}{p},\underset{\sim}{q})_i'\phi(\underset{\sim}{q})dq\ .$$

Our sign conventions ensure that all exterior equations carry the same signs as their interior counterparts. Hence for the exterior harmonic ϕ defined in B_e, such that $\phi \to O|\underset{\sim}{p}|^{-1}$ as $|\underset{\sim}{p}| \to \infty$, which assumes values ϕ on δB and normal derivatives ϕ_e' on δB, Green's formula take the form

$$\int_{\delta B} G(p,q)'_e \phi(q)dq - \int_{\delta B} G(p,q)\phi'_e(q)dq = \phi(p); \; q\in\delta B, p\in B_e \quad (13)$$

where $G(p,q)'_e$ represents the exterior normal derivative of G at q keeping p fixed. When p is a point on δB, as before,

$$\int_{\delta B} G(p,q)'_e \phi(q)dq - \int_{\delta B} G(p,q)\phi'_e(q)dq = \tfrac{1}{2}\phi(p); \; p,q\in\delta B \quad (14)$$

and for a point p in B_i, by virtue of a further jump in the double layer integral,

$$\int_{\delta B} G(p,q)'_e \phi(q)dq - \int_{\delta B} G(p,q)\phi'_e(q)dq = 0; \quad p\in B_i, q\in\delta B . \quad (15)$$

It is interesting to examine the behavior of ϕ defined by (13), at infinity. Given ϕ and ϕ'_e on δB, from (13) we have

$$\phi(p) = 0|p|^{-2} \int_{\delta B} \phi(q)dq - 0|p|^{-1} \int_{\delta B} \phi'_e(q)dq, \quad (16)$$

since $G = 0|p|^{-1}$ and $G' = 0|p|^{-2}$ when $|p| \to \infty$.

In contrast with the interior problem, where

$$\int_{\delta B} \phi'_i(q)dq = 0$$

for the interior harmonic ϕ (Gauss condition)

$$\int_{\delta B} \phi'_e(q)dq \neq 0 \quad (17)$$

necessarily. This does not contradict the Gauss condition if we bear in mind the compensating contribution from a large sphere at infinity.

CHAPTER 2

FORMULATION OF DIRICHLET AND NEUMANN PROBLEMS BY FREDHOLM INTEGRAL EQUATIONS

Dirichlet Problem

If the simple source potential V represents a harmonic function characterised by the boundary values ϕ, it must, from (2), satisfy the boundary equation

$$\phi(\underset{\sim}{p}) = \int_{\delta B} G(\underset{\sim}{p},\underset{\sim}{q})\sigma(\underset{\sim}{q})dq \; ; \; \underset{\sim}{p},\underset{\sim}{q}\in\delta B \tag{18}$$

which is a Fredholm integral equation of the 1st kind for σ in terms of ϕ on δB. If a solution of (18) exists, it generates an interior harmonic function

$$\phi(\underset{\sim}{p}) = \int_{\delta B} G(\underset{\sim}{p},\underset{\sim}{q})\sigma(\underset{\sim}{q})dq \; ; \quad \underset{\sim}{q}\in\delta B, \; \underset{\sim}{p}\in B_i$$

and an exterior harmonic function

$$\phi(p) = \int_{\delta B} G(\underset{\sim}{p},\underset{\sim}{q})\sigma(\underset{\sim}{q})dq \; ; \quad \underset{\sim}{q}\in\delta B, \; \underset{\sim}{p}\in B_e$$

such that $\phi(\underset{\sim}{p}) = 0|\underset{\sim}{p}|^{-1}$ as $|\underset{\sim}{p}| \to \infty$. Similarly if the double source potential W represents a harmonic function ϕ in B_i, it must, from (9) satisfy the boundary equation

$$\phi(\underset{\sim}{p}) = \tfrac{1}{2}\mu(\underset{\sim}{p}) + \int_{\delta B} G(\underset{\sim}{p},\underset{\sim}{q})^{1}_{i}\mu(\underset{\sim}{q})dq \; ; \; \underset{\sim}{p},\underset{\sim}{q}\in\delta B \tag{19}$$

which is a Fredholm integral equation of the 2nd kind for μ in terms of ϕ on δB.

Interior Neumann Problem

In the case of the interior Neumann problem, where ϕ_i^{1} is given on δB, it follows from (3) that

$$\phi_i^{1}(\underset{\sim}{p}) = -\tfrac{1}{2}\sigma(\underset{\sim}{p}) + \int_{\delta B} G_i^{1}(\underset{\sim}{p},\underset{\sim}{q})\sigma(\underset{\sim}{q})dq \; ; \; \underset{\sim}{p},\underset{\sim}{q}\in\delta B \,. \tag{20}$$

This is a Fredholm integral equation of the 2nd kind for the unknown boundary function σ .

Equation (19) is fully discussed by Kellogg but is not utilised in this thesis. Leaving aside (18) to be discussed later, the necessary and sufficient condition for the existance of a solution[1] of (20), by Kellogg, is

$$\int_{\delta B} \mu(\underset{\sim}{p})\phi_i^1(\underset{\sim}{p})dp = 0 \tag{21}$$

where μ is a solution of the transpose (or adjoint) hamogeneous equation

$$-\tfrac{1}{2}\mu(\underset{\sim}{p}) + \int_{\delta B} G(\underset{\sim}{p},\underset{\sim}{q})_i^1\mu(\underset{\sim}{q})dq = 0 \; ; \; \underset{\sim}{p},\underset{\sim}{q}\in\delta B \; . \tag{22}$$

This admits the non-trivial solution $\mu = 1$ by virtue of the Gauss flux theorem for the field point on δ B viz.

$$\int_{\delta B} G(\underset{\sim}{p},\underset{\sim}{q})_i^1 dq = -\int_{\delta B} G(\underset{\sim}{p},\underset{\sim}{q})_e^1 dq = \tfrac{1}{2}; \; \underset{\sim}{p},\underset{\sim}{q}\in\delta B \; . \tag{23}$$

Setting $\mu = 1$ in (21) we have the expected Gauss condition for the interior harmonic ϕ viz.

$$\int_{\delta B} \phi_i^1(\underset{\sim}{p})dp = 0 \; . \tag{24}$$

The general solution[1] of (20) is then given by

$$\sigma = \sigma_o + k\lambda$$

where σ_o is a particular solution of (20); k is an arbitrary constant and λ is a solution of the corresponding homogenous equation

$$-\tfrac{1}{2}\lambda(\underset{\sim}{p}) + \int_{\delta B} G_i^1(\underset{\sim}{p},\underset{\sim}{q})\lambda(\underset{\sim}{q})dq = 0; \; \underset{\sim}{p},\underset{\sim}{q}\in\delta B \; , \tag{25}$$

An alternative proof of (24) is as follows. Integrating both sides of (20) with respect to p and bearing in mind the Theorem (23):

$$\int_{\delta B} \phi_i^1(\underset{\sim}{p})dp = -\int_{\delta B} \tfrac{1}{2}\sigma(\underset{\sim}{p})dp + \int_{\delta B}\int_{\delta B} G_i^1(\underset{\sim}{p},\underset{\sim}{q})\sigma(\underset{\sim}{q})dq\, dp$$

$$= -\int_{\delta B} \tfrac{1}{2}\sigma(\underset{\sim}{p})dp + \int_{\delta B} \tfrac{1}{2}\sigma(\underset{\sim}{q})dq = 0 \tag{26}$$

Exterior Neumann Problem

In the case of the exterior Neumann problem, where ϕ'_e is given on δB, it follows from (4) that

$$\phi^1_e(\underset{\sim}{p}) = -\tfrac{1}{2}\sigma(\underset{\sim}{p}) + \int_{\delta B} G^1_e(\underset{\sim}{p},\underset{\sim}{q})\sigma(\underset{\sim}{q})dq \;;\; \underset{\sim}{p},\underset{\sim}{q}\epsilon\delta B \;. \tag{27}$$

This has a solution, by Kellogg, if

$$\int_{\delta B} \phi^1_e(\underset{\sim}{p})\mu(\underset{\sim}{p})dp = 0 \tag{28}$$

where μ is a solution of the corresponding transpose homogeneous equation

$$-\tfrac{1}{2}\mu(\underset{\sim}{p}) + \int_{\partial B} G(\underset{\sim}{p},\underset{\sim}{q})^1_e\mu(\underset{\sim}{q})dq = 0; \; \underset{\sim}{p},\underset{\sim}{q}\epsilon\delta B \;. \tag{29}$$

The equation (29) in three dimensions has no non-trivial solution, since its transpose

$$-\tfrac{1}{2}\lambda(\underset{\sim}{p}) + \int_{\partial B} G^1_e(\underset{\sim}{p},\underset{\sim}{q})\lambda(\underset{\sim}{q})dq = 0; \; \underset{\sim}{p},\underset{\sim}{q}\epsilon\delta B \tag{30}$$

as shown in the next chapter, has no non-trival solution. As a result, by Kellogg, (27) has always a unique solution.

Integrating both the sides of (27) with respect to p, we find

$$\int_{\delta B} \phi^1_e(\underset{\sim}{p})dp = -\tfrac{1}{2}\int_{\delta B} \sigma(\underset{\sim}{p})dp + \int_{\delta B}\int_{\delta B} G^1_e(\underset{\sim}{p},\underset{\sim}{q})\sigma(\underset{\sim}{q})dq\; dp$$

$$= -\tfrac{1}{2}\int_{\delta B} \sigma(\underset{\sim}{p})dp - \tfrac{1}{2}\int_{\delta B} \sigma(\underset{\sim}{q})dq = -\int_{\delta B} \sigma(\underset{\sim}{q})dq \tag{31}$$

which, in contrast with (26), does not equal zero necessarily. This is completely in accordance with (17) in Chapter 1.

Green's Boundary Formula

In Green's formula (10), the interior harmonic function ϕ is expressed in terms of the values of ϕ and ϕ'_i on δB. These over-prescribe[3] the boundary data and, therefore, the formula cannot be used directly to solve the boundary value problems. This is because ϕ alone on δB, or ϕ'_i alone on δB, or any admissible local relation between ϕ and ϕ'_i on δB, suffices to determine ϕ throughout B_i. One way out of this difficulty is to take the field point $\underset{\sim}{p}$ on δB itself, which is Green's boundary formula (11). This may be viewed as a constraint between ϕ and

ϕ'_i on δB that defines one in terms of the other . Given ϕ on δB (Dirichlet problem), (11) becomes a Fredholm integral equation on the 1st kind for ϕ'_i viz.

$$\int_{\delta B} G(\underset{\sim}{p},\underset{\sim}{q})\phi'_i(\underset{\sim}{q})dq = -\tfrac{1}{2}\phi(\underset{\sim}{p}) + \int_{\delta B} G(\underset{\sim}{p},\underset{\sim}{q})'_i\phi(\underset{\sim}{q})dq \; ; \; \underset{\sim}{p},\underset{\sim}{q}\in\delta B \; . \tag{32}$$

Conversely, given ϕ'_i on δB (Neumann problem), (11) becomes a Fredholm integral equation of the 2nd kind for ϕ viz.

$$-\tfrac{1}{2}\phi(\underset{\sim}{p}) + \int_{\delta B} G(\underset{\sim}{p},\underset{\sim}{q})'_i\phi(\underset{\sim}{q})dq = \int_{\delta B} G(\underset{\sim}{p},\underset{\sim}{q})\phi'_i(\underset{\sim}{q})dq \; ; \; \underset{\sim}{p},\underset{\sim}{q}\in\delta B \; . \tag{33}$$

Leaving equation (32) to be discussed in the next chapter, we come to equation (33) which, by Kellogg, has a solution if

$$\int_{\delta B} \lambda(\underset{\sim}{p})dp \int_{\delta B} G(\underset{\sim}{p},\underset{\sim}{q})\phi'_i(\underset{\sim}{q})dq = 0 \; ; \; \underset{\sim}{p},\underset{\sim}{q}\in\delta B \; . \tag{34}$$

Here λ is a solution of (25), which is the transpose of homogeneous part of (33) viz.

$$-\tfrac{1}{2}\phi(\underset{\sim}{p}) + \int_{\partial B} G(\underset{\sim}{p},\underset{\sim}{q})'_i\phi(\underset{\sim}{q})dq = 0 \; ; \; \underset{\sim}{p},\underset{\sim}{q}\in\delta B \; . \tag{35}$$

This equation (35), by virtue of (23), exhibits a non-trivial solution $\phi = 1$. Hence (25), which is the transpose of (35), has a non-trivial solution λ . Interchanging the order of integration in the left hand side of (34), we have

$$\int_{\delta B} \lambda(\underset{\sim}{p})dp \int_{\delta B} G(\underset{\sim}{p},\underset{\sim}{q})\phi'_i(\underset{\sim}{q})dq = \int_{\delta B} \phi'_i(\underset{\sim}{q})dq \int_{\delta B} G(\underset{\sim}{q},\underset{\sim}{p})\lambda(\underset{\sim}{p})dp = 0 \, ,$$

since $G(\underset{\sim}{p},\underset{\sim}{q}) = G(\underset{\sim}{q},\underset{\sim}{p})$ and $\int_{\delta B} G(\underset{\sim}{q},\underset{\sim}{p})\lambda(\underset{\sim}{p})dp = \phi = 1.$

The above condition is in agreement with the condition derived in (24).

The general solution of (33) is given by

$$\phi = \phi_o + k\eta$$

where ϕ_o is a particular solution of (33); k is an arbitrary constant and $\eta = 1$ is a solution of the corresponding homogeneous equation (35).

Given ϕ_e' on δB (the exterior Neumann problem), (14) becomes a Fredholm integral equation of the 2nd kind for ϕ viz.

$$-\tfrac{1}{2}\phi(\underset{\sim}{p}) + \int_{\delta B} G(\underset{\sim}{p},\underset{\sim}{q})_e^{1}\phi(\underset{\sim}{q})dq = \int_{\delta B} G(\underset{\sim}{p},\underset{\sim}{q})\phi_e^{1}(\underset{\sim}{q})dq \;;\; \underset{\sim}{p},\underset{\sim}{q}\in\delta B \;. \tag{36}$$

This has a solution, by Kellogg, if

$$\int_{\partial B}\lambda(\underset{\sim}{p})dp\int_{\partial B}G(\underset{\sim}{p},\underset{\sim}{q})\phi_e^{1}(\underset{\sim}{q})dq = 0 \;;\; \underset{\sim}{p},\underset{\sim}{q}\in\delta B$$

where λ is a solution of (30) which is a transpose of the homogeneous part of (36). It is discussed earlier that in three dimensions, equation (30) has no non-trivial solution. Hence in three dimensions, by Kellogg, (36) has a unique solution.

Confining our discussion to three dimensions, we find the exterior Neumann problem, in contrast with the interior Neumann problem, has always a solution and that it is unique.

CHAPTER 3

EXISTENCE AND UNIQUENESS OF THE SOLUTION OF FREDHOLM INTEGRAL EQUATION OF THE 1ST KIND

The Electrostatic Equation

If we put $\phi = 1$ in (18), we obtain the electrostatic equation

$$\int_{\delta B} G(\underset{\sim}{p},\underset{\sim}{q})\lambda(\underset{\sim}{q})dq = 1 \; ; \; \underset{\sim}{p},\underset{\sim}{q}\in\delta B \quad . \tag{37}$$

Since $\phi = 1$ on δB, it follows that $\phi = 1$ everywhere in B_i. Hence taking the interior normal derivative of (37), we have

$$-\tfrac{1}{2}\lambda(\underset{\sim}{p}) + \int_{\delta B} \overset{1}{G_i}(\underset{\sim}{p},\underset{\sim}{q})\lambda(\underset{\sim}{q})dq = 0 \; ; \; \underset{\sim}{p},\underset{\sim}{q}\in\delta B \; . \tag{38}$$

This equation exhibits a non-trivial solution λ, since its transpose

$$-\tfrac{1}{2}\mu(\underset{\sim}{p}) + \int_{\delta B} G(\underset{\sim}{p},\underset{\sim}{q})\overset{1}{_i}\mu(\underset{\sim}{q})dq = 0 \; ; \; \underset{\sim}{p},\underset{\sim}{q}\in\delta B \; ,$$

has, by virtue of (23), a non-trivial solution $\mu = 1$. The solution of (38) generates an interior simple source potential

$$\chi(p) = \int_{\delta B} G(p,q)\lambda(q)dq \; ; \; \underset{\sim}{q}\in\delta b, \; \underset{\sim}{p}\in B_i \tag{39}$$

characterised by

$$\overset{1}{\chi_i}(\underset{\sim}{p}) = 0 \; ; \; \underset{\sim}{p}\in\delta B \; . \tag{40}$$

It follows that χ = Constant on δB. Hence the solution λ either satisfies (37) or possibly satisfies

$$\int_{\delta B} G(\underset{\sim}{p},\underset{\sim}{q})\lambda(\underset{\sim}{q})dq = 0 \; ; \; \underset{\sim}{p},\underset{\sim}{q}\in\delta B \; . \tag{41}$$

Let us assume the non-trivial solution λ of (38) satisfies (41). Hence it generates an exterior simple source potential

$$\chi(\underset{\sim}{p}) = \int_{\delta B} G(\underset{\sim}{p},\underset{\sim}{q})\lambda(\underset{\sim}{q})dq \quad ; \underset{\sim}{q}\in\partial B, \underset{\sim}{p}\in B_e \tag{42}$$

characterised by

$$\chi(\underset{\sim}{p}) \to 0|\underset{\sim}{p}|^{-1}\int_{\partial B}\lambda(q)dq \quad \text{as} \quad |\underset{\sim}{p}| \to \infty \quad . \tag{43}$$

The combination of (43) with (41), i.e. $\chi = 0$ on δ B, implies by a classical existence theorem[1] that $\chi = 0$ everywhere in B_e.
Hence

$$\chi^1_e(\underset{\sim}{p}) = 0 \; ; \; \underset{\sim}{p}\in\delta B \quad . \tag{44}$$

Bearing in mind $\chi^1_i\,(\underset{\sim}{p}) = 0$; $\underset{\sim}{p} \in \delta B$, by (6),
it follows that

$$-\lambda(\underset{\sim}{p}) = \chi^1_i(\underset{\sim}{p}) + \chi^1_e(\underset{\sim}{p}) = 0 \quad .$$

This shows that the equation (41) has no non-trivial solution. Hence λ satisfies (37), and the solution of (37) is unique. In two dimensional potential theory

$$\chi(\underset{\sim}{p}) = O(\log|\underset{\sim}{p}|)\int_{\delta B}\lambda(\underset{\sim}{q})dq \quad \text{as } |\underset{\sim}{p}| \to \infty$$

and hence we can not conclude that $\chi = 0$ everywhere in B_e even though $\chi = 0$ on δ B. In two-dimensions, therefore, equation (41) may exhibit a non-trivial solution (Γ contour case, Jaswon 1963).

Generalisation of Electrostatic Equation

To show that the more general equation (18) has a unique solution, let us consider its equivalent normal derivative equation (20).
It has already been shown that the general solution of (20) is

$$\sigma = \sigma_o + k\lambda \tag{45}$$

where σ_o is a particular soluton of (20); k is an arbitrary constant and λ is a solution of the corresponding homogeneous equation (25). This solution generates a simple source potential that differs from $\phi(\underset{\sim}{p})$ of (18) only by a constant, which may be eliminated by choosing a suitable value of k. Hence $\sigma_o + k\lambda$ provides a unique solution of (18). This discussion covers the equation (32) though it remains to be proved that $\phi_i^{\prime}(\underset{\sim}{p})$ of (32) satisfies (24). Operating on both sides of (32) by $\int \cdots\cdots \lambda(\underset{\sim}{p})dp$ and interchanging the order of integration (Fubini's theorem), we have

$$\int_{\delta B} \lambda(\underset{\sim}{p})dp \int_{\delta B} G(\underset{\sim}{p},\underset{\sim}{q})\phi_i^{\prime}(\underset{\sim}{q})dq = \int_{\delta B} \lambda(\underset{\sim}{p})dp \int_{\delta B} G(\underset{\sim}{p},\underset{\sim}{q})_i^{\prime}\phi(\underset{\sim}{q})dq - \tfrac{1}{2}\int_{\delta B} \lambda(\underset{\sim}{p})\phi(\underset{\sim}{p})dp$$

i.e. $$\int_{\delta B} \phi_i^{\prime}(\underset{\sim}{q})dq \int_{\delta B} G(\underset{\sim}{q},\underset{\sim}{p})\lambda(\underset{\sim}{p})dp = \int_{\delta B} \phi(\underset{\sim}{q})dq \int_{\delta B} G(\underset{\sim}{p},\underset{\sim}{q})_i^{\prime}\lambda(\underset{\sim}{p})dp - \tfrac{1}{2}\int_{\delta B} \lambda(\underset{\sim}{p})\phi(\underset{\sim}{p})dp$$

i.e. $$\int_{\delta B} \phi_i^{\prime}(\underset{\sim}{q})dq = \tfrac{1}{2}\int_{\delta B} \phi(\underset{\sim}{q})\lambda(\underset{\sim}{q})dq - \tfrac{1}{2}\int_{\delta B} \lambda(\underset{\sim}{p})\phi(\underset{\sim}{p})dp$$

i.e. $$\int_{\delta B} \phi_i^{\prime}(\underset{\sim}{q})dq = 0 \quad .$$

Relation between formulations

We have two formulations (18) and (32) of the Dirichlet problem, both of which are Fredholm integral equations of the 1st kind. Neither of these coincide with the classical formulation (19), which is a Fredholm integral equation of the 2nd kind. To establish a connection between (18), (19) and (32) let us introduce Green's identity (15) for an exterior function Ψ in B_e, characterised by the behaviour $O\,|\underset{\sim}{p}|^{-1}$ as $|\underset{\sim}{p}| \to \infty$,

$$\int_{\delta B} G(\underset{\sim}{p},\underset{\sim}{q})'_e \Psi(\underset{\sim}{q})dq - \int_{\delta B} G(\underset{\sim}{p},\underset{\sim}{q})\Psi'_e(\underset{\sim}{q})dq = 0 \ ; \ \underset{\sim}{p}\in B_i, q\in\delta B \ . \tag{46}$$

Superimposing (10) and (46), and bearing in mind the relation (5), we find

$$\int_{\delta B} G(\underset{\sim}{p},\underset{\sim}{q})'_i\left[\phi(\underset{\sim}{q})-\Psi(\underset{\sim}{q})\right]dq - \int_{\delta B} G(\underset{\sim}{p},\underset{\sim}{q})\left[\phi'_i(\underset{\sim}{q})+\Psi'_e(\underset{\sim}{q})\right]dq = \phi(\underset{\sim}{p}) \ . \tag{47}$$

There are two distinct possibilities for Ψ :

(i) $\Psi = \phi$ on δB, whence

$$\phi(\underset{\sim}{p}) = -\int_{\delta B} G(\underset{\sim}{p},\underset{\sim}{q})\left[\Psi'_e(\underset{\sim}{q})+\phi'_i(\underset{\sim}{q})\right]dq \ ; \ \underset{\sim}{q}\in\delta B, \underset{\sim}{p}\in B_i \ . \tag{48}$$

Putting $\Psi'_e(\underset{\sim}{q}) + \phi'_i(\underset{\sim}{q}) = -\sigma(\underset{\sim}{q})$, (48) identifies with (18).

(ii) $\Psi'_e(\underset{\sim}{q}) = -\phi'_i(\underset{\sim}{q})$ on δB, whence

$$\phi(\underset{\sim}{p}) = \int_{\delta B}\left[\phi(\underset{\sim}{q})-\Psi(\underset{\sim}{q})\right]G(\underset{\sim}{p},\underset{\sim}{q})'_i dq \ ; \ \underset{\sim}{p}\in B_i, \underset{\sim}{q}\in\delta B \ . \tag{49}$$

Putting $\phi(\underset{\sim}{q}) - \Psi(\underset{\sim}{q}) = \mu(\underset{\sim}{q})$, (49) identifies with (19) when $\underset{\sim}{p}$ is taken on δB.

CHAPTER 4

SOME APPLICATIONS OF POTENTIAL THEORY

Electrostatic Capacity

It has been shown that the 'electrostatic' equation

$$\int_{\delta B} G(\underset{\sim}{p},\underset{\sim}{q})\lambda(\underset{\sim}{q})dq = 1 \ ; \ \underset{\sim}{p},\underset{\sim}{q}\in\delta B \tag{50}$$

exhibits a unique solution λ. To prove that λ has the same sign everywhere on δB, we note δB is an equipotential of the exterior harmonic functionn χ of (42). Hence χ'_e has the same sign everywhere on δB. Now

$$\chi = O|\underset{\sim}{r}|^{-1} \text{ as } |\underset{\sim}{r}| \to \infty ,$$

Therefore, $\chi^1_e(\underset{\sim}{p}) < 0$ (51)

everywhere on δB. Bearing in mind $\chi'_i(\underset{\sim}{p}) = 0$, we see that, by (6),

$$\lambda(\underset{\sim}{p}) = -(\chi^1_i(\underset{\sim}{p}) + \chi^1_e(\underset{\sim}{p})) > 0$$

on δB. The quantity

$$\kappa = \int_{\delta B} \lambda(\underset{\sim}{p})dp > 0 \tag{52}$$

is defined to be the electrostatic capactity of δB.
The electrostatic density λ which generates the potential $\phi = 1$ on δB can be obtained by solving the equation (50). The capacity κ then may be computed using this λ in (52).

Potential Fluid Motion

An inviscid incompressible fluid is flowing from infinity with uniform velocity $\underset{\sim}{U}$. In the finite region it passes round a fixed obstacle B which distrubs the flow. If Ψ is the velocity potential of the free flow, and if ϕ is the perturbation of this potential by the presence of B, then the total velocity potential is

$$\Phi = \phi + \Psi \tag{53}$$

where $-\nabla\Psi = \underset{\sim}{U} =$ a constant, (54)

and $\phi = O|\underset{\sim}{p}|^{-1}$, by (16), as $|\underset{\sim}{p}| \to \infty$.

The normal velocity component is zero at the boundary δB, and so

$$\Phi_e^1(\underset{\sim}{p}) = \phi_e^1(\underset{\sim}{p}) + \Psi_e^1(\underset{\sim}{p}) = 0 \; ; \; \underset{\sim}{p} \in \delta B \; . \tag{55}$$

From (55), $\phi_e^1(\underset{\sim}{p}) = -\Psi_e^1(\underset{\sim}{p})$; $\underset{\sim}{p} \in \delta B$. Since Ψ_e^1 is known ϕ_e^1 is therefore known on δB. Hence the determination of ϕ becomes an exterior Neumann problem which, as shown earlier, has always a unique solution.

Since $\phi_e^1 = -\Psi_e^1$ on δB,

we have

$$\int_{\delta B} \phi_e^1(\underset{\sim}{p})dp = -\int_{\delta B} \Psi_e^1(\underset{\sim}{p})dp = 0 \qquad , \qquad \text{by (54)} \quad . \tag{56}$$

Putting (56) in (16), we find in the case of potential flow, that the perturbation ϕ is of order $|\underset{\sim}{p}|^{-2}$ as $|\underset{\sim}{p}| \to \infty$.

Given ϕ_e^1 on δB, the perturbation ϕ can be obtained in two ways:-

(i) It can be generated by a simple source distribution of density σ on δB such as (18) i.e.

$$\phi(\underset{\sim}{p}) = \int_{\delta B} G(\underset{\sim}{p},\underset{\sim}{q})\sigma(\underset{\sim}{q})dq \; ; \; \underset{\sim}{q} \in \delta B \tag{57}$$

where σ is obtained by solving the integral equation (27) viz.

$$-\tfrac{1}{2}\sigma(\underset{\sim}{p}) + \int_{\delta B} G_e^1(\underset{\sim}{p},\underset{\sim}{q})\sigma(\underset{\sim}{q})dq = \phi_e^1(\underset{\sim}{p}) \; ; \; \underset{\sim}{p},\underset{\sim}{q} \in \delta B \tag{58}$$

in which $\phi_e^1(\underset{\sim}{p})$ is given by (55). The σ's in (58) have the property, by (31),

$$\int_{\delta B} \sigma(\underset{\sim}{q})dq = -\int_{\delta B} \phi_e^1(\underset{\sim}{p})dp = 0 \qquad , \text{ by (56)} \quad . \tag{59}$$

(ii) ϕ can directly be obtained by solving the integral equation (36) viz.

$$-\tfrac{1}{2}\phi(\underset{\sim}{p}) + \int_{\delta B} G(\underset{\sim}{p},\underset{\sim}{q})_e^1\phi(\underset{\sim}{q})dq = \int_{\delta B} G(\underset{\sim}{p},\underset{\sim}{q})\phi_e^1(\underset{\sim}{q})dq \; ; \; \underset{\sim}{p},\underset{\sim}{q} \in \delta B \tag{60}$$

where ϕ_e^1 on δB is given by (55).

PART II

NUMERICAL PROCEDURES

CHAPTER 5

NUMERICAL SOLUTION OF FREDHOLM INTEGRAL EQUATION

First Kind

To solve a boundary integral equation analytically is, generally speaking, out of the question. A straightforward numerical approach replaces the equation by a system of simultaneous linear algebraic equations, referring to a set of nodal points spaced over the boundary. The equations are then assembled and solved by writing a digital computer program.

For a numerical solution we divide the surface ∂B into N intervals i.e. sub-areas, and then we make the fundamental assumption that

(1) THE SOURCE DENSITY REMAINS CONSTANT OVER A SUB-AREA .

On the basis of this assumption, for a particular field point $\underset{\sim}{p}$, equation (18) becomes

$$\sum_{j=1}^{N} \sigma_j \int_j G(\underset{\sim}{p},\underset{\sim}{q})\, dq = \phi(\underset{\sim}{p}) \quad , \tag{61}$$

where σ_j stands for the constant value of σ over the j th sub-area. To make further progress, we introduce a pivotal point $\underset{\sim}{q}_k$ within the k th sub-area, which is normally the centroid of the sub-area, and we put

$$\underset{\sim}{p} = \underset{\sim}{q}_1 \, , \underset{\sim}{q}_2 \, , \underset{\sim}{q}_3 \cdot \cdot \cdot \underset{\sim}{q}_N$$

successively. As a result (61) becomes

$$\sum_{j=1}^{N} \sigma_j \int_j G(\underset{\sim}{q}_k,\underset{\sim}{q})\, dq = \phi(\underset{\sim}{q}_k) \; ; \quad k = 1, 2, \cdot \cdot \cdot N . \tag{62}$$

This is a discrete system of N linear algebraic equations for the N unknowns .

Equations (62) can be put in the matrix form

$$[A]\,[\sigma] = [\phi] \tag{63}$$

where $[\sigma]$ is a column vector with the elements σ_j and $[\phi]$ is a column vector with N elements $\phi(q_j)$; $[A]$ is a N x N matrix with elements

$$a_{kj} = \int_j G(\underset{\sim}{q}_k, \underset{\sim}{q})\, dq \tag{64}$$

i.e. the integral of G $(\underset{\sim}{q}_k, \underset{\sim}{q})$ over the jth sub-area keeping $\underset{\sim}{q}_k$ fixed. In principle this can be computed as it stands, but simple approximations to it suffice for our purposes. Two distinct cases arise:

(a) when $j \neq k$, the integrand is finite. To approximate it we make the assumption that

(2) THE KERNEL REMAINS CONSTANT THROUGHOUT THE SUB-AREA, ITS VALUE BEING ASSOCIATED WITH THE PIVOTAL POINT $\underset{\sim}{q}_k$.

On this basis, we find

$$a_{kj} = G(\underset{\sim}{q}_k, \underset{\sim}{q}) \int_j dq \quad ; \qquad j \neq k \quad . \tag{65}$$

(b) when $j = k$, the integrand is singular, but integrable, and it may be evaluated analytically (Appendix I).

Given ϕ on ∂B, (63) represents a system of N linear algebraic equations for σ_k. These can be solved either by the matrix inversion method or, since $a_{kk} \neq 0$, by the Gauss - Seidel iterative method.

<u>Second Kind</u>

Following the basic assumptions and procedures adopted with equation (18), we write equations (20) and (27) as

$$-\frac{\sigma_k}{2} + \sum_{j=1}^{N} \sigma_j \int_j G'(\underset{\sim}{q}_k, \underset{\sim}{q})\, dq = \phi'(\underset{\sim}{q}_k) \quad ; \quad k = 1, 2, \cdots N . \tag{66}$$

Given $\phi'(\underset{\sim}{q}_k)$ on ∂B, this represents a system of N linear algebraic equations for the unknowns $\sigma_1, \sigma_2, \ldots\ldots \sigma_N$ of the form

$$[B][\sigma] = [\phi'] \quad . \tag{67}$$

The element b_{kj} of the N x N matrix $[B]$ is given by

$$b_{kj} = \int_j G'(\underset{\sim}{q}_k, \underset{\sim}{q})\, dq \quad ; \qquad j \neq k \quad , \tag{68}$$

$$= -\frac{1}{2} + \int_j G'(\underset{\sim}{q}_k, \underset{\sim}{q})\, dq \quad ; \qquad j = k \ . \tag{69}$$

The integrand in (68) is finite and on the basis of the assumption 2 it becomes

$$b_{kj} = G'(\underset{\sim}{q}_k, \underset{\sim}{q}) \int_j dq \quad ; \qquad j \neq k \ . \tag{70}$$

The integrand in (69) is apparently indeterminate but integrable, and may be evaluated analytically (Appendix II)

Similarly following the same assumptions and procedures, we write equations (33) and (36) as

$$-\frac{\phi(\underset{\sim}{q}_k)}{2} + \sum_{j=1}^{N} \phi(\underset{\sim}{q}_j) \int_j G(\underset{\sim}{q}_k, \underset{\sim}{q})'\, dq = \sum_{j=1}^{N} \phi'(\underset{\sim}{q}_j) \int_j G(\underset{\sim}{q}_k, \underset{\sim}{q})\, dq \ ; \ k = 1, 2, \cdots N \ . \tag{71}$$

Given $\phi'(\underset{\sim}{q}_k)$ on ∂B, this equation represents a system of N linear algebraic equations for the unknowns $\phi(\underset{\sim}{q}_1)$, $\phi(\underset{\sim}{q}_2)$, ... $\phi(\underset{\sim}{q}_N)$, of the form

$$[C][\phi] = [D] \ . \tag{72}$$

The element C_{kj} of the N x N matrix $[C]$ is given by

$$C_{kj} = \int_j G(\underset{\sim}{q}_k, \underset{\sim}{q})'\, dq \quad ; \qquad j \neq k \ , \tag{73}$$

$$= -\frac{1}{2} + \int_j G(\underset{\sim}{q}_k, \underset{\sim}{q})'\, dq \ ; \quad j = k \ . \tag{74}$$

The integrand in (73) is finite and, as before, on the basis of assumption 2, it becomes

$$C_{kj} = G(\underline{q}_k, \underline{q})' \int_j dq \quad ; \quad j \neq k \quad . \tag{75}$$

When j = k, the integrand is apparently indeterminate but integrable, and may be evaluated analytically (Appendix II). The column vector $[D]$ has N elements

$$d_k = \sum_{j=1}^{N} \phi'(\underline{q}_j) \int_j G(\underline{q}_k, \underline{q}) dq \quad ; \quad k = 1, 2, \cdots N \; .$$

The above integral for j = 1, 2, ... N is evaluated in the same way as (64).

From (69) and (74) we find that the diagonal element in any of the matrices $[B]$ and $[C]$ is a fairly large element in a row. This makes the equations amenable to solution by the Gauss-Seidel iterative method.

Singular Matrix

In the electrostatic problem $\phi_i' = 0$ on ∂B, so that (20) becomes the homogeneous equation

$$-\frac{1}{2}\lambda(\underline{p}) + \int G'_{int.}(\underline{p}, \underline{q}) \lambda(\underline{q}) dq = 0 \quad , \tag{76}$$

where int. stands for interior normal (replacing i of Part I).
On discretisation (76) gives (67) with $\phi' = 0$, and $[\sigma]$ is replaced by $[\lambda]$ i.e.

$$[B][\lambda] = 0 \quad .$$

It has already been shown in Chapter 2, that the equation (76) has a non-trival solution. Hence the matrix $[B]$ must be singular. This property must be ensured by our numerical procedure. How can this be done? Since (76) has a non-trivial solution, it follows that

$$\int_{\partial B} dp \left[-\frac{1}{2}\lambda(\underline{p}) + \int_{\partial B} G'_i(\underline{p}, \underline{q}) \lambda(\underline{q}) dq \right] = 0 \; ,$$

$$\text{i.e.} \quad \int_{\partial B} -\tfrac{1}{2}\lambda(\underset{\sim}{p})\,dp + \int_{\partial B}\int_{\partial B} G_i^{\,|}(\underset{\sim}{p},\underset{\sim}{q})\,\lambda(\underset{\sim}{q})\,dq\,dp = 0 \;,$$

$$\text{i.e.} \quad \int_{\partial B} -\tfrac{1}{2}\lambda(\underset{\sim}{p})\,dp + \int_{\partial B}\lambda(\underset{\sim}{q})\,dq \int_{\partial B} G_i^{\,|}(\underset{\sim}{p},\underset{\sim}{q})\,dp = 0 \;.$$

Our numerical approach should theoretically ensure that

$$\int_{\partial B} G_i^{\,|}(\underset{\sim}{p},\underset{\sim}{q})\,dp = \tfrac{1}{2} \;. \tag{77}$$

This result suggests that we should define b_{kk}, given by (69), so that

$$b_{kk} + \sum_{j=1}^{N}{}^{*} \int_{k} G_i^{\,|}(\underset{\sim}{q}_j,\underset{\sim}{q})\,dq = 0 \;;\quad k = 1,2,\cdots N \;,$$

$$\text{i.e. by (68)}\;, \quad b_{kk} + \sum_{j=1}^{N}{}^{*} b_{jk} = 0 \;;\quad k = 1,2,\cdots N \;, \tag{78}$$

where $\sum^{*}$ indicates omission of $j = k$ in the sequence $j = 1,2,\ldots N$. This means that the sum of each column of $[B]$ is zero, and hence evaluation of b_{kk} by (78) ensures that the matrix $[B]$ is singular.

The homogeneous part of (33), i.e.

$$-\tfrac{1}{2}\phi(\underset{\sim}{p}) + \int_{\partial B} \phi(\underset{\sim}{q})\,G(\underset{\sim}{p},\underset{\sim}{q})^{\,|}_{\,i}\,dq = 0 \;, \tag{79}$$

on discretisation gives (72) with $[D] = 0$, i.e.

$$[C][\phi] = 0 \;.$$

Since (79) has a non-trivial solution, shown in Chapter 2, the matrix $[C]$ must be singular. This property must be ensured by our numerical procedure. Adding all the elements in a k th row of $[C]$, we obtain, by 23,

$$\sum_{j=1}^{N} C_{kj} = -\frac{1}{2} + \sum_{j=1}^{N} \int_j G(\underset{\sim}{q}_k, \underset{\sim}{q})'_i \, dq$$

$$= -\frac{1}{2} + \int_{\partial B} G(\underset{\sim}{q}_k, \underset{\sim}{q})'_i \, dq = 0 \; ; \quad k = 1, 2, \cdots N \, .$$

Hence our numerical approach should ensure that

$$\int_{\partial B} G(\underset{\sim}{q}_k, \underset{\sim}{q})'_i \, dq = \frac{1}{2} \; ; \quad k = 1, 2, \cdots N \, . \tag{80}$$

This result suggests that we should define C_{kk}, given by (74), so that

$$C_{kk} + \int^{*} G(\underset{\sim}{q}_k, \underset{\sim}{q})'_i \, dq = 0 \tag{81}$$

where $\int^{*}$ indicates omission of the k th interval. Evaluation of C_{kk} by (81) ensures that the matrix $[C]$ is singular.

In the case of the exterior Neumann problem, the homogeneous equations (29) and (30), shown in Chapter 2, have no non-trivial solutions. Hence the matrix $[C]$ and $[B]$, obtained on discretisation of (29) and (30) respectively, are not generally singular. In such cases we assume

(3) THE SUB-AREAS ARE PIECEWISE FLAT .

On this basis, by Appendix II, we find

$$\int_k G'(\underset{\sim}{q}_k, \underset{\sim}{q}) \, dq = \int_k G(\underset{\sim}{q}_k, \underset{\sim}{q})' \, dq = 0 \quad . \tag{82}$$

CHAPTER 6

PRINCIPLES OF DIVISION OF A SURFACE INTO SUB-AREAS

Introduction

We now consider in detail the problem of dividing a surface into sub-areas. In the case of a flat surface, say the surface of a cube no difficulty arises. We simply divide each side into equal squares. On the other hand, in the case of a sphere, it is not immediately obvious how to proceed. The possible sub-division of a spherical surface is given in Figure 3. This suggests that the optimum sub-division will be a mixture of squares and triangles.

It is also necessary to consider that, generally, the charge density is not constant. It varies over an interval and therefore our fundamental assumption i.e. the charge density is constant over a sub-area, brings in some error. The question now arises how we can minimise this error by a suitable choice of sub-area.

Variation of density

To carry out our numerical analysis, we divide a curve, a surface or a volume into smaller intervals and we assume that the density σ over each interval is a continuous function which spreads uniformly in all directions from the centroid. Following Weierstrass's theorem[4], we know, any continuous function can be represented as accurately as we please, over a finite range of its arguments, by a polynomial of sufficiently high degree. Hence σ at a point (x, y, z) can be approximated by

$$\sigma = \sum_{n} F_n(x, y, z) \quad , \tag{83}$$

where F_n is a piecewise continuous symmetric polynomial function of degree n.

On rearrangement, F can be written as

$$F = \sum_{j} \sum_{k} A_{kj} P_{kj} \quad , \tag{84}$$

where P_{kj} is a homogeneous polynomial of degree j which remains invariant under any permutation of x, y and z.

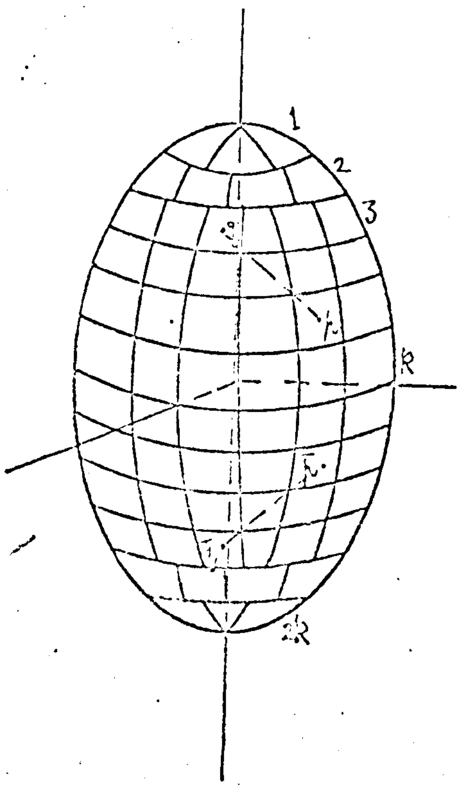

Fig. 3

SUB-AREAS ON THE SURFACE OF A SPHÈRE

To simplify our numerical calculations, we approximate the value of σ over an interval by taking only the first term in its Taylor expansion about the centroid of the interval. As a result, the approximate value of σ becomes a constant over an interval, which agrees with our fundamental assumption.

At any point $\underset{\sim}{q}\left(x_0+\delta x\,,\,y_0+\delta y\,,\,z_0+\delta z\right)$, we may write

$$\sigma(\underset{\sim}{q}) = \sum_n \left[F_n(x_0, y_0, z_0) + \delta x \frac{\partial F_n}{\partial x} + \delta y \frac{\partial F_n}{\partial y} + \delta z \frac{\partial F_n}{\partial z} + \cdots \right] , \tag{85}$$

where (x_o, y_o, z_o) are the co-ordinates of the centroid $\underset{\sim}{q}_o$ of the q th interval. According to our approximation,

$$\sigma(\underset{\sim}{q}) = \sum_n F_n(x_0, y_0, z_0) \quad . \tag{86}$$

Neglecting higher-order quantities, the significant part of the error in (86), as compared with (85), is given by

$$\epsilon = \sum_n \int_q \left(\frac{\partial F_n}{\partial x} \delta x + \frac{\partial F_n}{\partial y} \delta y + \frac{\partial F_n}{\partial z} \delta z \right) dq \;, \tag{87}$$

where the integral is taken over the q th interval and dq stands for the volume element dxdydz at (x, y, z). Transferring the origin of the reference frame to (x_o, y_o, z_o), we find, by Euler's theorem on homogeneous functions,

$$\epsilon = \sum_n \int_q \left(x \frac{\partial F_n}{\partial x} + y \frac{\partial F_n}{\partial y} + z \frac{\partial F_n}{\partial z} \right) dx\, dy\, dz \;,$$

$$= \sum_n n \int_q F_n(x, y, z)\, dx\, dy\, dz \quad . \tag{88}$$

Some special Intervals

Taking z = 0, a typical term of ϵ is given by

$$I = \int_{q} \left(x^m y^n + x^n y^m\right) dx\, dy \quad . \tag{89}$$

(i) For a circular area with radius 'a',

$$I_c = 4\iint \left(x^m y^n + x^n y^m\right) dx\, dy$$

$$= 4\int_{\theta=0}^{\frac{\pi}{2}} \int_{r=0}^{a} r^{m+n+1}\left(\cos^m\theta \sin^n\theta + \cos^n\theta \sin^m\theta\right) d\theta\, dr$$

$$= 8\,\frac{a^{m+n+2}}{m+n+2} \int_{\theta=0}^{\frac{\pi}{2}} \cos^m\theta \sin^n\theta\, d\theta \quad . \tag{90}$$

This can be computed for any choice of m and n:

(a) $n = 1,\ m \geqslant 0$ or $m = 1,\ n \geqslant 0$ gives

$$I_c = \frac{8a^{m+n+2}}{m+n+2} \cdot \frac{1}{(m+n)} \quad ;$$

(b) $n > 1,\ m = 0$ gives

$$I_c = \frac{8a^{m+n+2}}{m+n+2}\left[\frac{(n-1)(n-3)\cdots 3\cdot 1}{n(n-2)\cdots\cdots 4\cdot 2}\ \frac{\pi}{2}\right] \quad ; \text{ when n is an even integer,}$$

$$= \frac{8a^{m+n+2}}{m+n+2}\left[\frac{(n-1)(n-3)\cdots 4\cdot 2}{n(n-2)\cdots\ 5\cdot 3\cdot 1}\ 1\right] \quad ; \text{ when n is an odd integer.}$$

(c) $n > 1$, $m > 1$ gives

$$I_c = \frac{8a^{m+n+2}}{m+n+2}\left[\frac{1\cdot3\cdot5\cdots(n-1)\cdot1\cdot3\cdot5\cdots(m-1)}{2\cdot4\cdot6\cdots(m+n)}\cdot\frac{\pi}{2}\right] \quad ; \quad \text{when both m and n are even,}$$

$$= \frac{8a^{m+n+2}}{m+n+2}\left[\frac{2.4.6\cdots(m-1)}{(n+1)(n+2)\cdots(m+n)}\right] \quad ;$$

when any one of them, say m, is an odd integer ;

(ii) For a rectangular area with sides 2a and 2b,

$$I_R = 4\int_{x=0}^{a}\int_{y=0}^{b}\left(x^m y^n + x^n y^m\right)dx\,dy \quad ,$$

$$= 4\frac{1}{(m+1)(n+1)}\left[a^{m+1}b^{n+1} + a^{n+1}b^{m+1}\right] . \tag{91}$$

(iii) For an isoceles triangular area (Fig. 4)

$$I_T = \int_q \left(x^m y^n + x^n y^m\right)dq \quad ,$$

Putting $x = r\,\mathrm{Cos}\,\theta$,
$y = r\ \mathrm{Sin}\,\theta$
and $H = r\ \mathrm{Sec}\,\theta$

$$= 2\sum_{j=1}^{3}\int_{\theta=0}^{\theta_j}\left[\left(\cos^m\theta\,\sin^n\theta + \sin^m\theta\,\cos^n\theta\right)\int_{r=0}^{H_j\sec\theta} r^{m+n+1}\,dr\right]d\theta \quad ,$$

$$= 2\sum_{j=1}^{3}\frac{H_j^{m+n+2}}{m+n+2}\int_{\theta=0}^{\theta_j}\left(\tan^n\theta + \tan^m\theta\right)\sec^2\theta\,d\theta \quad ,$$

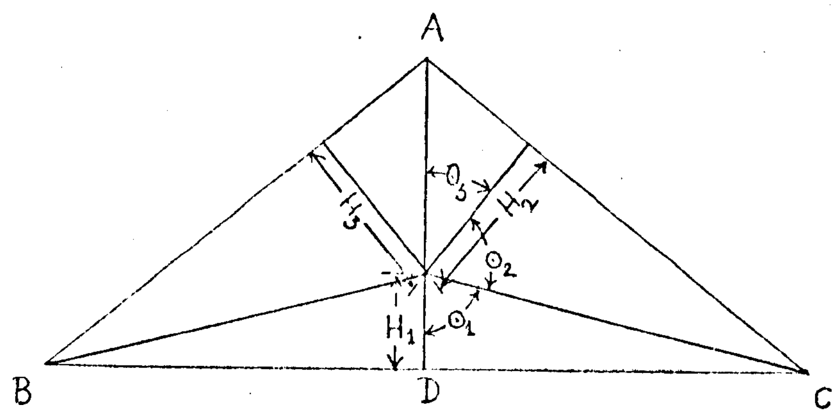

Fig. 4

$$= 2 \sum_{j=1}^{3} \frac{H_j^{m+n+2}}{m+n+2} \left(\frac{\operatorname{Tan}^{n+1} \Theta_j}{n+1} + \frac{\operatorname{Tan}^{m+1} \Theta_j}{m+1} \right) . \tag{92}$$

Optimum Choice of Interval

The integral I_R in (91) varies with a and b. For a given rectangular area, I_R has a minimum when a = b. Hence by (91)

$$I_R = I_{sq} = \frac{8}{(m+1)(n+1)} a^{m+n+2} \quad , \quad \text{when } a = b \quad . \tag{93}$$

Similarly, I_T in (92) attains a minimum when the triangular interval of a given area is an equilateral triangle. This is evident from Table 1 in which I_T (Θ) refers to the value of I_T for the isosceles triangle with base angles Θ . The triangular areas considered therein are each of unit area. From Table 1 it is clear that for all values of m and n, for a given area

$$I_T(15^\circ) > I_T(30^\circ) > I_T(45^\circ) > I_T(60^\circ) < I_T(75^\circ) . \tag{94}$$

Further for a given area

$$I_c < I_{sq} < T_T(60^\circ) . \tag{95}$$

This is evident from Table 2 in which the areas considered are each of unit area.

All the relations mentioned above are true for every term of (88) and therefore these are true for (88) itself.

ESTIMATION OF ERROR ON UNIT TRIANGULAR AREAS

m	n	m+n	$I_T(15^o)$	$I_T(30^o)$	$I_T(45^o)$	$I_T(60^o)$	$I_T(75^o)$
0	1	1	0·80765	0·64138	0·56929	0·54574	0·58422
1	1	2	0·25881	0·21605	0·17901	0·16667	0·17328
2	1	3	0·16290	0·10582	0·07344	0·06302	0·07260
3	1	4	0·16603	0·06883	0·03601	0·02673	0·03972
3	2	5	0·04918	0·02713	0·01453	0·01067	0·01361
4	2	6	0·05655	0·01993	0·00805	0·00499	0·00856

Table 1

ESTIMATION OF ERROR ON DIFFERENT FIGURES OF UNIT AREA

m	n	m+n	I_c	I_{sq}	$I_T(60^o)$
0	1	1	0·47890	0·50000	0·54574
1	1	2	0·10132	0·12500	0·16667
2	1	3	0·03049	0·04167	0·06302
3	1	4	0·01075	0·01563	0·02673
3	2	5	0·00408	0·00521	0·01067
4	2	6	0·00101	0·00208	0·00499

Table 2

General Rules for Sub-division

In numerical analysis, the entire curve or surface or volume under consideration should be covered by intervals keeping no gap between them. The spherical intervals can not be fitted together to cover a volume in the above fashion. The next most suitable intervals are the regular polygons, of which the simplest interval is a cube. Similarly, in the case of a surface, the most suitable interval i.e. sub-area is a square or an equilateral triangle.

Bearing these considerations in mind, we lay down the following general procedures:

1. It is recommended to cover a curve, a surface or a volume by the same type of intervals as far as possible.
2. In case of a surface it needs, in general, a mixture of triangular and rectangular sub-areas to fit together. The triangular sub-areas should be as far as near to equilateral form. The rectangular sub-areas should be kept near to the square form.
3. It is found, in general, that σ changes rapidly as we approach a sharp edge or a corner on a surface. In fact it can not properly be represented by (83) near a sharp edge or a corner. Hence in general, one should not expect to obtain an accurate measure of σ at these points by our numerical methods. To achieve a tolerable approximation to σ near such a point:
   (a) The sub-areas should become smaller in size as we approach such a point.
   (b) The reduction in size of the sub-area should be gradual.

CHAPTER 7

APPROXIMATE INTEGRATION

Introduction

To evaluate analytically an integral of the form

$$I = \int_{\partial B} F(\underset{\sim}{p},\underset{\sim}{q})\, d\underset{\sim}{q} \tag{96}$$

the first requirement, in general, is that the integrand should have an analytic expression in terms of the co-ordinates of $\underset{\sim}{q}$. Further, the boundary surface ∂B should also have an analytic expression. For bodies with definite regular geometrical shapes, there are analytic expressions for ∂B, but sometimes it happens that even for these the evaluation of (96) becomes very complicated. For a body with an irregular boundary different parts of it may require different analytic expressions, in which case the evaluation of (96) becomes extremely complicated. Often in practice, only the numerical values of the integrand are available at the pivotal points of ∂B. Accordingly this is not generally possible to evaluate (96) analytically.

In view of the above difficulties, we must think of an operation to approximate (96) over any surface ∂B over which $F(\underset{\sim}{p},\underset{\sim}{q})$ is defined. It is desirable that the operation should be simple on the one hand and, on the other hand, it should be capable of approximating (96) within a tolerable error.

When $F(\underset{\sim}{p},\underset{\sim}{q})$ is a function of a single variable, as happens with the plane curves, the Simpson and the Trapezoidal rules of approximate integration produce results to a sufficient degree of accuracy. Unfortunately, there are, in general, no such analogous rules to effect an approximate integration when the integrand is a function of two or more independent variables.

Approximation Methods

When $F(\underset{\sim}{p},\underset{\sim}{q})$ is a function of two or more variables, we propose two methods to approximate the integral over ∂B:

(i) The AVERAGING method of approximation.

(ii) The CENTROID method of approximation.

In both these methods, we divide ∂B into N intervals i.e. sub-areas, operate on each of the sub-areas separately, and then add them up to approximate the integral over ∂B.

(i) AVERAGING METHOD

If the k th interval, i.e. sub-area, is an m sided polygon, the averaging approximation to (96) over this area is defined by

$$I_A = \sum_{k=1}^{N} \frac{\sum_{j=1}^{m+1} F(\underset{\sim}{p}, \underset{\sim}{q}_{j-1})}{m+1} \int_k dq \quad ; \quad \underset{\sim}{p} \notin \partial B , \tag{97}$$

where $\underset{\sim}{q}_1, \underset{\sim}{q}_2, \ldots\ldots \underset{\sim}{q}_m$ define the m corner points of the polygon and $\underset{\sim}{q}_o$ defines the pivotal point (centroid) of the polygon.

(ii) CENTROID METHOD

If I_c represents the approximation to (96) by the centroid method of approximation, then I_c is defined by

$$I_c = \sum_{k=1}^{N} F(\underset{\sim}{p}, \underset{\sim}{q}_o) \int_k dq \quad ; \quad \underset{\sim}{p} \notin \partial B , \tag{98}$$

where, as before, $\underset{\sim}{q}_o$ defines the centroid of the k th sub-area.

The centroid method of approximation is nothing but the application of assumption 2 in the evaluation of (96). The averaging method may well be looked upon as an extension of the above principle.

If the integrand has a factor $|\underset{\sim}{p} - \underset{\sim}{q}|$ then, depending upon the position of $\underset{\sim}{p}$ two distinct cases arise:

(i) If $\underset{\sim}{p} \neq \underset{\sim}{q}$, the integrand is finite and evaluation of (97) as well as of (98) is straight-forward.

(ii) If $\underset{\sim}{p} = \underset{\sim}{q}$, the integrand is singular and, the integral must be evaluated analytically.

A Comparative Study of the TWO Methods

To make a comparative study of the merits of the two approximations, we consider the analytic value of the integral (96) for a particular F. In this thesis, we deal mainly with integrals of the type

$$I = \int_{\partial B} \frac{dq}{|\underset{\sim}{p} - \underset{\sim}{q}|} \quad , \quad J = \int_{\partial B} \frac{dq}{|\underset{\sim}{p} - \underset{\sim}{q}|'} \; .$$

Let us therefore take

$$I = \int_{\partial B} \frac{dq}{|p - q|} \tag{99}$$

as a test case for a comparative study of the two approximations.

Using a cartesian frame of reference, let ∂B be a rectangular area defined by $z = 0$, $x = \pm a$, $y = \pm b$. Since $q \in \partial B$, we may write $q = (x, y, 0)$ and a field point may be represented by $p = (X,Y,Z)$. By appendix I,

$$I = \int_{\partial B} \frac{dq}{|p - q|}$$

$$= \int_{y=-b}^{b} \int_{x=-a}^{a} \frac{dx\ dy}{\sqrt{(X-x)^2 + (Y-y)^2 + Z^2}} \quad , \tag{100}$$

$$= \left[\log\left\{ \left(\frac{C+\sqrt{k^2+D^2}}{E+\sqrt{k^2+F^2}}\right)^{k} \frac{\left(k+\sqrt{k^2+D^2}\right)^{C}}{\left(k+\sqrt{k^2+F^2}\right)^{E}} \right\} + Z\left\{ \sin^{-1}\left(\frac{F^2+E\sqrt{k^2+F^2}}{F\left(E+\sqrt{k^2+F^2}\right)}\right) - \sin^{-1}\left(\frac{D^2+C\sqrt{k^2+D^2}}{D\left(C+\sqrt{k^2+D^2}\right)}\right) \right\} \right]_{k=Y-b}^{k=Y+b} ,$$

where $C = X+a$, $D^2 = C^2 + Z^2$, $E = X-a$, $F^2 = E^2 + Z^2$ and $k = Y - y$.

Choosing $a = b = 1$ to ease the numerical work and treating ∂B as a single sub-area and not sub-dividing it any further, we compute I_A, I_c for (100) for various locations of p as indicated in Table 3.

From Table 3 we find that, for all locations of the field point,

$$|I - I_c| < |I - I_A| \quad . \tag{101}$$

APPROXIMATIONS TO AN INTEGRAL

CO-ORDINATES OF p x y z	DISTANCE FROM CENTRE	I	I_c	I_A	% ERROR IN I_C
0·750, 0, 0	0·750	1·41929	1·33333	1·76736	6·06
1·750, 0, 0	1·750	0·57898	0·57143	0·41027	1·30
2·750, 0, 0	2·750	0·36562	0·36364	0·18502	0·54
3·750, 0, 0	3·750	0·26745	0·26667	0·11217	0·29
0·750, 0·750, 0	1·061	0·99118	0·94281	2·09872	4·88
1·750, 1·750, 0	2·475	0·40697	0·40406	0·22494	0·72
2·750, 2·750, 0	3·889	0·25786	0·25713	0·10625	0·28
3·750, 3·750, 0	5·303	0·18885	0·18856	0·06669	0·15
0 , 0, 0·500	0·500	1·58672	2·00000	1·46667	26·00
0 , 0, 1·750	1·750	0·55671	0·57143	0·33885	2·64
0 , 0, 2·750	2·750	0·35972	0·36364	0·17195	1·09
0 , 0, 4·500	4·500	0·22132	0·22222	0·08300	0·41

Table 3

This means that the centroid method produces a better approximation than that of the averaging method. When we divide ∂B into N sub-areas to evaluate I_A and I_c by a more general application of (97) and (98), relation (101) remains valid for each of the N sub-areas. Hence (101) remains valid when these are added over the whole of ∂B, It may be mentioned that the centroid method not only yields a better approximation than the averaging method but is also simpler to compute.

Error in the Centroid Method

If ∂B forms a single sub-area, and $p \notin \partial B$, we see from Table 3 and Fig. 5 that:

(i) The error in I_c diminishes asymptotically to zero as $\underset{\sim}{p}$ tends to infinity.

(ii) For a given distance from the centroid of ∂B, the error is a maximum when $\underset{\sim}{p}$ lies on the normal to ∂B through its centroid. Further, it is evident that, for all locations of $\underset{\sim}{p}$,

$$\epsilon_{max} \leqslant 1\% \qquad \text{when} \qquad \left|\underset{\sim}{p} - \underset{\sim}{q}_o\right| \geqslant 2\, D_{max} \;, \tag{102}$$

where ϵ_{max} represents the maximum of the errors in I_c for various positions of $\underset{\sim}{p}$ and D_{max} represents the greatest diagonal of the largest interval i.e. sub-area.

Now let us divide ∂B into N sub-areas and examine the behaviour of the error in I_c as N gradually increases. We define I_c at a point $\underset{\sim}{p}$ $(\underset{\sim}{p} \notin \partial B)$ by

$$I_{cp} = \sum_{j=1}^{N} I_{cj} \;, \tag{103}$$

where I_{cj} represents the value of I_c over the j th sub-area. The field point $\underset{\sim}{p}$ lies outside ∂B at a perpendicular distance d from the boundary point $\underset{\sim}{p}_B$ [Fig. 6 (a)], such that

$$d = \left| \underset{\sim}{p}_B - \underset{\sim}{p} \right| = \frac{L_{min}}{2} \;, \tag{104}$$

where L_{min} is the minimum distance between the two nodal points of the N sub-areas. Hence, as N increases, $\underset{\sim}{p} \rightarrow \underset{\sim}{p}_B$. Taking ∂B to be a unit area

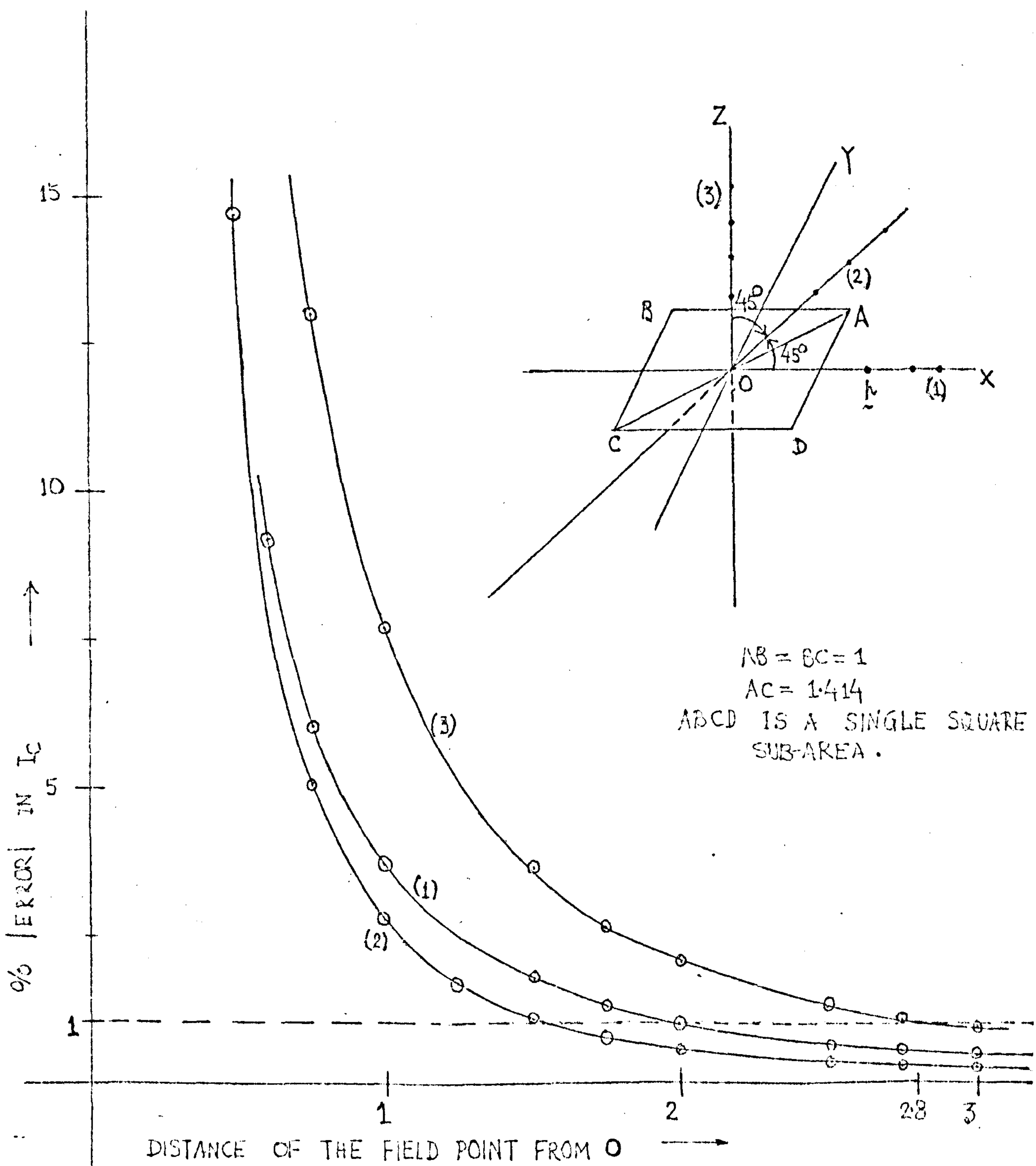

Fig. 5

ESTIMATION OF ERROR IN THE APPROXIMATION TO $\int \frac{1}{|r-y|}\, d_y$ OVER A SINGLE SUB-AREA.

and dividing it into N sub-areas, I_{cp} and I are evaluated for different values of N. For each choice of N, the field point $\underset{\sim}{p}$ always satisfied the relation (104). The values of I_{cp} and I for different values of N and for different positions of $\underset{\sim}{p}$ are given in Table 4.

This Table shows clearly that, as N increases, though the field point $\underset{\sim}{p}$ approaches the boundary of ∂B, the percentage error in I_{cp} gradually decreases. The same conclusion holds good when ∂B is a triangular surface [Fig. 6 (b)] of unit area with N triangular sub-areas.

If ∂B is divided into N sub-areas, and $\underset{\sim}{p} \in \partial B$, $\underset{\sim}{p}$ will either be an interior point of a sub-area or it will be a boundary point of two or more sub-areas. In such a case, as stated earlier, we must evaluate the integral analytically over the sub-area for which $\underset{\sim}{p}$ is an interior or a boundary point. Evaluating the integral over the rest of the sub-areas by (103), we find

$$I_{cp} = \sum_j I_{cj} + \sum_k I_k \quad , \tag{105}$$

where I_{cj} refers to the sub-area not containing $\underset{\sim}{p}$ and I_k refers to the sub-area for which $\underset{\sim}{p}$ is an interior or a boundary point.

If $\underset{\sim}{p}$ satisfies (104), from Fig. 6(1) and Fig. 6(5) it follows that

$$\epsilon_{IN} \leqslant \epsilon_{OUT} \tag{106}$$

for the same sub-division of ∂B and for all values of N, where ϵ_{IN}, ϵ_{OUT} respectively stand for the % errors in I_{cp} when $\underset{\sim}{p} \in \partial B$ and $p \notin \partial B$. Accordingly, when dealing with boundary value problems, the above approximations produce a better result when the field point $\underset{\sim}{p}$ is on the boundary itself than when it is outside the boundary and obeys relation (104).

Application of the Approximation to Some Test Cases

We know, by the Gauss flux theorem (23) of Chapter 2, that

$$J = \int_{\partial B} \frac{dq}{|\underset{\sim}{p}-\underset{\sim}{q}|'_{int.}} = 2\pi \quad ; \quad \underset{\sim}{p} \in \partial B \ , \tag{107}$$

ERROR IN APPROXIMATION DEPENDING UPON THE POSITION OF THE FIELD POINT

CO-ORDINATES OF p (x, y, z)	TOTAL SUB-AREAS N	$d=\lvert \underset{\sim}{p}-\underset{\sim}{p}_B \rvert$	I	I_C	% ERROR IN I_C
0·6250, 0·1250, 0	16	0·1250	1·23059	1·22175	0·718
0·5625, 0·0625, 0	64	0·0625	1·41726	1·41122	0·359
0·5417, 0·0417, 0	144	0·0417	1·50030	1·49673	0·238
0·5250, 0·0250, 0	400	0·0250	1·58055	1·57832	0·141
0·5179, 0·0179, 0	784	0·0179	1·62084	1·61922	0·099

Table 4

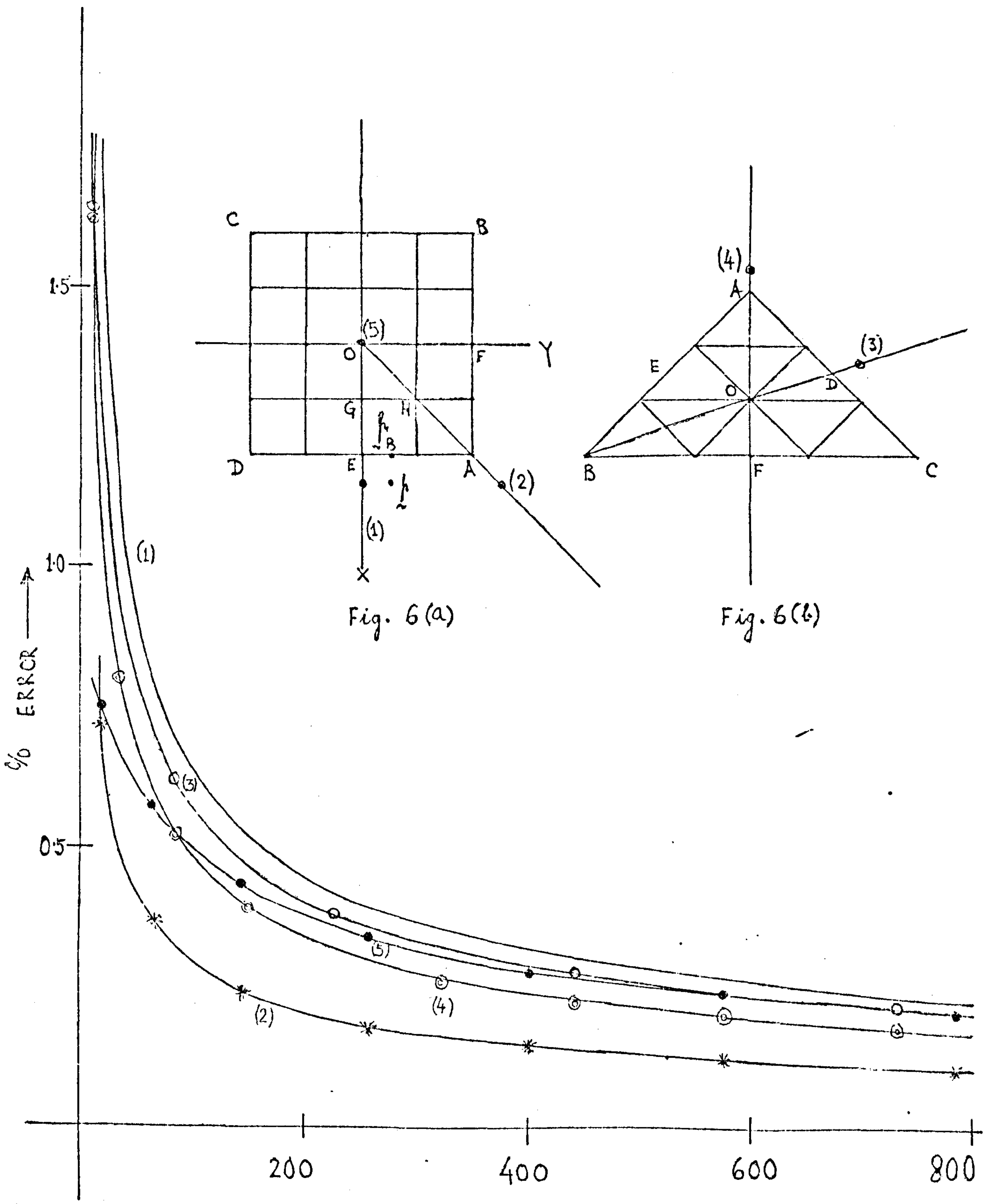

ERROR IN THE APPROXIMATION AS THE NUMBER OF SUB-AREAS INCREASES

Fig. 6

where $|\underset{\sim}{p} - \underset{\sim}{q}|'_{int.}$ represents the interior derivative of $|\underset{\sim}{p} - \underset{\sim}{q}|$ at the point $\underset{\sim}{q}$ keeping $\underset{\sim}{p}$ fixed. On discretisation, (107) can be represented as

$$J_k = \sum_{j=1}^{N} \int_j \frac{dq}{|\underset{\sim}{q}_k - \underset{\sim}{q}|'_{int.}} , \tag{108}$$

where $\underset{\sim}{q}_k = \underset{\sim}{p}$. When j successively assume values 1, 2, ... K, ... N there arise two distinct cases:

(i) when $j \neq k$, by assumption 2

$$\int_j \frac{dq}{|\underset{\sim}{q}_k - \underset{\sim}{q}|'_{int.}} = \frac{(\underset{\sim}{q}_k - \underset{\sim}{q}_j) \cdot \hat{n}_{ext.}(\underset{\sim}{q}_j)}{|\underset{\sim}{q}_k - \underset{\sim}{q}_j|^3} \int_j dq , \tag{109}$$

where $\hat{n}_{ext.}(\underset{\sim}{q}_j)$ represents the exterior unit normal at the pivotal point $\underset{\sim}{q}_j$.

(ii) when $j = k$, the integrand is singular. But by assumption 3 and Appendix II, we may approximate this to zero i.e.

$$\int_k \frac{dq}{|\underset{\sim}{q}_k - \underset{\sim}{q}|'_{int.}} = 0 .$$

By (109) ,

$$J_k = \sum_j^{*} \frac{(\underset{\sim}{q}_k - \underset{\sim}{q}_j) \cdot \hat{n}_{ext.}(\underset{\sim}{q}_j)}{|\underset{\sim}{q}_k - \underset{\sim}{q}_j|^3} \int_j dq + \int_k \frac{dq}{|\underset{\sim}{q}_k - \underset{\sim}{q}|'_{int.}} , \tag{110}$$

where J_k represents the approximated value of J at the point $\underset{\sim}{q}_k \in \partial B$ and $\sum^{*}$ represents the summation over all the sub-areas except the k th sub-area.

Let ∂B be a surface of a unit cube whose 6 sides are given by

$$x = \pm\tfrac{1}{2} \quad , \quad y = \pm\tfrac{1}{2} \quad \text{and} \quad z = \pm\tfrac{1}{2} \quad .$$

Dividing ∂B into N square sub-areas (Fig. 7), the value of J_k is computed by (110). This value, as expected, is most inaccurate when k defines a sub-area nearest to a corner. The value of J_k at the points $\underset{\sim}{q}_k$ are computed and exhibited in Table 5 for comparison with the analytic value $2\pi \simeq 6{\cdot}28318$.

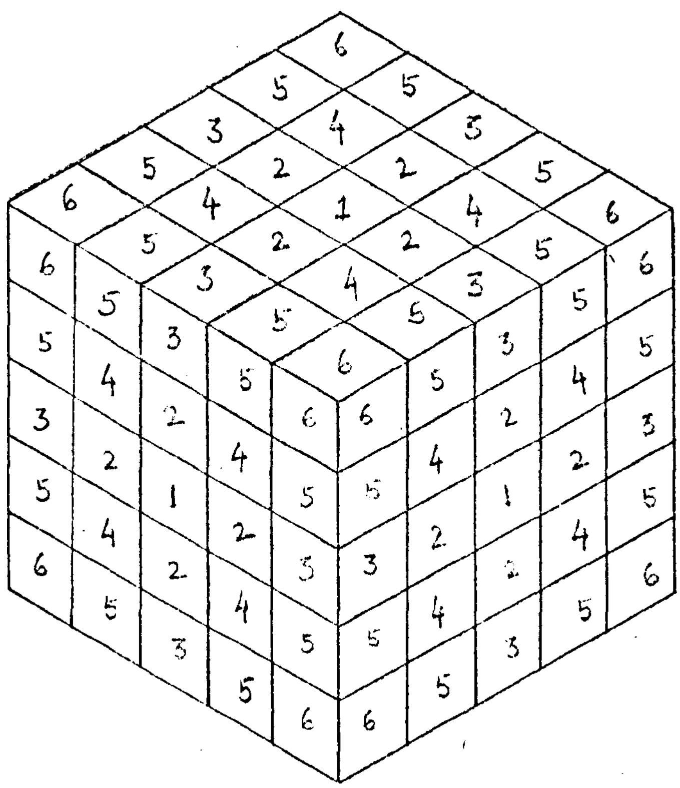

Fig. 7

SUB-AREAS ON THE SURFACE OF A CUBE

TESTING OF THE APPROXIMATION ON THE SURFACE OF A UNIT CUBE

CO-ORDINATES OF q_k (x, y, z)	TOTAL SUB-AREAS N	J_k	% ERROR
0·000, 0·000, 0·500	216	6·30768	0·389
0·000, 0·000, 0·500	1944	6·28591	0·043
0·000, 0·000, 0·500	5400	6·28417	0·017
0·417, 0·417, 0·500	216	6·19087	1·469
0·472, 0·472, 0·500	1944	6·18639	1·540
0·483, 0·483, 0·500	5400	6·18614	1·544

Table 5

Let ∂B be the spherical surface

$$x^2+y^2+z^2 = 1 \quad .$$

It is divided into N sub-areas as in Fig. 3. The sub-areas adjacent to the poles are approximately triangular in form and the rest all are approximately trapezoidal in form. The value of J_k at the point $\underset{\sim}{q}_k$ is then computed by application of (110) for different values of N and for different positions of the field point, as exhibited in Table 6.

For a given value of N the error is a maximum when the field point is nearest to the pole, which is expected because of the size and the form of the sub-areas at that region.

TESTING OF THE APPROXIMATION ON THE SURFACE OF A UNIT SPHERE

CO-ORDINATES OF q_k x y z	TOTAL SUB-AREAS N	J_k	% ERROR
0·9997, 0, 0·0228	2544	6·16661	1·855
0·9998, 0, 0·0175	9264	6·20372	1·265
0·9999, 0, 0·0135	20184	6·22496	0·927
0·9999, 0, 0·0110	35304	6·23724	0·731
0·0906, 0, 0·9959	2544	6·08119	3·215
0·0453, 0, 0·9989	9264	6·18188	1·612
0·0302, 0, 0·9995	20184	6·21561	1·075
0·0227, 0, 0·9997	35304	6·23325	0·807

Table 6

PART III
CAPACITY OF CONDUCTORS

CHAPTER 8

ELECTROSTATIC CAPACITY

Recapitulation of Equations

We now regard ∂B as a closed perfectly conducting surface brought to a unit potential by the introduction of charges. If $\lambda(\underset{\sim}{q})$ is the equilibrium charge density at $\underset{\sim}{q}$, this distribution generates the potential

$$V(\underset{\sim}{p}) = \int_{\partial B} \frac{\lambda(\underset{\sim}{q})\,dq}{|\underset{\sim}{p}-\underset{\sim}{q}|}$$

at $\underset{\sim}{p}$, which exists and is continuous everywhere including ∂B. Hence λ must satisfy the integral equation

$$\int_{\partial B} \frac{\lambda(\underset{\sim}{q})\,dq}{|\underset{\sim}{p}-\underset{\sim}{q}|} = 1 \quad ; \quad \underset{\sim}{p} \in \partial B \,, \tag{111}$$

of which a unique solution has been proved to exist. It has also been proved, in Chapter 4, that λ has the same sign (>0) everywhere on ∂B. This enables us to define the essentially positive quantity

$$K = \int_{\partial B} \lambda(\underset{\sim}{q})\,dq \,,$$

which is known as the capacity of ∂B.

On discretisation, (111) gives N linear algebraic equations for λ viz.

$$\sum_{j=1}^{N} a_{kj}\,\lambda_j = 1 \quad ; \quad k = 1, 2 \cdots N \,, \tag{112}$$

where

$$a_{kj} = \int_j \frac{dq}{|\underset{\sim}{q}_k - \underset{\sim}{q}|} \,, \tag{113}$$

and
$$k = \sum_{j=1}^{N} \lambda_j \, ds_j \tag{114}$$

where ds_j represents the area of the j th sub-area.

Solution of Equations

After evaluation of the a_{kj} by the procedures discussed in Chapter 5, equations (112) are solved by the Gauss-Seidel interative[5] method. In this method, after each iteration, we obtain a set of values of $\lambda_1, \lambda_2 \ldots \lambda_N$ at the N pivotal points $\underset{\sim}{q}_1, \underset{\sim}{q}_2, \ldots \underset{\sim}{q}_N$ on ∂B. After the r th iteration these values are denoted $\lambda_1^r, \lambda_2^r \ldots \lambda_N^r$, and so at the pivotal point $\underset{\sim}{q}_k$ we have, after n iterations, a sequence of n values

$$\left\{ \lambda_k^r \right\} ; \qquad r = 1, 2 \cdots n, \tag{115}$$

which are successive approximations to the exact value $\lambda(q_k)$.

If for a pre-assigned small positive quantity ϵ (ϵ = 00·0001 say), there exists a number M such that

$$\left| \lambda_k^r - \lambda_k^{r-1} \right| \leq \epsilon \ , \text{ for } \ r = M, \tag{116}$$

at every pivotal point $\underset{\sim}{q}_1, \underset{\sim}{q}_2 \ldots \underset{\sim}{q}_N$, then at this the approximate solutions are given by

$$\lambda_k^M \ ; \ k = 1, 2, \cdots N \ . \tag{117}$$

Determination of The Optimum Value of N

Our preceding analysis has dealt with a fixed number N of nodal points. From the fundamental assumption that the source density is constant over a sub-area, it appears that the computed source density at a nodal point approaches its analytic value at that point as $N \to \infty$. But because of the rounding-off errors involved in the computations, after a certain stage, the result becomes distorted as N increases. Hence the problem arises of finding the optimum value of N. To find this we start with a small value of N and gradually increase it until a stage comes when either

(i) p ceases to behave monotonically,

or (ii) the density distribution along a line on ∂B changes sign.

At this stage, the optimum value of N is given by the value of N considered in the previous stage.

Intrinsic Test of Accuracy

The solution of (112) yields the numerically generated potential

$$V(\underset{\sim}{p}) = \sum_{j=1}^{N} \lambda_j \int_j \frac{dq}{|\underset{\sim}{p}-\underset{\sim}{q}|} \tag{118}$$

at any point $\underset{\sim}{p} \in B + \partial B$. This automatically has the value $V = 1$ at the nodal points on ∂B, but will generally deviate from 1 at any other point. For a particular sub-area,

$$\left|1 - V(\underset{\sim}{p})\right| \begin{array}{ll} = 0 & \text{when } \underset{\sim}{p} \text{ is a nodal point on } \partial B, \\ > 0 & \text{when } \underset{\sim}{p} \text{ is not a nodal point on } \partial B. \end{array}$$

Since $1 - V(\underset{\sim}{p})$ is a harmonic function in B, its modulus $\left|1 - V(\underset{\sim}{p})\right|$ attains a maximum[1] for some point $\underset{\sim}{p}$ on ∂B. We may therefore approximately determine $\left|1 - V(\underset{\sim}{p})\right|_{max}$ by generating $V(\underset{\sim}{p})$ at a number of representative non-pivotal points on ∂B.

CHAPTER 9

CAPACITY OF THIN CONDUCTORS

Square Plate

Let the periphery of a thin square conductor ABCD (Fig. 8) of unit area in the plane z = 0 be given by

$$x = \pm \tfrac{1}{2} \quad \text{and} \quad y = \pm \tfrac{1}{2} \ .$$

It is divided into N equal square sub-areas of area ds each, where

$$N = k^2 \ ; \quad k = 2m+1 \ ; \quad m = 1, 2, \cdots n \ ,$$

and $$ds = N^{-1} \ . \tag{119}$$

Of these N sub-areas, there is a sub-area with its nodal point at the centroid of the plate, which concides with the origin of the reference frame OXYZ. Further, there are 4 rows of sub-areas with nodal points on the lines x = 0, y = 0, x = y and x = -y respectively. This pattern of sub-division helps us to obtain the density and the potential distribution along these lines directly from (112) and (118) respectively.

According to (112), there are N linear algebraic equations for λ. By symmetry, the number of equations reduces to

$$\begin{aligned} N^* &= 1 + 2 + \cdots + (k+1)/2 \\ &= \frac{k+1}{2}\left(\frac{k+1}{2} + 1\right)\Big/ 2 \\ &= (k+1)(k+3)/8 \ . \end{aligned} \tag{120}$$

In this particular case, the sub-areas are all squares. The elements a_{kj} of (112) are evaluated as in Chapter 5. The diagonal element a_{kk}, by Appendix I, is

$$a_{kk} = 4h \log (1 + \sqrt{2}),$$

where h denotes the edge length of the square sub-area.

Starting with a small value of N, equations (112) are constructed and solved for λ by the Gauss-Seidel iterative method with $\epsilon = 0{\cdot}0001$, with the help of the I.C.L. 1905 computer at the City University.

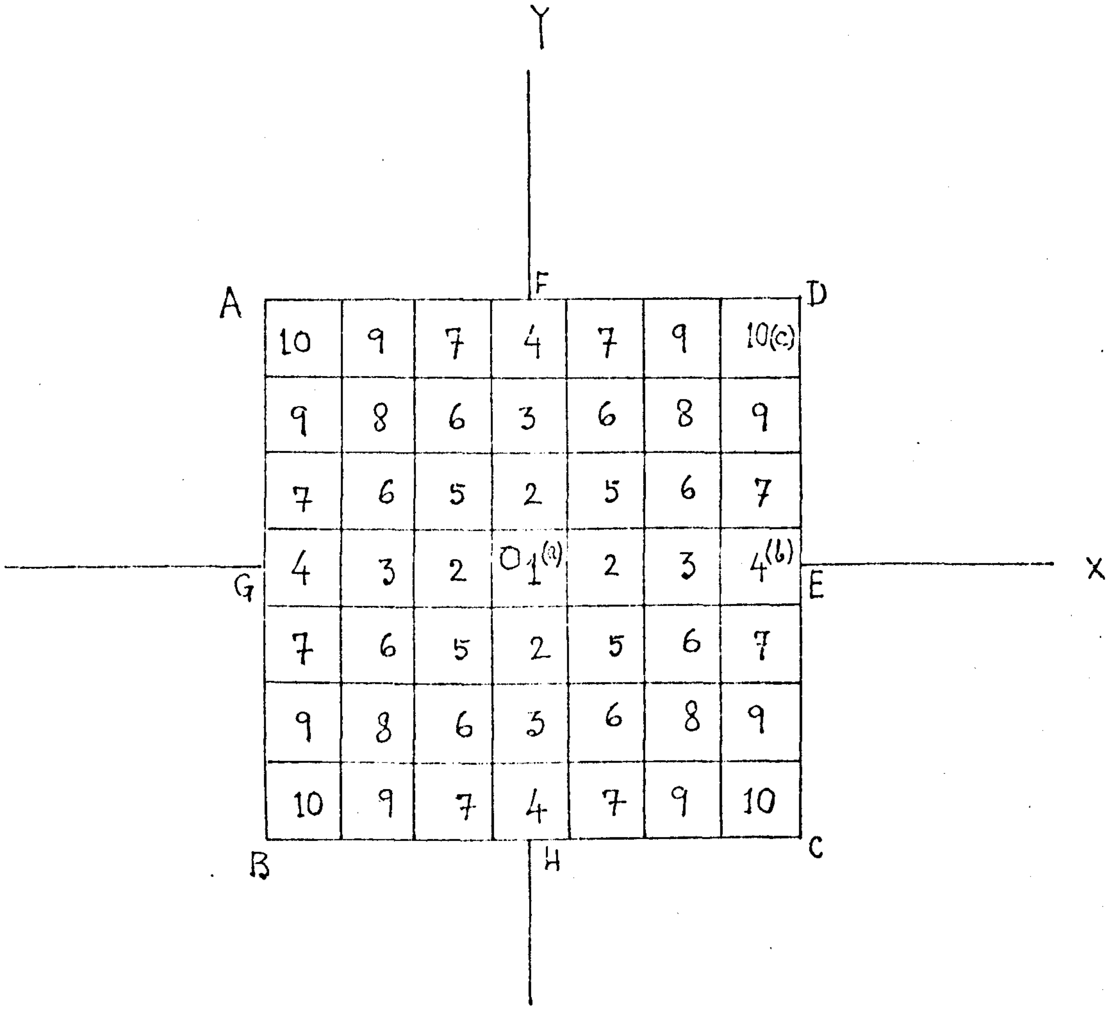

FIG. 8

SUB-AREAS ON A SQUARE PLATE.

From the λ so computed, we calculate the capacity K from (114) using (119).

The values of the electrostatic capacity of a thin square conductor of unit area for increasing values of N are given in Table 7. It is evident from this Table that, when N = 361, the density distribution at some points becomes negative. This marks the optimum stage in the numerical procedures. At this stage $K = 0{\cdot}36188$ and it is attained for N = 289 as discussed in Chapter 8.

If 'a' represents the edge length of the thin square plate, then according to Polya and Szego,[6] the capacity lies between the bounds

$$0{\cdot}35917\, a < K < 0{\cdot}37570\, a \quad . \tag{121}$$

It will be seen that our computed value lies well within the bounds given in (121).

The figures 8(a) and 8(b) show the density distribution along the lines x = 0 and x = y respectively. This is a minimum at the centre and it increases gradually as we go towards the rim in any direction. This behaviour compares with the known density behaviour for the circular plate as we move from the centre towards its rim (Chapter 10).

To examine the accuracy attained in generating V on ∂B, V has been calculated by (118) for N = 289, taking $\underset{\sim}{p}$ as the corner points of the sub-areas. The λ used in (118) were obtained from (112) for the same value of N i.e. N = 289. Table 7(a) shows the generated values of V at the corner points of the sub-areas along the diagonal of the square.

It is evident from Table 7(a) and from figure 8(c) that $|V - 1|$ is minimum near the centre of the plate and gradually increases as we move towards the rim. It is maximum, as expected, at a corner of the plate.

<u>Rectangular Plate</u>

Let the unit rectangular plate ABCD (Fig. 9) be in the plane $z = 0$. The boundaries of ABCD are given by $x = \pm 2a$, $y = \pm a$. The breadth AB is divided into k parts by (k -1) lines drawn parallel to BC and the length BC is divided into 2 k parts by drawing (2 k - 1) lines parallel to AB. Hence the rectangular area ABCD is divided into

$$N = 2k^2 \tag{122}$$

equal square sub-areas.

ELECTROSTATIC CAPACITY OF A THIN SQUARE CONDUCTOR

SUB-AREA N	EQUATION N*	DENSITY AT THE CENTRE OF SUB-AREAS (a)	(b)	(c)	CAPACITY
25	6	0·18792	0·37434	0·56870	0·34845
49	10	0·18515	0·43358	0·71120	0·35390
81	15	0·18369	0·48609	0·84261	0·35690
121	21	0·18269	0·53336	0·96626	0·35886
169	28	0·18198	0·57679	1·08360	0·36018
225	36	0·18144	0·61724	1·19580	0·36115
289	45	0·18093	0·65537	1·30370	0·36188
361	55	Ill condition arises in the values of σ. Some of them become negative.			

Table 7

(This should be read in conjuction with Fig. 8)

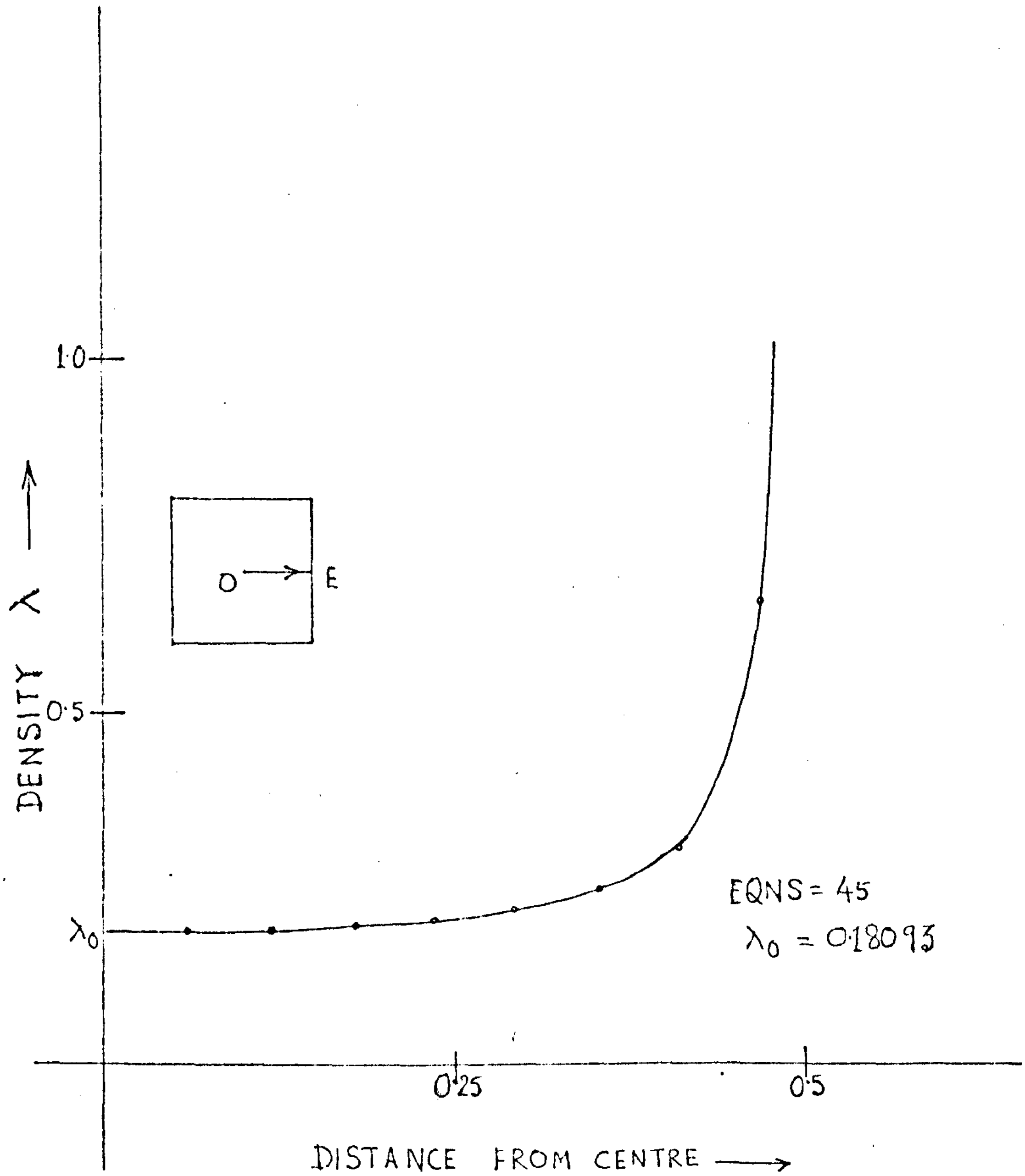

FIG. 8(a)

DENSITY DISTRIBUTION ALONG A CENTRAL LINE OE

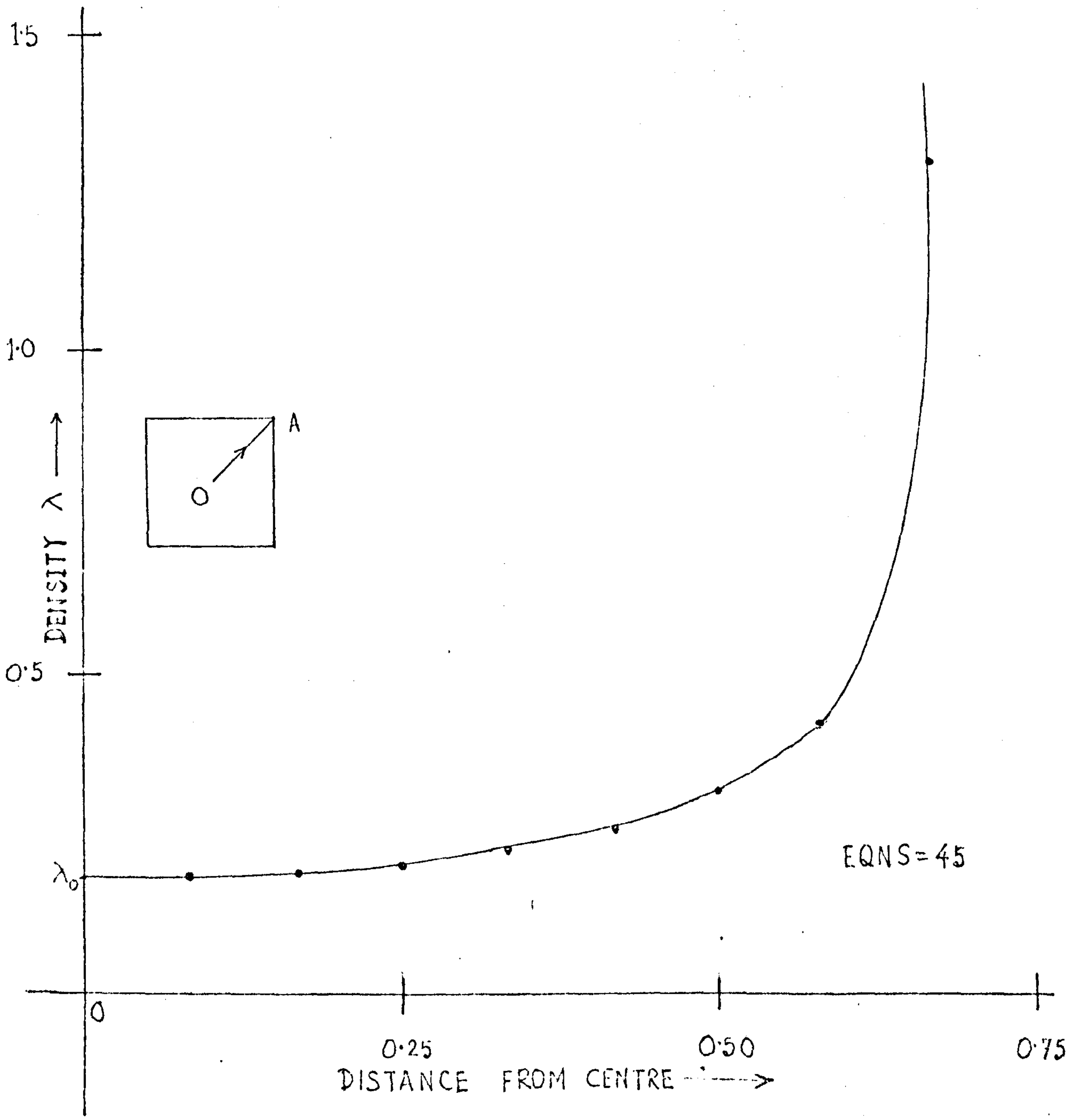

FIG. 8 (b)

DENSITY DISTRIBUTION ALONG A DIAGONAL OA

POTENTIALS GENERATED AT THE CORNER POINTS OF THE SUB-AREAS LYING ALONG A DIAGONAL OF THE THIN SQUARE PLATE

CO-ORD. OF THE CORNER POINTS X	Y	V	$\lvert V-1 \rvert$
0·02941	0·02941	1·00170	0·00170
0·08823	0·08823	1·00180	0·00180
0·14706	0·14706	1·00180	0·00180
0·20588	0·20588	1·00200	0·00200
0·26471	0·26471	1·00240	0·00240
0·32353	0·32353	1·00310	0·00310
0·38235	0·38235	1·00420	0·00420
0·44118	0·044118	1·03450	0·03450
0·50000	0·500000	0·76845	0·23155

Table 7(a)

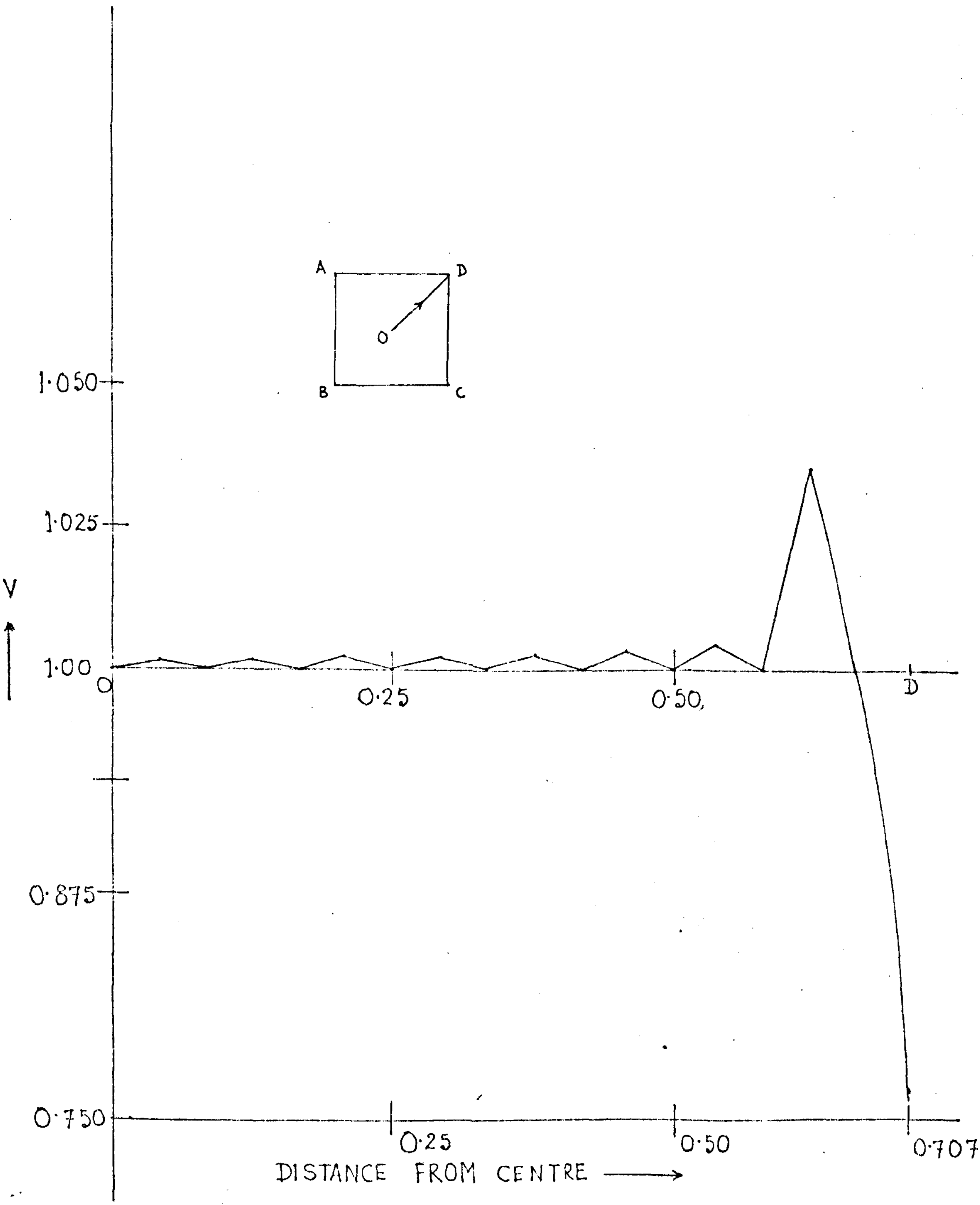

FIG. 8 (C)

VARIATION OF COMPUTED POTENTIAL ALONG A DIAGONAL OD.

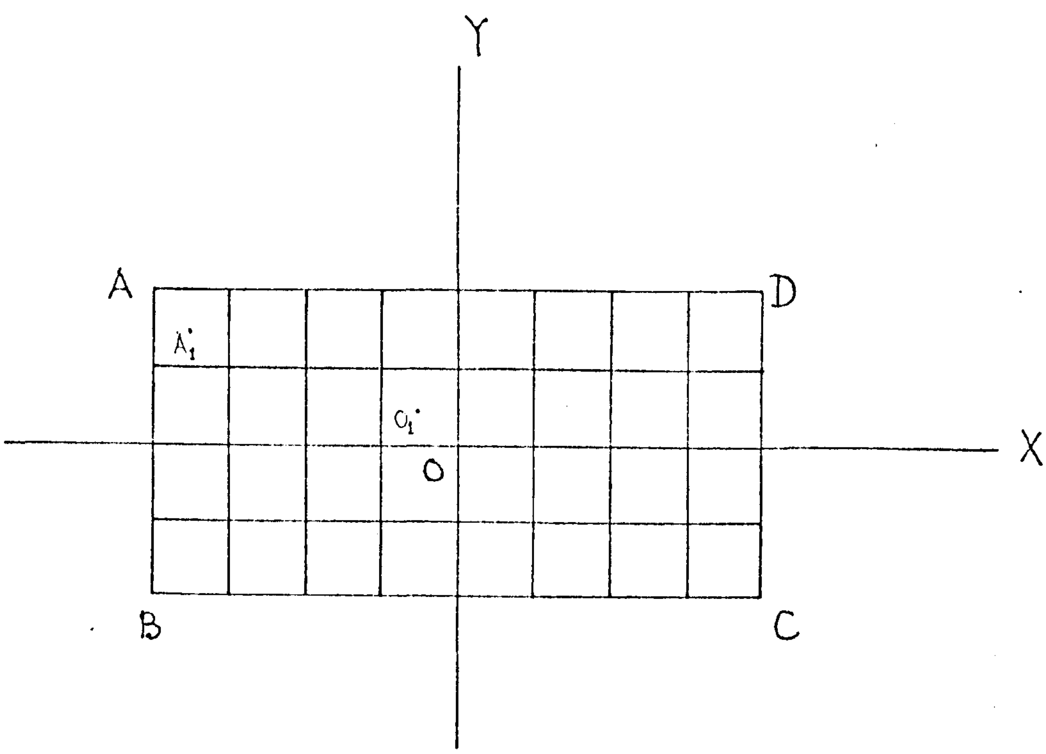

FIG. 9

SUB-AREAS ON A RECTANGULAR PLATE

Proceeding the same way as in the case of a square plate, we form the N equations

$$\sum_{j=1}^{N} a_{kj}\,\lambda_j = 1 \quad ; \quad k = 1, 2 \cdots N . \tag{123}$$

The N equations (123), from symmetry, reduce to

$$N^*\left(= \frac{N}{4} = \frac{k^2}{2}\right) \quad \text{equations} . \tag{124}$$

The equations are then solved by the Gauss-Seidel iterative method with ϵ = 0·0001 and the K is computed as before by (114). Table 8 exhibits the value of K as N increases.

In this case, K gradually increases from 0·35938 to 0·37431 as N increases from 32 to 1800. No ill conditioning was noticed in this range of N but the machine capacity forced us to stop at N = 1800. For the unit rectangular plate with edge ratio 1:2, we find K = 0·37431.

2. Isosceles Triangular Plate

Let a thin isosceles triangular conductor ABC (Fig. 10) have its centroid at the origin of a reference frame OXYZ and it lies in the plane z =0. Its boundaries are given by

$$x = d$$

$$y = x \tan\theta + 2d \tan\theta ,$$

$$y = -x \tan\theta - 2d \tan\theta ,$$

where the meridian AD = 3d, and θ is the angle made by AC with the axis of x.

The plate is divided into

$$N = k^2 \tag{125}$$

equal triangular sub-areas [Fig. 10(a)] by drawing 3 sets of (k -1) equidistant parallel lines, parallel to the sides of the triangle, and k in (125) is given by

$$k = 1 + (j-1)3 \quad ; \quad j = 2, 3, \cdots n . \tag{126}$$

ELECTROSTATIC CAPACITY OF A THIN RECTANGULAR PLATE

(EDGE RATIO 2:1)

SUB-AREA N	EQUATION N^*	DENSITY AT THE POINTS O_1(Centre)	A_1(Corner)	CAPACITY
32	8	0·20076	0·62369	0·35938
128	32	0·19321	0·99326	0·36815
288	72	0·19049	1·31218	0·37102
648	162	0·18872	1·73780	0·37288
968	242	0·18817	1·99826	0·37354
1352	338	0·18780	2·24514	0·37399
1800	450	0·18758	2·48107	0·37431

Table 8

(This should be read in conjuction with Fig. 9)

This pattern of sub-divisions gives us 3 rows of sub-areas whose nodal points lie on the 3 meridians of the triangle along with a sub-area whose nodal point lies at the centroid of the triangle. Further the sub-areas thus formed are all equal in size and in form [Fig. 10(a)].

From symmetry, the number of independent equations reduces to

$$N^* = \frac{1+(j-1)3}{2}\left\{2+(j-1)3\right\} ; \quad j = 2, 3 \cdots n . \tag{127}$$

For the equilateral triangular plate

$$N^* = \frac{j}{2}\left\{2+(j-1)3\right\} ; \quad j = 2, 3 \cdots n . \tag{128}$$

The co-efficients a_{kj} of (112) are computed over the sub-areas, as before, by the centroid method when $j \neq k$. When $j = k$, by Appendix I,

$$a_{kk} = \sum_{j=1}^{m} \frac{2\Delta_j}{a_j} \log\left(\frac{L_j + L_{j+1} + a_j}{L_j + L_{j+1} - a_j}\right) , \tag{129}$$

where Δ_j is the area of the triangle formed by the sides L_j, L_{j+1} and a_j [Fig. 10(b)]. When $j = m$, in (129) $j + 1$ should be replaced by 1 instead of $m + 1$; m denotes the number of sides of the polygon.

Equilateral Plate of unit area

For an equilateral plate of unit area $\theta = 30^\circ$, and a side BC is given by

$$\frac{1}{2} \text{ BC. AC Sin } 60^\circ = 1$$

$$\text{or} \quad \frac{1}{2} \text{ BC} \cdot \text{BC Sin } 60^\circ = 1 \text{ or } \text{BC} = \left(\frac{2}{\text{Sin } 60^\circ}\right)^{\frac{1}{2}} .$$

The meridian AD is given by

$$\text{AD} = 3d = \text{BC Cos } 30^\circ .$$

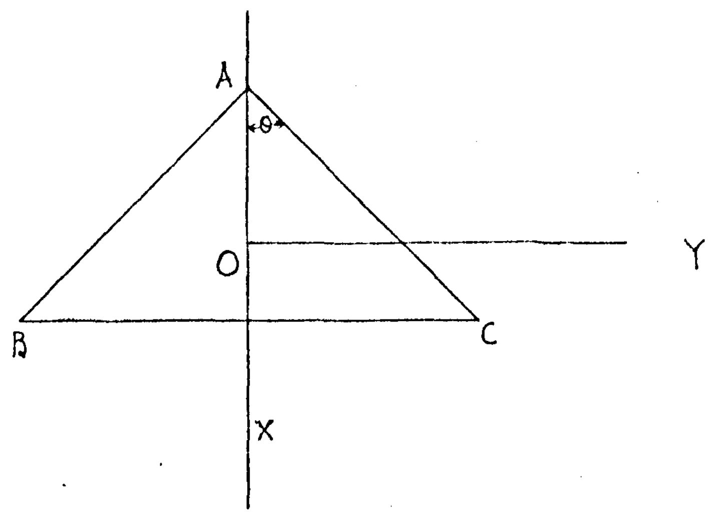

Fig. 10

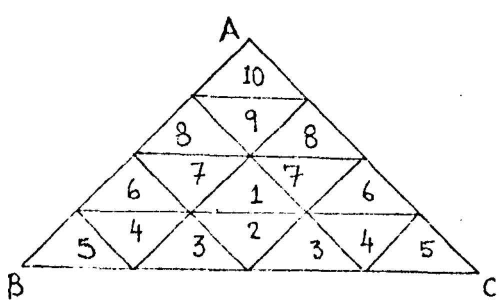

Fig. 10(a)

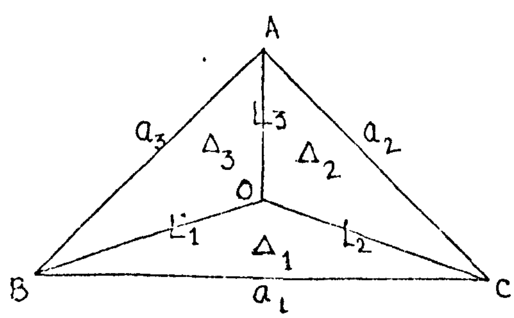

Fig. 10(b)

After evaluation of the co-efficients a_{kj} of (112) over the triangular sub-areas, the N^* equations, where N^* is given by (128), are then solved by the Gauss-Seidel iterative method with $\epsilon = 0{\cdot}0001$. The λ_j thus obtained are used in (114) to evaluate the capacity of the plate.

The values of the capacity of the thin equilateral triangular conductor of unit area for increasing values of N are given in Table 9. It is evident from the Table that the capacity of the plate is $K = 0{\cdot}38308$, and this value is attained when N = 361. The density λ distributed along a median, for the above value of N, is given in the Fig. 10(c).

For N = 361, the potential V is calculated at the corner points of the sub-areas along a median of the plate. The reference frame is taken as in Fig. 10. The values of $|V - 1|$ thus computed are exhibited in Table 9 (a). It is evident from this Table that the value of $|V - 1|$ is the lowest when $\underset{\sim}{p}$ is near the centroid of the plate and gradually increases as we move towards the periphery. The maximum value of it, as expected, lies at an apex of the plate.

Right angled isosceles triangular plate of Unit Area

A thin isosceles triangular plate of unit area with base angles 45° each is divided into N sub-areas by the procedure stated before. In this case $\theta = 45^\circ$ and hence

$$AD = AB \quad \mathrm{Sin}\ 45^\circ$$

and $\frac{1}{2}$ BC. AD = 1 i.e. $\frac{1}{2}$ (2 AB Cos 45°) (AB Sin 45°) = 1 .

Hence AB = $\sqrt{2}$ and BC = 2.

As in the former case, the N equations (112) are constructed. From symmetry, the N equations reduce to N^* equations where N^* is given by (127). The equations are then solved, as before, by the Gauss-Seidel iterative method and then K is computed by (114). The values of K for a range of values of N are given in Table 10.

In this case K gradually increases from $0{\cdot}36174$ to $0{\cdot}40025$ as N increases from 16 to 361. No ill conditioning was noticed in this range of N but the machine capacity forced us to stop at N = 361. The value of the capacity attained at this stage is found to be $K = 0{\cdot}40025$.

Following the same procedure, the capacity of an isosceles triangular plate (120°, 30°, 30°) of unit area is computed for increasing value of N, and are exhibited in Table 11. The capacity of the plate, from Table 11, is $K = 0{\cdot}41011$.

ELECTRO-STATIC CAPACITY OF A THIN EQUILATERAL PLATE

i	SUB-AREA N	EQUATION N^*	DENSITY AT CENTROID	CAPACITY
2	16	5	0·18340	0·35361
3	49	12	0·18610	0·36527
4	100	22	0·18397	0·37010
5	109	35	0·18277	0·37273
6	256	51	0·18200	0·37438
7	361	70	0·18136	0·38308
8	484	92	0·18086	0·38139

Table 9

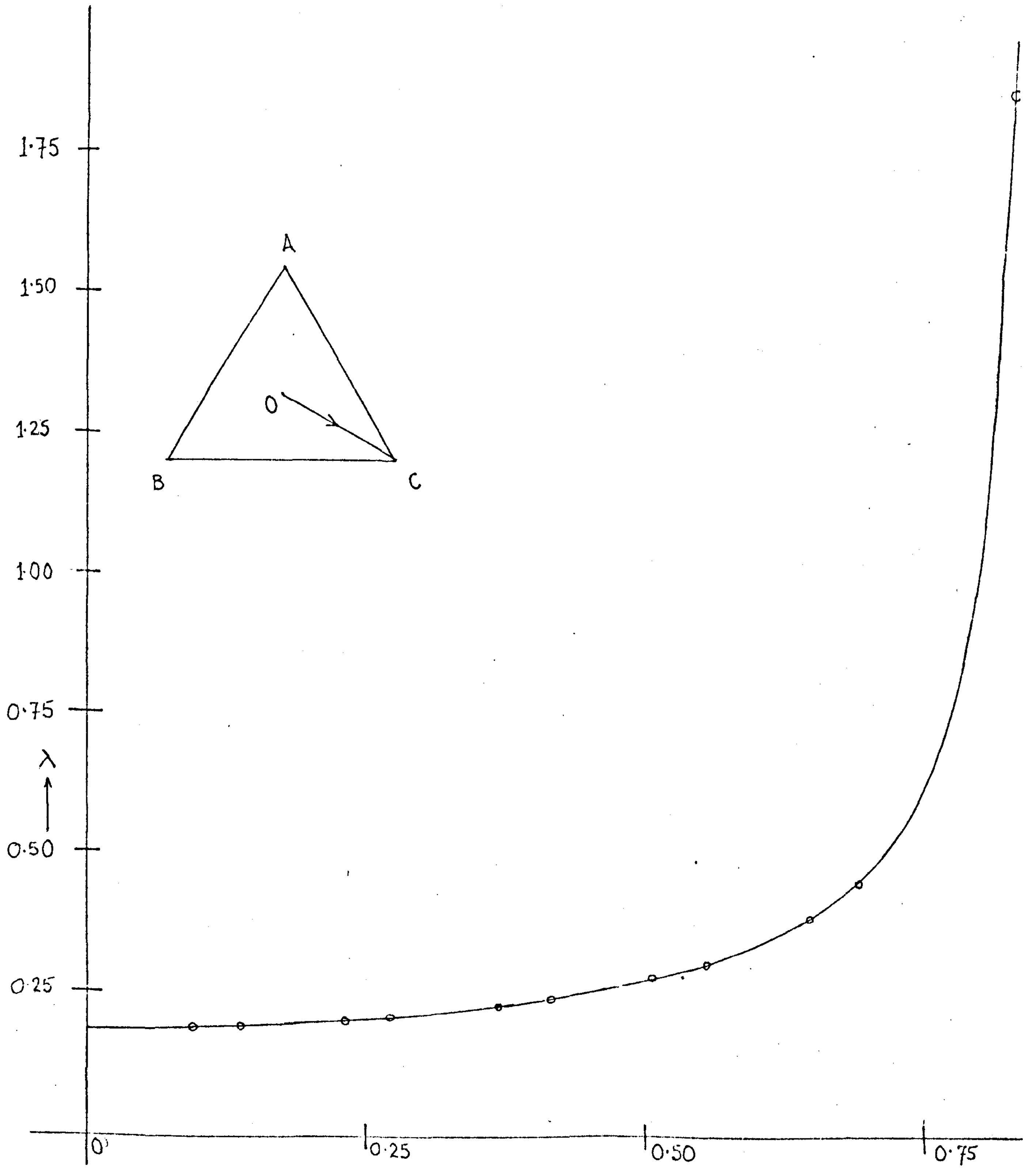

Fig. 10(c)

DENSITY DISTRIBUTION ALONG A MEDIAN OC

POTENTIALS GENERATED AT THE CORNER POINTS OF SUB-AREAS LYING ALONG A MEDIAN OF THE THIN EQUILATERAL TRIANGULAR PLATE

CO-ORD. OF THE CORNER POINTS X	Y	V	$\lvert V - 1 \rvert$
0·02309	0·03999	1·00131	0·00131
0·09236	0·15997	1·00142	0·00142
0·16162	0·27994	1·00165	0·00165
0·23089	0·39991	1·00215	0·00215
0·30016	0·51989	1·00346	0·00346
0·36942	0·63986	1·02819	0·02819
0·43869	0·75984	0·70133	0·29867

Table 9 (a)

ELECTROSTATIC CAPACITY OF A RIGHT ANGLED ISOSCELES TRIANGULAR PLATE OF UNIT AREA

i	SUB-AREA N	EQUATION N*	DENSITY AT CENTROID	CAPACITY
2	16	10	0·1845	0·36174
3	49	28	0·1890	0·37372
4	100	55	0·1869	0·37866
5	169	91	0·1859	0·38135
6	256	136	0·1850	0·38303
7	361	190	0·1849	0·40025

Table 10

ELECTROSTATIC CAPACITY OF AN ISOSCELES (120^{o}, 30^{o}, 30^{o}) TRIANGULAR PLATE OF UNIT AREA

i	SUB-AREA N	EQUATION N^*	DENSITY AT CENTROID	CAPACITY
2	16	10	0·1800	0·38498
3	49	28	0·1978	0·39829
4	100	55	0·1932	0·40384
5	169	91	0·1934	0·40688
6	256	136	0·1930	0·40879
7	361	190	0·1930	0·41011

Table 11

General Conclusions

It is interesting to note how K varies for different shaped triangles of unit area. This is exhibited in Table 12. From this, we see that K decreases as the symmetry increases, reaching its minimum for the equilateral plate. Table 12(a) exhibits the capacity of unit plates of different shape. It appears from Table 12(a) that, for regular polygons of unit area, K decreases as the number of sides increases, reaching its minimum for a circular plate (Chapter 10).

ELECTROSTATIC CAPACITY OF UNIT THIN TRIANGULAR PLATES OF DIFFERENT SHAPE

ANGLES OF THE PLATE IN DEGREES			CAPACITY
60	60	60	0·38139
90	45	45	0·40025
120	30	30	0·41011

Table 12

ELECTROSTATIC CAPACITY OF THIN PLATES OF UNIT AREA

PLATE	CAPACITY
EQUILATERAL TRIANGULAR PLATE	0·38139
SQUARE "	0·36188
CIRCULAR "	0·35917

Table 12(a)

CHAPTER 10
CAPACITY OF A THIN CIRCULAR DISC

Analytical Solution

Let V be the potential due to an electrified flat circular disc of unit radius. The centre of the disc defines the origin of a system of cylindrical polar co-ordinates, of which the Z-axis lies perpendicular to the plane of the disc. In cylindrical co-ordinates, V satisfies

$$\nabla^2 V = \frac{\partial^2 V}{\partial r^2} + \frac{1}{r}\frac{\partial V}{\partial \theta} + \frac{\partial^2 V}{\partial z^2} = 0 \;, \tag{130}$$

with boundary conditions, for $z = 0$ (i.e. plane of the disc)

$$V = 1 \quad , \quad 0 \leq r < 1 \tag{131}$$

$$\frac{\partial V}{\partial z} = 0 \quad , \qquad r > 1 \;. \tag{132}$$

The 2nd condition (132) comes from the symmetry of V across $z = 0$ and absence of charges outside the disc.

The solution of (130) under the above conditions, according to Tranter[7], is

$$V = \frac{2}{\pi}\int_0^\infty p^{-1} e^{-pz} J_0(rp) \sin p \, dp \;. \tag{133}$$

For $\quad r < 1$

$$\left(\frac{\partial V}{\partial z}\right)_{z=0} = \frac{2}{\pi}\int_0^\infty J_0(rp) \sin(-p) \, dp \;,$$

which is the imaginary component of

$$I = \frac{2}{\pi}\int_0^\infty J_0(r p)\, e^{-ip}\, dp \quad . \tag{134}$$

From Watson,[8]

$$I = \frac{2}{\pi}\, \frac{1}{\sqrt{(-i)^2 + r^2}} = \frac{2}{\pi}\, \frac{-i}{\sqrt{1-r^2}} \quad ,$$

$$\therefore \left(\frac{\partial V}{\partial z}\right)_{z=0} = -\frac{2}{\pi}\, \frac{1}{\sqrt{1-r^2}} \quad . \tag{135}$$

By relation (6) of Chapter 1, and from symmetry,

$$-4\pi\lambda = \left[\left(\frac{\partial V}{\partial z}\right)_{int.} + \left(\frac{\partial V}{\partial z}\right)_{ext.}\right]_{z=0} = 2\left(\frac{\partial V}{\partial z}\right)_{z=0}$$

$$= -\frac{4}{\pi}\, \frac{1}{\sqrt{1-r^2}} \quad .$$

Therefore

$$\lambda = \frac{1}{\pi^2}\, \frac{1}{\sqrt{1-r^2}} \quad , \tag{136}$$

Where λ is the density at a radial distance r from the centre. For a disc of radius a, at a distance r from the centre

$$\lambda = \frac{1}{\pi^2}\, \frac{1}{\sqrt{1-\left(\frac{r}{a}\right)^2}} \quad .$$

The capacity k of the disc of radius 'a' is

$$k = \int_{\partial B} \lambda(q)\, dq = \int_{r=0}^{a} \int_{\theta=0}^{2\pi} \frac{1}{\pi^2}\, \frac{1}{\sqrt{1-\left(\frac{r}{a}\right)^2}}\, r\, d\theta\, dr$$

$$= \frac{2\pi}{\pi^2} \int_{r=0}^{a} \frac{r\,dr}{\sqrt{1-\left(\frac{r}{a}\right)^2}} = a\left(\frac{2}{\pi}\right)$$

$$\simeq 0{\cdot}6366203 \quad , \quad \text{when} \quad a = 1 \ . \tag{137}$$

Numerical Approach

Apart from the analytical approach, already discussed, the integral equation formulae provide a straightforward numerical approach to solve the problem numerically. Let a density distribution λ on ∂B (thin circular plate of unit radius) generate the potential V which satisfies the equation (130) i.e.

$$\nabla^2 V = 0$$

with boundary conditions (131) and (132) i.e.

$$V(\underset{\sim}{r}) = 1 \ ; \ \underset{\sim}{r} \in \partial B$$

and on $z = 0$,

$$V'(\underset{\sim}{r}) = 0 \quad ; \ |\underset{\sim}{r}| > a$$

respectively. In the integral equation method the boundary condition (131) is sufficient to solve the problem and hence the condition (132) is redundant in this case. This is essentially because our formulation is a Dirichlet formulation, which confines us to ∂B, whereas Tranter's formulation is a mixed formulation for which we must go outside ∂B.

Since V = 1 on ∂B, λ satisfies the equation (111) which, on discretisation, takes the form (112) i.e.

$$\sum_{j=1}^{N} a_{kj}\,\lambda_j = 1 \quad ; \quad k = 1,2 \cdots N \ .$$

Division of a circular domain into sub-areas

To find a numerical solution of (112), it is necessary to divide ∂B into sub-areas. To affect the sub-division the circular domain is divided into n annular rings and each ring in its turn is divided into M sub-areas except the inner most ring which is divided into M_1 sub-areas (Fig. 11). For sub-areas of equal area we have in a j th ring

$$\frac{\pi\left(\overset{*}{r}{}_j^2 - \overset{*}{r}{}_{j-1}^2\right)}{M} = \frac{\pi \overset{*}{r}{}_1^2}{M_1} ,$$

i.e. $$\overset{*}{r}{}_j^2 - \overset{*}{r}{}_{j-1}^2 = \left(\frac{M}{M_1}\right)\overset{*}{r}{}_1^2 . \tag{138}$$

Putting $j = 2, 3, \ldots . n$ in succession and adding them up, we obtain

$$\overset{*}{r}{}_n^2 = \left\{(n-1)\left(\frac{M}{M_1}\right)+1\right\}\overset{*}{r}{}_1^2 .$$

Since $r_n = a$ (=1, the radius of the disc),

$$\overset{*}{r}{}_1^2 = a^2 \Big/ \left[(n-1)\left(\frac{M}{M_1}\right)+1\right] .$$

Using this value of $\overset{*}{r}_1$ in (138) and putting $j = 2, 3, \ldots . n$ in succession, we obtain n annular rings on the circular domain. The value of M_1 usually equals 6 to obtain the sub-areas, nearly of equilateral form, in the inner-most ring and, M is determined by

$$M = 6\left(2^{k-1}\right) \quad ; \quad k \leqslant n . \tag{139}$$

n may have any value but to keep the sub-areas in the outermost ring near to square form, we choose n such that it approximately satisfies

$$\frac{2\pi r_n}{M} \simeq \frac{r_n}{n} \quad \text{ie} \quad \frac{6\cdot 28318}{6\left(2^{k-1}\right)} \simeq \frac{1}{n} .$$

Hence for a particular choice of k , a choice for n, from above, is given by

$$n = 2^{k-1} . \tag{140}$$

This sub-division gives very thin trapezoidal sub-areas in a few of the inner rings, which are not suitable for numerical work. To eliminate the thin sub-areas, the width of the m th ring is diminished by the adjustment given by

$$T_m = p\left(T_m^1\right) , \quad p < 1$$

where T_m^1 represents the width of the m th ring in (138); m usually equals 4. The width of the rings inner to the m th ring are then determined by

$$T_j = p\left(T_{j+1}\right) ; \quad j = (m-1), (m-2) \cdots 2 . \tag{141}$$

The validity of (141) depends on the features of the inner rings

$$T_j^1 \geqslant T_{j+1}^1 \qquad \text{and} \qquad 0 < p < 1 .$$

Now the radii of the above m - 1 concentric rings are given by

$$r_j = r_m^* - \sum_{l=j}^{m} T_l + T_j \quad ; \quad j = 2, 3 \cdots m . \tag{142}$$

In the circular area of radius r_2, given by (142), k annular rings are introduced where k is given by (139). Each of the k rings has M_j equal sub-areas, where

$$M_j = 6\left(2^{j-1}\right) \quad ; \quad j = 1, 2, 3 \cdots k . \tag{143}$$

Of these k rings, if ρ_1 be the radius of the first circle, then ρ_1 is given by

$$\rho_1 = \left(\frac{2\pi r_2}{M}\right) q , \qquad 0 < q < 1 ,$$

where r_2 is given by (142). After determining ρ_1 with a starting value $q = 0{\cdot}9$, the radii of the remaining k - 1 circles are fixed by

$$\rho_j = \rho_{j-1} + \left(2\pi \rho_{j-1}/M_j\right) p_1 \quad ; \quad j = 2, 3 \cdots k , \tag{144}$$

where p_1 is usually set at 1·5. Now the annular gap, given by

$$D = r_2 - \rho_k ,$$

is divided into J parts to give J annular rings such that

$$\left| T_3 - \left(r_2 - \rho_{k+J-1} \right) \right| \leq \epsilon \quad , \tag{145}$$

where ϵ is a pre-assigned small +ve quantity (usually $< 0{\cdot}001$) and J is a +ve whole number given by the integral part of Q where,

$$Q = \frac{D}{\left(\frac{2\pi\rho_k}{M_k}\right)} - 1 \quad . \tag{146}$$

The radii of these J concentric circles are given by

$$\rho_{k+l} = \rho_{k+l-1} + SxT + (l-1)U \; ; \; l = 1, 2 \cdots J \; ,$$

where

$$SxT = \left(\frac{2\pi\rho_k}{M}\right) h_1$$

and

$$U = \left[r_2 - \left\{ \rho_k + (SxT)\, J \right\} \right] \Big/ \frac{(J-1)\,J}{2} \quad .$$

If $Q \leq 0$, q is gradually made smaller until $Q > 0$ and the adjustment is stopped at the stage when (145) is satisfied. At this stage ρ_{k+J} is readjusted by setting

$$\rho_{k+J} = r_2 \quad . \tag{147}$$

Now the total number of annular rings on the circular face becomes

$$N^* = (n-2) + k + J \quad , \tag{148}$$

and the radii of the concentric circles are given by

$$R_j = \rho_j \quad ; \quad j = 1, 2 \cdots (k+J) \quad ,$$

$$R_{k+J+l-2} = r_l \quad ; \quad l = 3, 4 \cdots m,$$

$$R_{k+J-2+s} = \overset{*}{r}_s \quad ; \quad s = (m+1), \cdots n .$$

The sub-areas in the 1st ring are quadrilaterals with shapes very near to that of an equilateral triangle. From the 2nd up to the (k - 1) th ring, the sub-areas are pentagons [Fig. 11 (a)] in which slant side BE of a sub-area is p_1 times the side BD. From the k th up to the ($\overset{*}{N}$ - 2) th ring, the sub-areas are trapezoidal in form. To make sub-areas smaller in size as we approach the rim, the number of sub-areas are doubled in the $\overset{*}{N}$ th ring by inserting radial line segments through the middle of each sub-area. The sub-areas in the ($\overset{*}{N}$ - 1) th and in the $\overset{*}{N}$ th ring are then made pentagonal in form [Fig 11(a)].

The total number of sub-areas on the circular plate is

$$N = \sum 6 * 2^{j-1} + (\overset{*}{N} - k + 1)\, 6 * 2^{k-1} + 2 * 6 * 2^{k-1} \quad . \tag{149}$$

Formulation and solution of equations

For the N sub-areas, there are N algebraic equations in N unknown λ_j given by (112). The co efficients a_{kj} of (112), are evaluated over the sub-areas, as before, by the centroid method when $j \neq k$ and analytically when $j = k$.

From symmetry, the N equations reduce to $\overset{*}{N}$ equations where $\overset{*}{N}$ is given by (148). The equations are then solved, as before by the Gauss-Seidel iterative method with $\epsilon = 0{\cdot}0001$.

Table 13 exhibits the value of the capacity of a thin plate of unit radius with increasing value of N. It is evident from the Table that $\kappa = 0{\cdot}6351872$. The analytic value of κ, by (137), is

$$\kappa = \frac{2}{\pi} \simeq 0{\cdot}6366203 \quad .$$

Table 14 exhibits the density distribution along a radius compared with that obtained analytically by (136). The numerical λ deviates only slightly from the analytical λ except in the neighbourhood of the rim. This behaviour of λ in the neighbourhood of the rim supports the conclusions drawn in Chapter 6. Fig. 12(a) gives the density profile based upon Table 14.

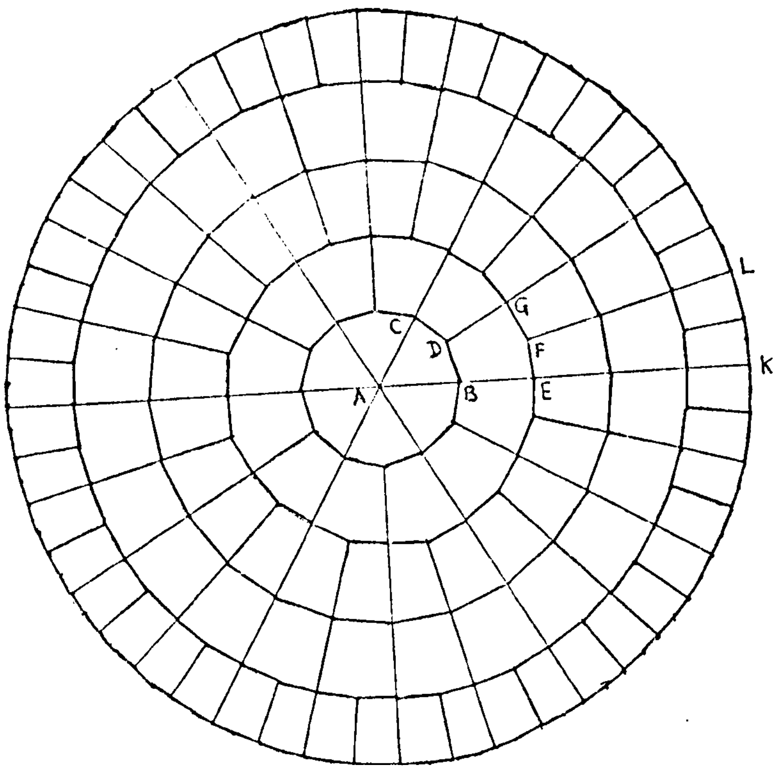

Fig. 11

SUB-AREAS ON A CIRCULAR DOMAIN

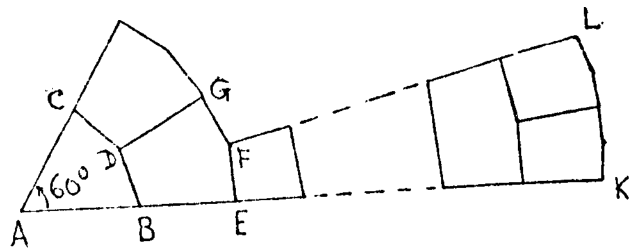

Fig. 11(a)

A SECTION OF FIG. 11 .

ELECTROSTATIC CAPACITY OF A THIN CIRCULAR PLATE COMPARED WITH ANALYTICAL VALUE $\kappa = 0{\cdot}6366$

SUB-AREA N	EQUATION N^*	NUMERICAL κ
162	7	0·6239460
522	12	0·6314764
2202	25	0·634633
2682	30	0·6351872
3162	35	0·6351505

Table 13

DENSITY DISTRIBUTION ON A CIRCULAR PLATE ALONG A RADIAL LINE

RADIAL DIST FROM CENTRE r	ANALYTICAL λ	NUMERICAL λ
0·02797	0·10136	0·10306
0·12294	0·10209	0·10194
0·19271	0·10326	0·10324
0·25042	0·10466	0·10456
0·32629	0·10719	0·10689
0·41929	0·11161	0·10647
0·52502	0·11905	0·12033
0·61273	0·12821	0·12982
0·72462	0·14702	0·14901
0·82141	0·17765	0·18016
0·93499	0·28567	0·27671
0·98732	0·63816	0·87936

Table 14

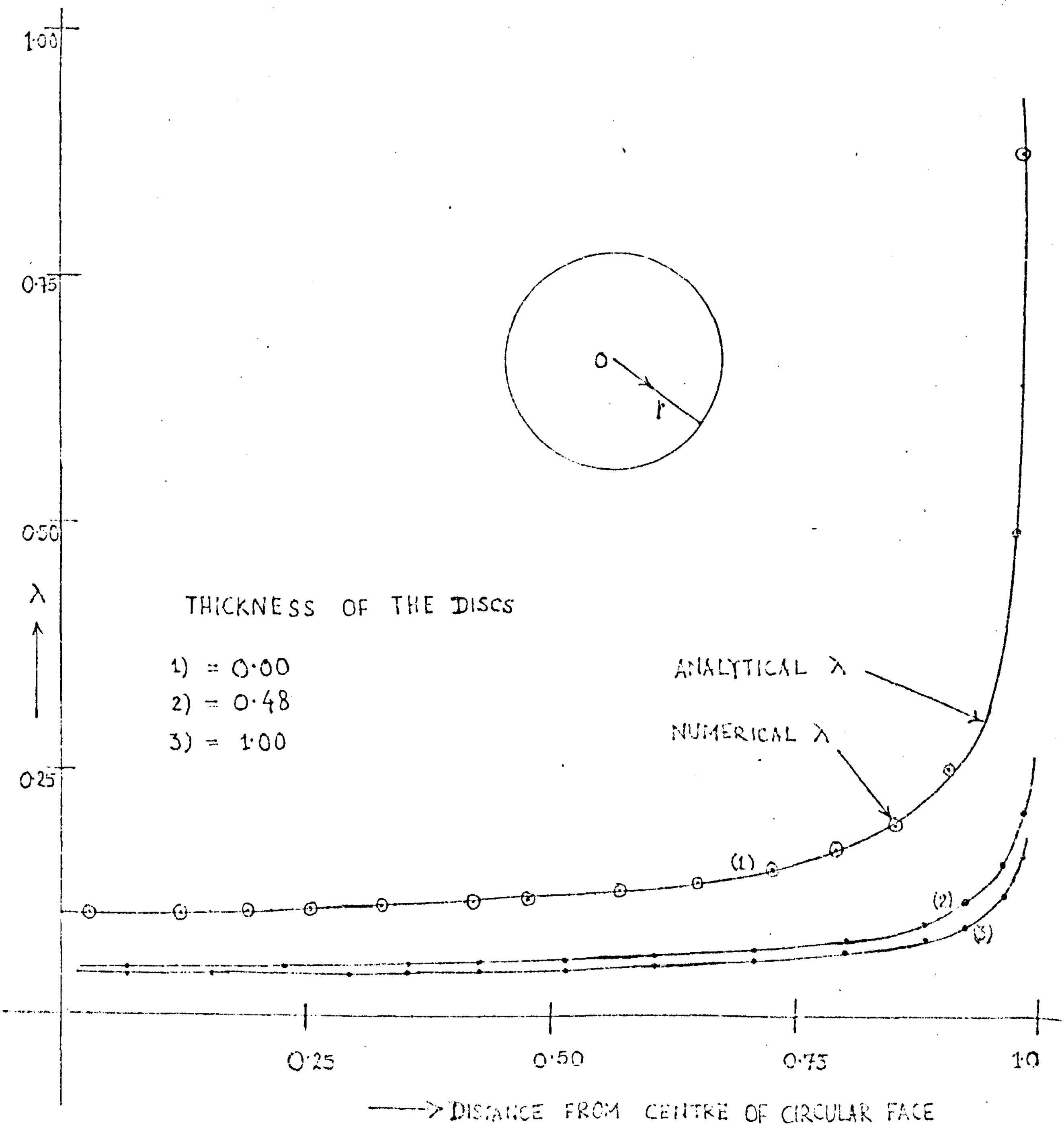

Fig. 12

DENSITY DISTRIBUTION ALONG A RADIAL LINE ON THE CIRCULAR FACE OF THICK DISCS OF UNIT RADIUS

CHAPTER 11

CAPACITY OF THICK CIRCULAR DISCS

Introduction

A thick circular disc (Fig. 13) may be viewed as a right circular cylinder with a small ratio H/a, where H defines the height and a defines the radius of the cylinder. Taking the origin of cylindrical polar co-ordinates at the centroid of the cylinder and the Z-axis to coincide with the axis of the cylinder, the plane boundaries at the ends are

$$z = \pm \frac{H}{2} \quad ,$$

the curved cylindrical boundary is

$$r = a \quad .$$

If V be the potential due to a equilibrium charge distribution on ∂B, V satisfies Laplace's equation

$$\nabla^2 V = 0$$

with boundary conditions (131) and (132) i.e.

$$V(\underset{\sim}{r}) = 1 \; ; \quad \underset{\sim}{r} \in \partial B$$

and on $z=0$,

$$V'(\underset{\sim}{r}) = 0 \; ; \quad |\underset{\sim}{r}| > a \quad .$$

Because of the form of ∂B, complications arise in solving the problem analytically. However, the integral equation formulation provides a straightforward numerical approach. In the integral equation method, the boundary condition (131) i.e.

$$V(\underset{\sim}{r}) = 1 \; ; \quad \underset{\sim}{r} \in \partial B \; ,$$

is sufficient to solve the problem and hence, as in the case of a thin plate, the boundary condition (132) is redundant. If the density distribution λ generates the potential $V = 1$ on ∂B, then λ satisfies (111) which, on discretisation, takes the form (112).

Division of the surface into sub-areas

Each of the plane circular faces is divided into sub-areas as the thin plate in the previous case. Hence if N^*_1 be the number of annular rings and N_1 be the total number of sub-areas on a plane face, by (148) and (149),

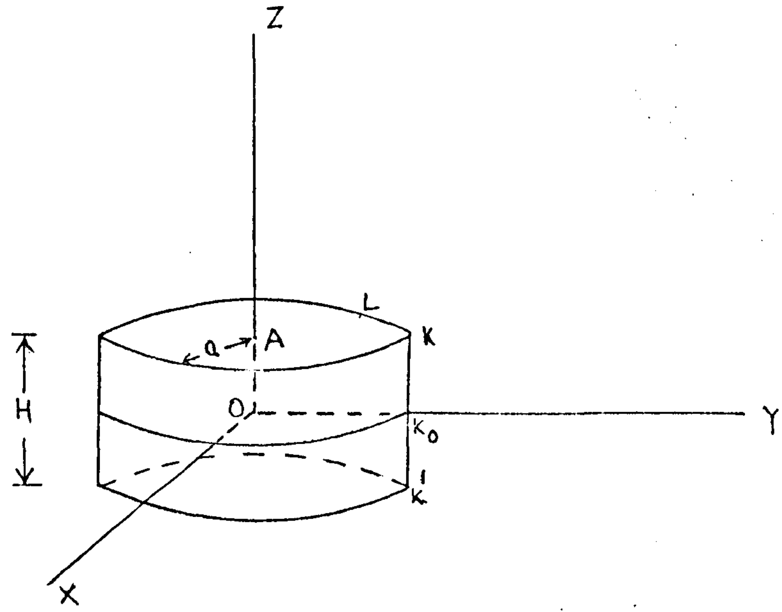

Fig. 13

A THICK CIRCULAR DISC

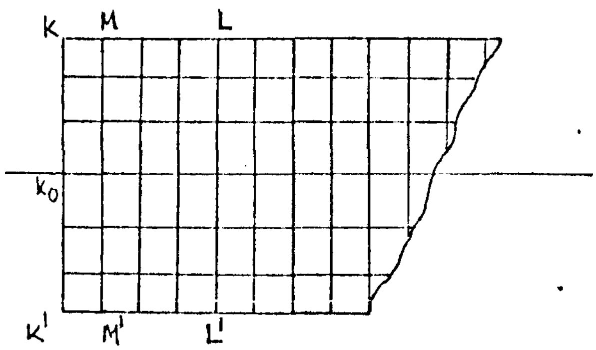

Fig. 13(a)

SUB-AREAS ON THE CYLINDRICAL SURFACE

$$N_1^* = (n-2) + k + J$$

and $$N_1 = \sum_{j=1}^{k} 6(2^{j-1}) + (N_1^* - k + 1)\{6(2^{k-1})\} + 2\{6(2^{k-1})\} \quad .$$

If we now insert N_2^* annular rings in the upper half of the cylindrical surface, then N_2^* is given by

$$N_2^* = L^* - 1 \tag{150}$$

where L^* is the integral part of

$$\left[\frac{H}{2} \Big/ \left(\frac{2\pi a}{4M}\right)\right] \quad .$$

If h_1 be the width of the ring nearest to the edge, then

$$h_1 = \left(\frac{2\pi a}{4M}\right) = h \quad (\text{Say}) \quad . \tag{151}$$

Further, if

$$U_1 = \left\{\frac{H}{2} - \left(\frac{2\pi a}{4M}\right) N_2^*\right\} \Big/ \left\{N_2^*(N_2^* - 1)/2\right\} \quad ,$$

the widths of the subsequent rings, as we move towards the plane $z = 0$, are given by

$$h_j = h + (j-1)U_1 \quad ; \quad j = 1, 2 \cdots N_2^* \, ,$$

when the breadth of each sub-area is kept constant at h given by (151).

Each of the N^*_2 rings contains 4M sub-areas, and hence the total number of sub-areas on the upper half of the cylindrical surface is

$$N_2 = 4(M)N_2^* \quad . \tag{152}$$

The total number of annular rings on the surface is

$$2N^* = 2\left(N_1^* + N_2^*\right) , \tag{153}$$

and the total number of sub-areas is

$$\begin{aligned} N &= 2\left(N_1 + N_2\right) , \\ &= 2\left[\sum_{j=1}^{k} 6\left(2^{j-1}\right) + \left(N_1^* - 1 - k\right)\left(2^{k-1}\right)6 + 2^{k-1}\left(12 + 24\, N_2^*\right)\right], \\ &= 2\left[\sum_{j=1}^{k} 6\left(2^{j-1}\right) + 6\left(2^{k-1}\right)\left(N_1^* + 1 + 4N_2^* - k\right)\right] . \end{aligned} \tag{154}$$

For $H = 0{\cdot}18$ and $k = 3$, it is found that $N^*_2 = 2$, $n = 4$, and $J = 2$. Hence $N^*_1 = 7$ and, by (153) and (154)

$$N^* = 9 \quad \text{and} \quad N = 708 .$$

The analysis of the sub-areas in each of the annular rings, for the above values of H and k, is given in Table 15.

Formulation and solution of the equations

For the N sub-areas, there are N algebraic equations in N unknowns given by (112). The co-efficients a_{kj} of (112), are evaluated over the sub-areas, as before, by the centroid method when $j \neq k$ and analytically when $j = k$.

From symmetry, the N equations reduce to N^* independent equations where N^* is given by (153). The equations are then solved, as before, by the Gauss-Seidel iterative method with $\epsilon = {\cdot}0001$.

Table 16 exhibits the value of κ of a thick plate of unit radius and thickness $H = 0{\cdot}18$ with increasing value of N.

SUB-AREAS ON THE SURFACE OF A THICK DISC (THICKNESS 0·48) OF UNIT RADIUS

NODAL POINTS		ARMS OF SUB-AREAS			AREA
RADIAL DIST r	Z	BD	GE	BE	
ON THE PLANE CIRCULAR SURFACE					
0·10066	0·2400	0·00	0·16184	0·16184	0·01310
0·22636	0·2400	0·08377	0·14957	0·12711	0·01506
0·34580	0·2400	0·07543	0·10505	0·11347	0·01015
0·48519	0·2400	0·10505	0·14630	0·15803	0·01969
0·62816	0·2400	0·14630	0·18312	0·14103	0·02303
0·77278	0·2400	0·18312	0·22159	0·14738	0·03037
0·92506	0·2400	0·11103	0·13081	0·15115	0·01838
ON THE CYLINDRICAL SURFACE					
1·00	0·20728	0·06545	0·06545	0·06545	0·00428
1·00	0·13455	0·06545	0·06545	0·08000	0·00524
1·00	0·04728	0·06545	0·06545	0·09455	0·00619

Table 15

[This should be read in conjuction with Fig. 11(a) and Fig. 13(a)]

Following the same procedure, the capacity of circular plates of unit radius with various thickness are evaluated and are given in Table 17.

Fitting of a polynomial through the capacity values

Our numerical approach gives the capacity for some discrete values of the thickness H. To approximate the capacity for any value of H in the above range, we attempt to fit a continuous curve through the computed values of capacity utilising the method of least squares.[9]

It appears from the difference columns (3) and (4) of Table 17 that the smoothest interpolating function may be a log function. Considering the analytic value of κ when the thickness is zero, we expect the form of the function to be

$$\kappa = f(H) = \frac{2}{\pi} \log \left(C_0 + \sum_{j=1}^{m} C_j H^j \right) , \tag{155}$$

where $C_0 = e$, the base of natural logarithms. For the 11 values of κ (Table 18), a polynomial of degree 10 will fit exactly through them. Starting with m = 1 and gradually increasing m in steps of 1, it is found that, for m = 5, the interpolating function (155) fits the computed values to an accuracy of 3 significant figures. Further when $H \to 0$, κ in (155) tends to $\frac{2}{\pi}$ as required.

For m = 5, the co-efficients are $C_0 = e = 2{\cdot}71828$, $C_1 = 2{\cdot}53801$, $C_2 = -2{\cdot}78274$, $C_3 = 4{\cdot}63385$ $C_4 = -3{\cdot}74689$ and $C_5 = 1{\cdot}18925$. Fig. 14 shows the relation between the computed values and the fitted values of κ , based on Table 18, for a disc of unit radius, as thickness varies from 0 to 1.

ELECTRO-STATIC CAPACITY OF A THICK DISC (THICKNESS 0·18) OF UNIT RADIUS

SUB-AREA N	EQUATION N^*	CAPACITY
708	9	0·72143804
1812	14	0·72189708
8244	30	0·72209634
10064	35	0·72201394

Table 16

ELECTRO-STATIC CAPACITY OF THICK CIRCULAR DISCS OF UNIT RADIUS AND THE DIFFERENCE COLOUMNS OF CAPACITY

THICKNESS H	CAPACITY κ	1ST ORDER DIFFERENCE δ^1	2ND ORDER DIFFERENCE δ^2
0·18	0·72209638		
		0·03615471	
0·28	0·75825109		– 0·0030993
		0·03314478	
0·38	0·79139585		– 0·00204284
		0·03110194	
0·48	0·82249781		– 0·00262198
		0·02847996	
0·58	0·85197777		– 0·00018507
		0·02829489	
0·68	0·88027266		– 0·00104826
		0·02724663	
0·78	0·90751929		– 0·00091254
		0·02633409	
0·88	0·93385338		– 0·00080316
		0·02553093	
0·98	0·93385338		

Table 17

CAPACITY OF THICK CIRCULAR DISCS FROM A FITTED POLYNOMIAL

THICKNESS H	COMPUTED κ	FITTED κ
0·00	0·63519	0·63662
0·18	0·72210	0·72197
0·28	0·75825	0·75843
0·38	0·79140	0·79141
0·48	0·82250	0·82237
0·58	0·85198	0·85196
0·68	0·88027	0·88034
0·78	0·90752	0·90757
0·88	0·93385	0·93378
0·98	0·95938	0·95941
1·00	0·96440	0·96453

Table 18

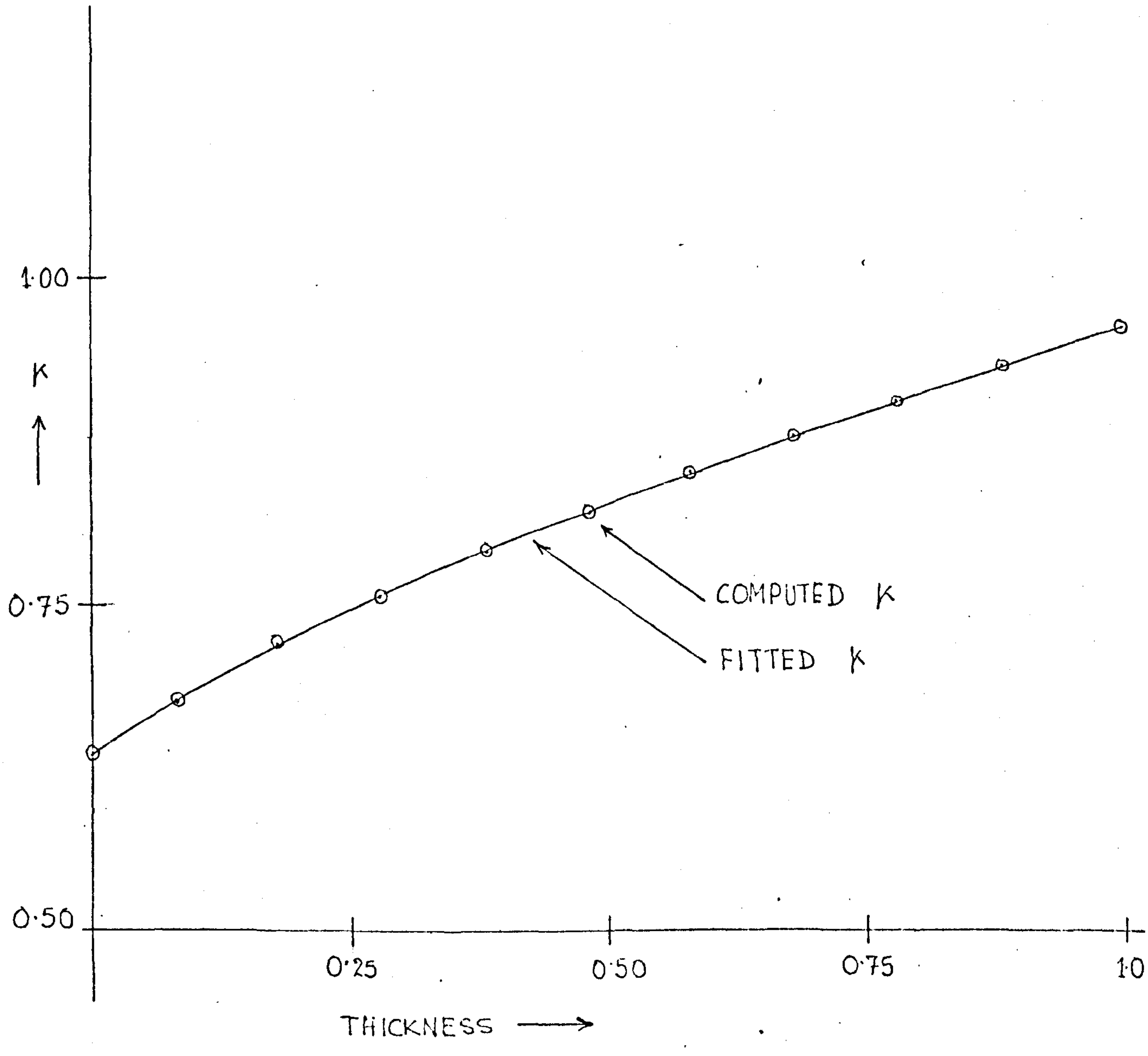

Fig.14

CAPACITY OF THICK CIRCULAR DISCS

CHAPTER 12

ELECTROSTATIC CAPACITY OF A CUBE

Division of surface into sub-areas

We choose a cartesian co-ordinate system so that the six faces of the cube have the equations

$$x = \pm a/2, \; y = \pm a/2 \quad \text{and} \quad z = \pm a/2.$$

As in the case of a square plate, each face of the cube is divided into

$$N_1 = k^2$$

square sub-areas where k is always an odd integer. The total number of sub-areas on the surface ∂B of the cube is

$$N = 6 N_1 = 6 k^2 . \tag{156}$$

Dirichlet Formulation

Let an equilibrium charge distribution λ on ∂B generate a potential V = 1 on ∂B. Hence λ satisfies the equation (111) i.e.

$$\int_{\partial B} \frac{\lambda(\underline{q})\, dq}{|\underline{p}-\underline{q}|} = 1 \quad .$$

on discretisation, as before, equation (111) gives N linear algebraic equations for the N unknown λ_j viz.

$$\sum_{j=1}^{N} \lambda_j \int_j \frac{dq}{|\underline{q}_k - \underline{q}|} = 1 \quad ; \quad k = 1, 2, 3 \cdots N ,$$

which is of the form

$$\sum_{j=1}^{N} a_{kj} \lambda_j = 1 , \qquad k = 1, 2, 3 \cdots N .$$

The co-efficients a_{kj} are evaluated, as before, by the centroid method of approximation when $k \neq j$. When $k = j$, the diagonal elements a_{kk} , for a square sub-area of edge length h, is given by (Appendix I)

$$a_{kk} = 4\, h \log (1 + \sqrt{2})$$

By symmetry, the N equations reduce to N* independent equations, where, from (120),

$$N^* = (k+1)(k+3)/8 \quad . \tag{157}$$

The equations are then solved by the Gauss-Seidel iterative method with $\epsilon = 0{\cdot}0001$ and the capacity K is then computed by (114). The capacity of the unit cube, computed for an increasing N is given in Table 19. The optimum N occurs at N = 1014, since the density λ_0 at the centre of a face has remained constant to the three preceding values of N. At this stage, $K = 0{\cdot}6595$.

The upper and the lower bounds for the capacity, determined by Polya and Szego, are

$$0{\cdot}6221\,a < K < 0{\cdot}7106\,a \quad .$$

Our value of K lies well within the bounds given above. The charge density at the centre of any face is approximately

$$\lambda_0 = 0{\cdot}0687 \quad .$$

Neumann Formulation

If the density distribution σ of (2) produces a constant potential on ∂B, then from (20) of Chapter 2

$$-\tfrac{1}{2}\sigma(\underset{\sim}{p}) + \int_{\partial B} G_i^{\prime}(\underset{\sim}{p},\underset{\sim}{q})\,\sigma(\underset{\sim}{q})\,dq = 0 \quad . \tag{158}$$

On discretisation, (158) gives N linear algebraic equations in N unknown σ_j which can be represented by (67) with $\phi_i^{\prime} = 0$ viz.

$$\left[B\right]\left[\sigma\right] = 0 \quad . \tag{159}$$

$[B]$ in (159) is a singular matrix, and the co-efficients b_{kj} are evaluated as in Chapter 5. As before, the N equations reduce to N* independent equations. To solve these equations we delete the N* th row, and we put $\sigma_{N^*} = 1$ in the N*th column. Hence (159) reduces to a system of N^*-1 equations in unknown ratios

$$X_j = \frac{\sigma_j}{\sigma_{N^*}} \quad ; \qquad j = 1, 2 \cdots (N^*-1) \quad . \tag{160}$$

CAPCITY OF A UNIT CUBE BY SOLVING DIRICHLET PROBLEM

SUB-AREA N	EQUATION N^*	DENSITY AT THE CENTRE OF THE FACE	CAPACITY
150	6	0·0691	0·65384292
294	10	0·0691	0·65677327
486	15	0·0687	0·65819403
726	21	0·0687	0·65899621
1014	28	0·0687	0·65945535
1350	36	0·0684	0·65977961

Table 19

Equation (159) now reduces to

$$\sum_{j=1}^{N^*-1} b_{kj} x_j = -b_{kN^*} \quad , \quad k = 1, 2 \cdots (N^*-1) \ , \tag{161}$$

and are solved by the Gauss-Seidel iterative method with $\epsilon = 0{\cdot}0001$.

The Neumann formulation (158) does not immediately give the capacity, since it only provides the relative charge density. However we know that if a conductor ∂B is raised to a constant potential V = c by a charge distribution σ on ∂B, then

$$\int_{\partial B} G(\underline{p}, \underline{q}) \sigma(\underline{q}) dq = C$$

so that

$$K = \frac{1}{C} \int_{\partial B} \sigma(\underline{q}) dq \ . \tag{162}$$

The numerical σ_j do not generate a constant V on ∂B. We therefore define

$$C = \left(\sum_{j=1}^{N} V_j \right) \Big/ N \ .$$

Putting this value of c in (162), we obtain K. The values of K thus found, for increasing N are exhibited in Table 20. By contrast with the Dirichlet formulation, no ill-conditioning appeared even at N = 2166. The capacity of the unit cube obtained by the Neumann formulation is

$$K \ (\text{Neumann}) = 0{\cdot}6475 \ ,$$

and that obtained by Dirichlet formulation is

$$K \ (\text{Dirichlet}) = 0{\cdot}6595 \ .$$

Each value is well within the bounds given by Polya and Szego . K (Neumann) appears to lie midway between the bounds whereas K (Dirichlet) lies close to the upper bound.

An alternative comparison with the Dirichlet formulation is possible. We scale the Neumann computed σ_j by a factor f so that

$$\int_{\partial B} f \ \sigma(\underline{q}) dq = f \int_{\partial B} \sigma(\underline{q}) dq = K \ (\text{Dirichlet}) \tag{163}$$

From (163),

$$\lambda \left(\text{Neumann}\right) = f \ \sigma \ . \tag{164}$$

CAPACITY OF A UNIT CUBE BY SOLVING NEUMANN PROBLEM

SUB-AREA N	EQUATION N^*	AVERAGE POTENTIAL C	TOTAL RATIO CHARGES	CAPACITY DIRCHLET	CAPACITY NEUMANN
294	10	4·80998	3·07528	0·65677	0·63935
486	15	4·07314	2·61327	0·65819	0·64159
726	21	3·54252	2·27895	0·65899	0·64331
1014	28	3·13809	2·02308	0·65946	0·64469
1350	36	2·81929	1·82072	0·65978	0·64581
1534	45	2·56049	1·65599	0·66001	0·64675
2166	55	2·33703	1·51328	- (-ve density appears)	0·64752

Table 20

This allows us to compare the charge densities yielding the same κ .

Table 21 exhibits the value of λ obtained from both formulations for N = 1014. The two solutions are in good agreement with one another except at the nodal points near the sharp edge and the corner of the cube.

COMPARISON OF DENSITY DISTRIBUTION ON THE SURFACE $z = 0\cdot5$

FIELD POINT		DENSITY	
X	Y	Dirichlet	Neumann
ALONG A DIAGONAL ON A FACE			
0·0	0·0	0·069	0·073
0·077	0·077	0·070	0·074
0·154	0·154	0·073	0·077
0·231	0·231	0·080	0·084
0·308	0·308	0·092	0·098
0·385	0·385	0·114	0·129
0·462	0·462	0·272	0·326
ALONG THE NODAL POINTS OF THE SUB-AREAS COMPRISING ANY OUTERMOST ROWS ON A FACE			
0·462	0·0	0·154	0·150
0·462	0·077	0·155	0·151
0·462	0·154	0·158	0·154
0·462	0·231	0·163	0·160
0·462	0·308	0·173	0·170
0·462	0·385	0·189	0·194
0·462	0·462	0·272	0·326

Table 21

PART IV

POTENTIAL FLOW OF A FLUID

CHAPTER 13

SUMMARY OF FORMULATIONS

Introduction

It has been shown in (57), Chapter 4, that for uniform potential flow perturbed by a fixed obstacle B, the disturbance potential ϕ can be generated by a simple source distribution of density σ on ∂B, i.e.

$$\phi(\underset{\sim}{p}) = \int_{\partial B} G(\underset{\sim}{p},\underset{\sim}{q})\,\sigma(\underset{\sim}{q})\,dq \quad ; \quad \underset{\sim}{p} \in B_e + \partial B \; . \tag{165}$$

The free flow potential ψ, by (54) of Chapter 4, is

$$\psi = -\underset{\sim}{U}\cdot\underset{\sim}{r} + c \tag{166}$$

where $\underset{\sim}{U}$ is the free flow velocity vector and c is an additive constant which does not affect the flow. The distribution σ in (165) satisfies the normal derivative equation

$$-2\pi\sigma(\underset{\sim}{p}) + \int_{\partial B} \frac{\sigma(\underset{\sim}{q})\,dq}{{}^{\prime}_{e}|\underset{\sim}{p}-\underset{\sim}{q}|} = \phi^{\prime}_{e}(\underset{\sim}{p}) \quad ; \quad \underset{\sim}{p} \in \partial B \; , \tag{167}$$

in which $\phi^{\prime}_{e}(\underset{\sim}{p})$ is given by (55), i.e.

$$\phi^{\prime}_{e}(\underset{\sim}{p}) = -\psi^{\prime}_{e}(\underset{\sim}{p}) \quad ; \quad \underset{\sim}{p} \in \partial B \quad . \tag{168}$$

It has already been shown in Chapter 2 that equation (167) has a unique solution σ which generates ϕ everywhere (including the surface ∂B) as the simple source potential

$$\phi(\underset{\sim}{p}) = \int_{\partial B} \frac{\sigma(\underset{\sim}{q})\,dq}{|\underset{\sim}{p}-\underset{\sim}{q}|} \quad . \tag{169}$$

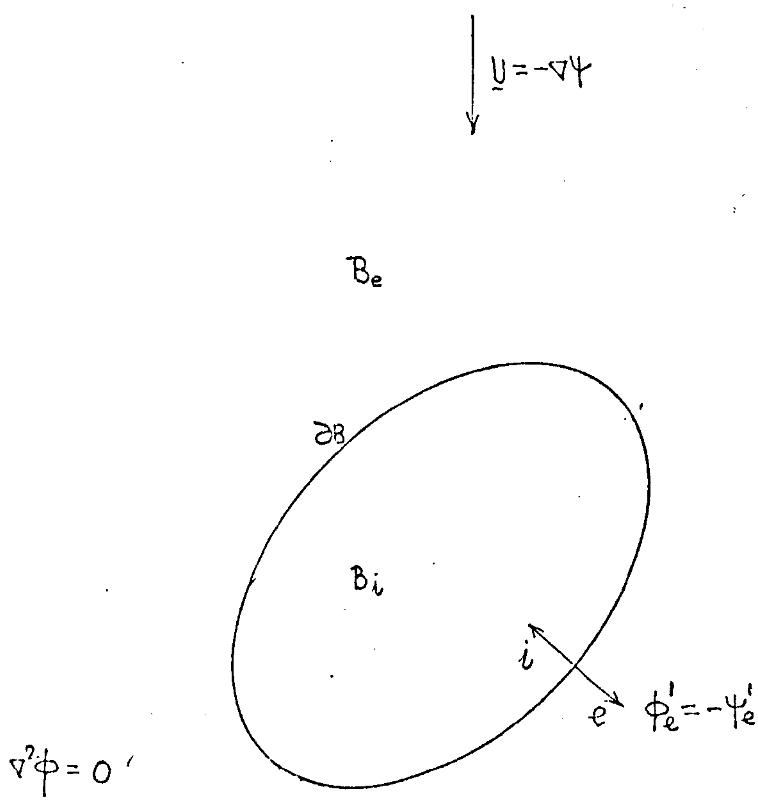

Fig. 15

FLOW PAST A FIXED BOUNDARY

Discretising, by Chapter 5,(167) becomes

$$-2\pi\sigma_k + \sum_{j=1}^{N} \sigma_j \int_j \frac{dq}{|q_k - q|} = \phi_e'(q_k) \; ; \; k = 1, 2, \cdots N \,, \tag{170}$$

and the computed σ_j generate ϕ according to the formula[10]

$$\phi(p) = \sum_{j=1}^{N} \sigma_j \int_j \frac{dq}{|p - q|} \quad . \tag{171}$$

Alternatively, utilising Green's boundary formula[11,12] (60) of Chapter 4, ϕ satisfies

$$-2\pi\phi(p) + \int_{\partial B} \frac{\phi(q)}{|p - q|_e'} dq = \int_{\partial B} \frac{\phi_e'(q)}{|p - q|} dq \; ; \; p, q \in \partial B \,. \tag{172}$$

It has been shown in (36), Chapter 2, that equation (172) has a unique solution ϕ on ∂B. On discretisation, by Chapter 5, (172) becomes

$$-2\pi\phi(q_k) + \sum_{j=1}^{N} \phi(q_j) \int_j \frac{dq}{|q_k - q|_e'} = \sum_{j=1}^{N} \phi_e'(q_j) \int_j \frac{dq}{|q_k - q|} \; ; \; k = 1, 2, \cdots N \,. \tag{173}$$

The tangential velocity v at a point p on ∂B is given by

$$v(p) = \left[\left(-\frac{\partial \Phi}{\partial s_1}\right)^2 + \left(-\frac{\partial \Phi}{\partial s_2}\right)^2 \right]^{\frac{1}{2}} \,, \tag{174}$$

where $\Phi = \phi + \Psi$ and s_1, s_2 are arc lengths along two mutually perpendicular tangential directions at $p \in \partial B$. When Φ is determined at discrete equidistant points along s_1, the tangential velocity[13] component along s_1 at $q_{j+\frac{1}{2}}$ is given by

$$v_1(q_{j+\frac{1}{2}}) = -\frac{1}{h_1}\left[\delta_1^1 - \frac{1}{24}\delta_1^3 + \frac{3}{640}\delta_1^5 - \cdots \right] \,, \tag{175}$$

where $q_{j+\frac{1}{2}}$ is the mid point between q_j and q_{j+1} ; δ_1^r is the difference of order r in a central difference table for Φ , and h_1 is the distance between any two equally spaced consecutive points along s_1 on ∂B i.e.,

$$h_1 = \left| q_{j+1} - q_j \right| .$$

Axial Flow Past A Symmetric Body

Let ∂B be an axially symmetric surface, and suppose the free flow is parallel to its axis of revolution. Let us now divide ∂B into 2K rings such that the plane of each ring is perpendicular to the axis of flow, and for a ring in the upper part of ∂B there is a ring of equal width in the lower part of ∂B. If p and $\bar{p}$ represent one such pair of rings in which p lies in the upper part and $\bar{p}$ lies in the lower part of ∂B (Fig. 16), the serial number of $\bar{p}$, counting from the top, is given by

$$\bar{p} = 2K - p + 1 \quad . \tag{176}$$

Similarly for a pair $q, \bar{q}$

$$\bar{q} = 2K - q + 1 \quad .$$

Since the plane of the rings are perpendicular to the direction of flow, at the nodal points in the p th ring σ and ϕ satisfy

$$(\phi)_p = (\phi_j)_p \; , \; (\phi')_p = (\phi'_j)_p \;\text{ and }\; (\sigma)_p = (\sigma_j)_p \; ; \; j = 1, \cdots MK(p) , \tag{177}$$

where MK(p) is the number of sub-areas in the p th ring.

(a) Simple Source Formulation

By virtue of (177), the N equations (170) for the N unknown σ_j reduce to 2K equations viz.

$$\sum_{q=1}^{2K} E_{pq} (\sigma)_q = (\phi'_e)_p \quad ; \quad p = 1, 2, \cdots 2K . \tag{178}$$

In (178) $(\sigma)_q$ is the discrete approximation to σ at any nodal point in the q th ring; $(\phi'_e)_p$ represents the exterior normal derivative of ϕ at any nodal

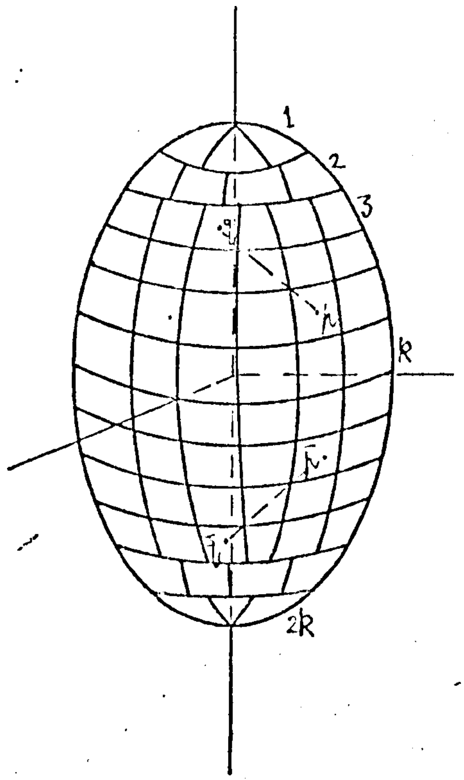

FIG. 16

SUB-AREAS ON THE SURFACE OF A SPHERE

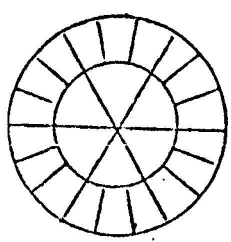

SUB AREAS AT THE TOP

FIG. 16(a)

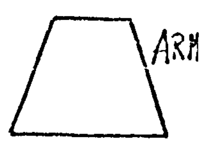

FIG. 16(b)

point in the p th ring, and E_{pq} stands for

$$E_{pq} = \sum_{j=1}^{MK(q)} \int_j \frac{dq}{{}_e^1|\underset{\sim}{p}-\underset{\sim}{q}|} \quad , \qquad q \neq p$$

$$= -2\pi + \sum_{j=1}^{MK(q)} \int_j \frac{dq}{{}_e^1|\underset{\sim}{p}-\underset{\sim}{q}|} \quad , \quad q = p$$

where $\underset{\sim}{p}$ is any nodal point in the p th ring.

If we take the Z-axis as the axis of flow, then for a pivotal point (X,Y,Z) in the p th ring there is a pivotal point (X,Y,-Z) in the $\bar{p}$ th ring on ∂B. Hence

$$E_{pq} = \int_q \frac{dq}{{}^1|\underset{\sim}{p}-\underset{\sim}{q}|} \quad , \qquad \text{over the q th ring}$$

$$= \int_{\bar{q}} \frac{d\bar{q}}{{}^1|\underset{\sim}{\bar{p}}-\underset{\sim}{\bar{q}}|} \quad , \qquad \text{over the } \bar{q} \text{ th ring}$$

$$= E_{\bar{p}\bar{q}} = E_{2K-p+1 \;\; 2K-q+1} \tag{179}$$

and $$(\phi^1)_p = -(\phi^1)_{\bar{p}} = -(\phi^1)_{2k-p+1} . \tag{180}$$

Further it is interesting to note that

$$E_{qp} = \int_p \frac{dp}{{}_e^1|\underset{\sim}{q}-\underset{\sim}{p}|} \neq \int_q \frac{dq}{{}_e^1|\underset{\sim}{p}-\underset{\sim}{q}|} = E_{pq} . \tag{181}$$

By virtue of (179) and (180), the system of equations (178) becomes

$$\begin{bmatrix} E_{11} & E_{12} & \cdots & E_{1K} & E_{1\,K+1} & \cdots & E_{1\,2K} \\ E_{21} & E_{22} & \cdots & E_{2K} & E_{2\,K+1} & \cdots & E_{1\,2K} \\ \vdots & \vdots & & \vdots & \vdots & & \vdots \\ E_{K1} & E_{K2} & \cdots & E_{KK} & E_{K\,K+1} & \cdots & E_{K\,2K} \\ E_{K\,2K} & E_{K\,2K-1} & \cdots & E_{K\,K+1} & E_{K\,K} & \cdots & E_{K\,1} \\ \vdots & \vdots & & \vdots & \vdots & & \vdots \\ E_{2\,2K} & E_{2\,2K-1} & \cdots & E_{2\,K+1} & E_{2K} & \cdots & E_{21} \\ E_{1\,2K} & E_{1\,2K-1} & \cdots & E_{1\,K+1} & E_{1K} & \cdots & E_{11} \end{bmatrix} \begin{bmatrix} (\sigma)_1 \\ (\sigma)_2 \\ \vdots \\ (\sigma)_K \\ (\sigma)_{K+1} \\ \vdots \\ (\sigma)_{2K-1} \\ (\sigma)_{2K} \end{bmatrix} = \begin{bmatrix} (\phi_e')_1 \\ (\phi_e')_2 \\ \vdots \\ (\phi_e')_K \\ -(\phi_e')_{K+1} \\ \vdots \\ -(\phi_e')_2 \\ -(\phi_e')_1 \end{bmatrix} . \quad (182)$$

The solution of (182) has the property (Appendix III)

$$(\sigma)_p = -(\sigma)_{2K-p+1} \quad ; \quad p = 1, 2, \cdots K . \qquad (183)$$

Hence (182) reduces to K equations viz.

$$\sum_{q=1}^{K} \left(E_{pq} - E_{p\;2K-q+1} \right) (\sigma)_q = (\phi_e')_p \quad ; \quad p = 1, 2, \cdots K . \qquad (184)$$

From (183) we see that for every positive source on ∂B there is a negative source of equal strength on ∂B and hence, in accordance with (59), the total source strength on ∂B is zero.

(b) Green's boundary formula

For a free flow parallel to the axis of revolution of a symmetric surface ∂B, the distrubance potential ϕ in every ring, shown earlier, satisfies relation (177). As a result the N equations (173), as before, reduce to 2K equations given by

$$\sum_{q=1}^{2K} H_{pq} (\phi)_q = D_p \quad ; \quad p = 1, 2, \cdots 2K \ , \tag{185}$$

where

$$H_{pq} = \sum_{j=1}^{MK(q)} \int_j \frac{dq}{|\underline{p}-\underline{q}|_e'} \quad ; \qquad q \neq p$$

$$= -2\pi + \sum_{j=1}^{MK(q)} \int_j \frac{dq}{|\underline{p}-\underline{q}|_e'} \ ; \quad q = p$$

and
$$D_p = \sum_{q=1}^{2K} (\phi_e')_q \int_q \frac{dq}{|\underline{p}-\underline{q}|} = \sum_{q=1}^{2K} (\phi_e')_q \sum_{j=1}^{MK(q)} \int_j \frac{dq}{|\underline{p}-\underline{q}|} \ .$$

As in the previous case, following the same procedures, it can be shown that

$$H_{pq} = H_{\bar{p}\bar{q}} = H_{2K-p+1 \ \ 2K-q+1} \tag{186}$$

and
$$D_p = -D_{\bar{p}} = -D_{2K-p+1} \ . \tag{187}$$

By virtue of the above results, the 2K equations in (185), as before, reduce to K equations viz.

$$\sum_{q=1}^{K} \left(H_{pq} - H_{p \ 2K-q+1} \right) (\phi)_q = D_p \quad ; \ p = 1, 2 \cdots K \ . \tag{188}$$

Test Function

It has already been shown that the approximation to an integral, over a given surface ∂B, approaches the analytic value as the number of sub-areas increases on ∂B. Further, by our fundamental assumption, the density distribution over a surface approaches its true value as the sizes of the sub-areas decrease and their number increases. Now the question arises what should be the minimum number of sub-areas, along with their respective sizes on ∂B, which will produce a sound value of the unknown on ∂B. Accordingly we first find a distribution of sub-areas on ∂B which will generate a test harmonic function h of the same nature as the required function ϕ .

The disturbance potential ϕ has the property

$$\phi = O|\underset{\sim}{r}|^{-2} \quad \text{as} \quad |\underset{\sim}{r}| \to \infty \quad .$$

Hence a comparable test function is

$$h = \frac{-\underset{\sim}{r} \cdot \hat{U}}{|\underset{\sim}{r}|^3} \quad , \tag{189}$$

where $\hat{U}$ defines a unit vector in the direction of the flow and h is a harmonic function with right behaviour at infinity i.e.

$$h = O|\underset{\sim}{r}|^{-2} \quad \text{as} \quad |\underset{\sim}{r}| \to \infty \quad .$$

The test function has been very useful in experimenting with the subdivision of ∂B and with our discretisation procedures.

CHAPTER 14

FLOW PAST A SPHERE

Introduction

A rigid sphere of radius 'a' is fixed with its centre at the origin O of spherical polar co-ordinates (Fig. 17). An inviscid incompressible fluid is flowing from infinity with uniform velocity $\underset{\sim}{U}$ given by

$$\underset{\sim}{U} = (0, 0, -U) = -\nabla\psi \quad , \tag{190}$$

where ψ is the free flow potential, and hence

$$\psi = Uz \quad , \tag{191}$$

taking the constant of integration to be zero. As already noticed in Chapter 4, the disturbance potential ϕ behaves as $O|\underset{\sim}{p}|^{-2}$ as $p \to \infty$, satisfies

$$\nabla^2\phi(\underset{\sim}{p}) = 0 \quad ; \quad \underset{\sim}{p} \in B_e \tag{192}$$

and on ∂B satisfies the boundary condition

$$\phi_e'(\underset{\sim}{p}) = -\psi_e'(\underset{\sim}{p}) = -U(z)_e' = -U\cos\Theta \ . \tag{193}$$

The solution[3] of (192) subject to boundary condition (193), in spherical polar co-ordinates, is

$$\phi = \frac{1}{2}\frac{Ua^3z}{r^3} \ . \tag{194}$$

The total velocity potential Φ, by (53), is

$$\Phi = \phi + \psi = \frac{1}{2}\frac{Ua^3z}{r^3} + Uz \ . \tag{195}$$

The fluid velocity on the surface of the sphere, by symmetry, is in the Θ increasing direction. This is given by

$$v_\theta = -\frac{1}{r}\frac{\partial\Phi}{\partial\theta} = \frac{1}{2}Ua\sin\theta + Ua\sin\theta = \frac{3}{2}Ua\sin\theta \ . \tag{196}$$

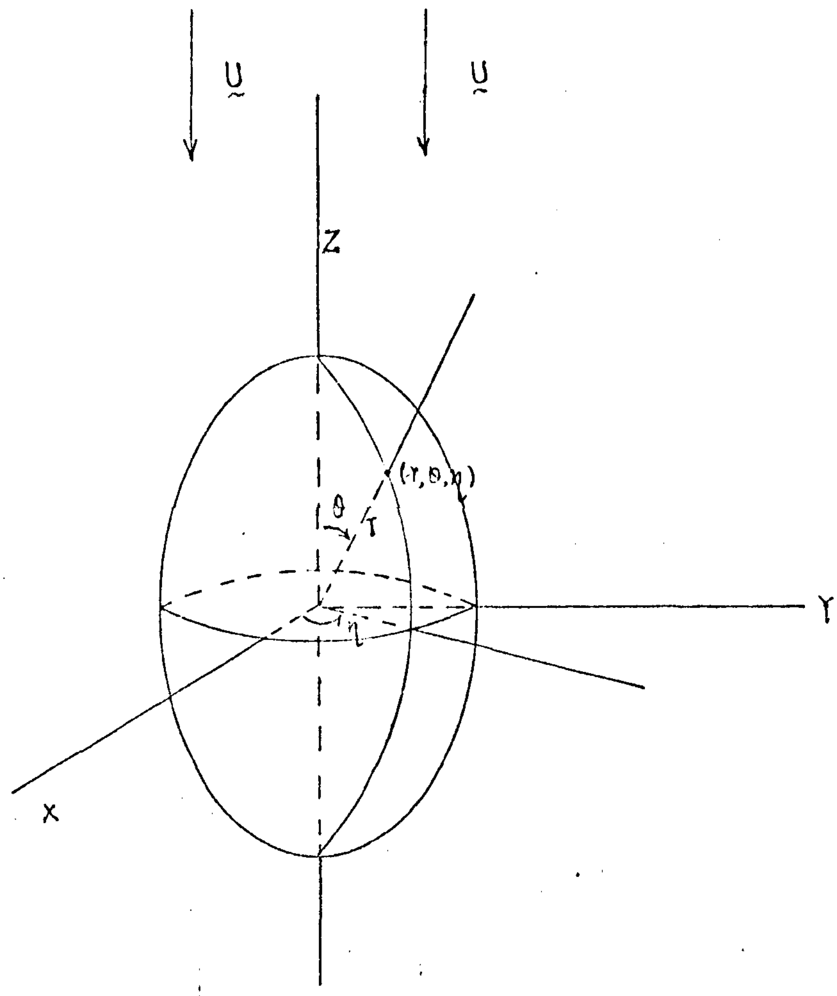

Fig. 17

FLOW PAST A FIXED SPHERE

Our aim is to compute an accurate approximation to (194) using the formulation of the last Chapter. Since the analytical solution of the problem is known, we have a chance to test the soundness of our numerical and geometrical procedures by obtaining a numerical solution for comparison with (194), taking a = 1. Since

$$\phi = \frac{1}{2}\frac{Ua^3 z}{r^3} = \frac{1}{2}\frac{z}{r^3} \quad \text{(taking } U = 1,\ a = 1\text{)} \tag{197}$$

$\phi_e'(\underset{\sim}{p})$ on ∂B is given by

$$\phi_e'(p) = \nabla\phi \cdot \hat{n}_e$$

$$= -\frac{1}{2}\left[\frac{3zx}{r^5}\ ,\ \frac{3yz}{r^5}\ ,\left(\frac{3z^2}{r^5} - \frac{1}{r^3}\right)\right]\cdot(x,y,z)\,a^{-1}$$

$$= -\frac{1}{2}\ \frac{2z}{r^3}\,a^{-1} = -\frac{1}{a}\ \frac{\cos\theta}{r^2} = -\cos\theta \quad (\because\ a = 1 \text{ and } r = 1 \text{ on } \partial B)$$

$$= -\psi_e'(\underset{\sim}{p}) \quad \left[\text{ by } (168)\right], \tag{198}$$

where $\hat{n}_e = (x,y,z)a^{-1}$ at $\underset{\sim}{p} \in \partial B$. Introducing (198) in (172), Green's Boundary Formula (Jaswon)[11,12] defines an equation for ϕ on ∂B with exact solution (197). Alternatively, introducing (198) in (167) the Simple Source Formulation (A.M.O. Smith)[10] defines an equation for σ with exact solution*

$$\sigma = \frac{3\cos\theta}{8\pi}. \tag{199}$$

This σ, by (165), generates ϕ in (197).

---

* $$-4\pi\sigma = \phi_e' + \phi_i' = \frac{1}{2}\left[\left(\frac{z}{r^3}\right)_e' + z_i'\right]_{r=a=1}$$

$$= \frac{1}{2}\left[\frac{d}{dr}\left(\frac{\cos\theta}{r^2}\right) - \frac{d}{dr}(r\cos\theta)\right]_{r=1} = -\frac{3}{2}\cos\theta\ .$$

$$\therefore \quad \sigma = \frac{3\cos\theta}{8\pi}.$$

Division of the surface into sub-areas

To solve the equations (167) and (172) numerically, the surface ∂B is to be divided into sub-areas. The upper half of the spherical surface $x^2 + y^2 + z^2 = a^2$ is divided into K horizontal rings. Each of the 1st KN($<$ K) rings, starting from the pole, is divided into MK_j equal sub-areas by MK_j meridian line segments where MK_j is given by

$$MK_j = 6\left[1+(j-1)2\right], \quad j = 1, 2, \cdots KN .$$

Starting from (KN + 1) up to the K th ring, each ring is divided into M equal sub-areas where

$$M = MK_j = 6(1+2KN) \; ; \quad j = (KN+1), \cdots K .$$

The total number of rings on the upper hemispherical surface is given by

$$K = KN + KT = KN + \left(\frac{M+2}{4}\right) = 4KN + 2 . \tag{200}$$

Any half meridian is divided into K equal parts to give the height h_k of a trapezoidal sub-area (Fig. 16) adjacent to the equatorial line which is divided into M equal parts to give the breadth b_k of the same sub-area. From the above, the ratio $h_k : b_k$ is given by

$$r = \frac{h_k}{b_k} = \frac{\frac{\pi a}{2}/2(2KN+1)}{2\pi a/6(2KN+1)} = \frac{3}{4} ,$$

where ideally r = 1 (see Chapter 6). If h_k is increased keeping b_k fixed and vice versa, the form of the trapezoidal sub-areas near the polar region deviates from the ideal form. This justifies the value of K chosen in (200).

If $d\phi_j$ be the angle between any two consecutive meridian line segments in the j th ring, then

$$d\phi_j = \frac{2\pi}{MK_j} \; ; \quad j = 1, 2, \cdots K .$$

The width of the 1st ring is tentatively taken to be ℓ_1 where

$$\ell_1 = \left(\frac{\pi a}{2}/KT\right)\Delta_1 \; ; \quad 1 < \Delta_1 < 2 .$$

This subtends an angle θ_1 at the centre of the sphere where

$$\theta_1 = \ell_1 a^{-1} .$$

The width of the j th ring is given by

$$\ell_j = \Delta_j \left(a \sin\theta_{j-1}\right) d\phi_j \; ; \quad j = 2, 3, \cdots KN ,$$

where $\theta_j = l_j a^{-1}$ and $1 < \Delta_j < 2$. Normally Δ_j is kept fixed at 1·5. From the (KN + 1) th up to the K th ring, the width of a sub-area is given by

$$l_{KN+j} = D + j(UT) \; ; \; j = 1, 2 \cdots KT ,$$

where
$$D = \frac{3}{2} a \left(\sin \theta_{KN} \right) d\phi_{KN+1}$$

and
$$UT = \left\{ a \left(\frac{\pi}{2} - \theta_{KN} \right) - (KT) D \right\} \Big/ \left\{ KT (KT+1)/2 \right\} .$$

The total number of sub-areas is

$$N = 2 \left[6 \left\{ \frac{KN}{2} \left(2 + \overline{KN-1} \; 2 \right) \right\} + M(KT) \right]$$

$$= 12 \left(7 \, KN^2 + 7 \, KN + 2 \right) . \tag{201}$$

The analysis of the sub-areas thus formed, for KN = 5, is given in Table 22. It is evident from this Table that:

(1) The sides of the triangular sub-areas adjacent to the pole are nearly equal.

(2) From the 2nd up to the KN th ring the width of any sub-area is nearly 1·5 times its average breadth.

(3) The change in the size of the sub-areas, as we move from the top to the equatorial line, follows a continuous pattern.

Computation of Disturbance Potential

Now we proceed to solve the equations (167) and (172) numerically. Dealing first with the Simple Source Formulation (167), we find, on discretisation, that this gives (170), a system of N linear algebraic equations in N unknown σ_j. From symmetry of ∂B and for relation (180), the N equations reduce to K equations given by (184). The co-efficients E_{pq} are evaluated as discussed in Chapter 5 and the equations are then solved by the Gauss-Seidel iterative method with ϵ = 0·0001.

ANALYSIS OF SUB-AREAS ON A SPHERICAL SURFACE

RING	SUB-AREA	AREA	UPPER SIDE AB	LOWER SIDE CD	ARM AD
1	6	0.12893E-01	0.00000E 00	0.16382E 00	0.15708E 00
2	18	0.71676E-02	0.54606E-01	0.88728E-01	0.99929E-01
3	30	0.56405E-02	0.53237E-01	0.71326E-01	0.90503E-01
4	42	0.48543E-02	0.50947E-01	0.62751E-01	0.85337E-01
5	54	0.42684E-02	0.48806E-01	0.57145E-01	0.80530E-01
6	66	0.39215E-02	0.46755E-01	0.53113E-01	0.78493E-01
7	66	0.42877E-02	0.53113E-01	0.58993E-01	0.76457E-01
20	66	0.47242E-02	0.94217E-01	0.94781E 01	0.49982E-01
21	66	0.45528E-02	0.94781E-01	0.95099E-01	0.47945E-01
22	66	0.43689E-02	0.95099E-01	0.95200E-01	0.45908E-01

Table 22

(This should be read in conjunction with Fig.16, Fig.16(a), Fig.16(b).)

The σ_j thus obtained satisfy the relation (183). These computed σ_j when used in (171), generate the required potential ϕ given by (197). Table 23 exhibits the computed σ (K = 46) compared with analytical σ given by (199). Table 24 exhibits the ϕ in (197), generated by the above σ_j, for the same value of K along with the analytical ϕ at the respective points on ∂B. Fig.18 exhibits the graphs of analytical and numerical σ based on Table 23.

The total velocity potential Φ is then obtained by (53) viz.

$$\Phi = \phi + \psi \quad , \tag{202}$$

where $\psi = Uz = z$ ($\because U = 1$). The graphs in Fig.19 exhibit ϕ and Φ, based on Table 24, on the upper hemispherical surface of the sphere.

In (172) ϕ_e^1 is given by (198). On discretisation, (172) gives N linear algebraic equations in N unknown $\phi(q_j)$. By virtue of the symmetry of ∂B and for (180), the N equations reduce to K equations given by (188). After evaluation of the H_{pq} and the D_p, of (188), the equations are solved by the Gauss-Seidel iterative method with $\epsilon = 0{\cdot}0001$. The $(\phi)_k$ thus obtained for K = 46, are exhibited in Table 24. The total potential Φ is then obtained by (202). The ϕ and the Φ thus obtained, for K = 46, are exhibited in Fig. 19.

Equipotentials

The σ which generates the required disturbance potential ϕ, for ϕ_e^1 given by (193), is obtained by solving the equation (167) numerically, as discussed earlier. These σ_j then generate the ϕ_k by (171) at any point $p \in B_e + \partial B$. The total velocity potential Φ is then obtained by (202).

For K = 46, the total potential Φ is then obtained at M^* points outside ∂B along with those at the nodal points, each lying on a separate ring, on the upper hemispherical part of ∂B. The equipotentials are then drawn from the K nodal points $\underset{\sim}{q}_1, \underset{\sim}{q}_2, \ldots \underset{\sim}{q}_K$ of ∂B through those points $\underset{\sim}{p}_j$ for which

$$|\Phi(\underset{\sim}{q}_m) - \Phi(\underset{\sim}{p}_j)| \leq 0{\cdot}001 \; ; \; \underset{\sim}{q}_m \in \partial B \, , \; j = 1, 2, \cdots (M^* + K) \, .$$

The equipotentials, thus found, are given in Fig. 20.

DISTRIBUTION OF SOURCE DENSITY ON A UNIT SPHERE

POLAR DISTANCE IN RADIAN	DENSITY σ	
	ANALYTICAL	NUMERICAL
0.041	0.11926	0.12073
0.179	0.11746	0.11835
0.290	0.11439	0.11512
0.390	0.11042	0.11105
0.484	0.10564	0.10623
0.579	0.09989	0.10053
0.675	0.09321	0.09387
0.771	0.08565	0.08629
0.867	0.07726	0.07787
0.964	0.06810	0.06867
1.061	0.05826	0.05876
1.159	0.04781	0.04824
1.257	0.03686	0.03719
1.356	0.02550	0.02573
1.455	0.01383	0.01396
1.554	0.00198	0.00199

Table 23

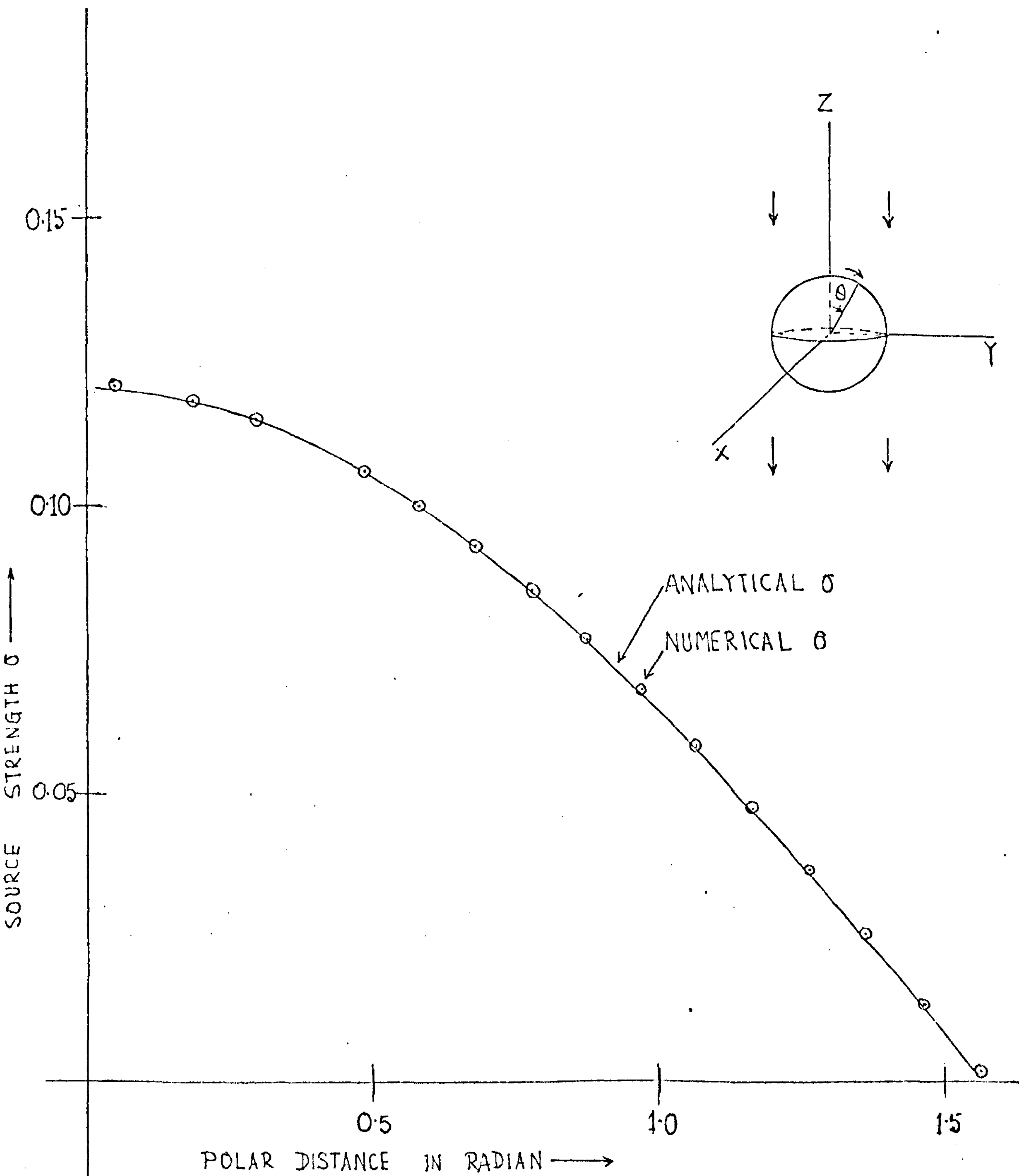

Fig. 18

SOURCE DISTRIBUTION ON THE SURFACE OF A SPHERE

GENERATION OF ϕ ON THE SURFACE OF A UNIT SPHERE

POLAR DISTANCE IN RADIAN	ANALYTIC ϕ	S.L.POTENTIAL (Smith)	%ERROR	G.B.FORMULA (Jaswon)	%ERROR
0.412E-01	0.49958E 00	0.50019E 00	0.124	0.50197E 00	0.478
0.956E-01	0.49772E 00	0.49917E 00	0.293	0.50009E 00	0.476
0.139E 00	0.49520E 00	0.49713E 00	0.389	0.49757E 00	0.478
0.179E 00	0.49201E 00	0.49414E 00	0.433	0.49435E 00	0.474
0.217E 00	0.48822E 00	0.48612E 00	0.449	0.49045E 00	0.457
0.643E 00	0.40020E 00	0.40195E 00	0.437	0.40186E 00	0.412
0.675E 00	0.39046E 00	0.39215E 00	0.433	0.39211E 00	0.423
0.707E 00	0.38030E 00	0.38194E 00	0.434	0.38194E 00	0.431
0.739E 00	0.36973E 00	0.37133E 00	0.433	0.37137E 00	0.441
0.771E 00	0.35877E 00	0.36033E 00	0.435	0.36039E 00	0.452
0.139E 01	0.90639E-01	0.91079E-01	0.485	0.91173E-01	0.589
0.142E 01	0.74345E-01	0.74707E-01	0.487	0.74785E-01	0.592
0.145E 01	0.57944E-01	0.58226E-01	0.487	0.58288E-01	0.594
0.149E 01	0.41453E-01	0.41655E-01	0.487	0.41700E-01	0.595
0.152E 01	0.24891E-01	0.25013E-01	0.486	0.25040E-01	0.598
0.155E 01	0.82761E-02	0.83163E-02	0.486	0.83255E-02	0.597

Table 24

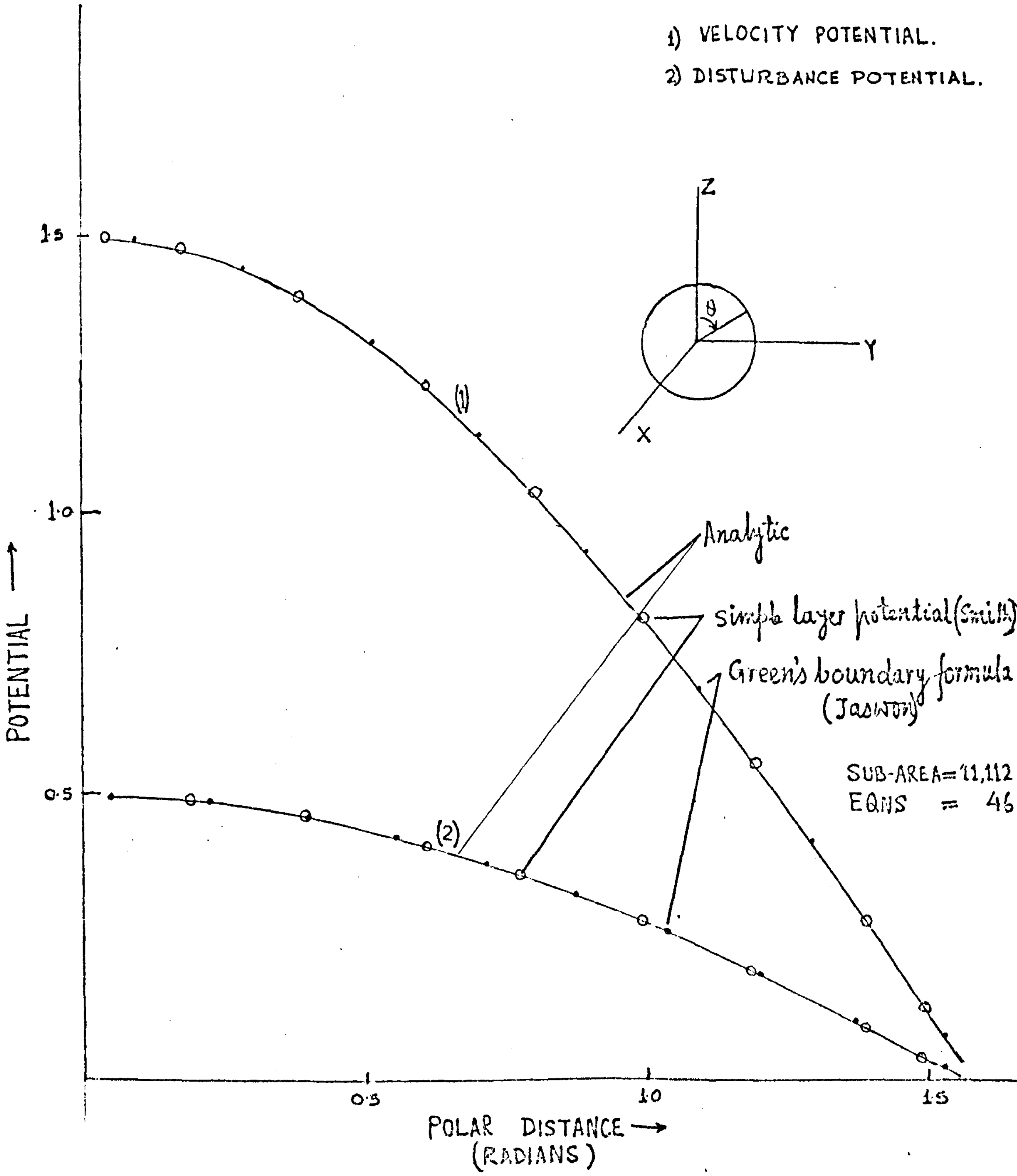
1) VELOCITY POTENTIAL.
2) DISTURBANCE POTENTIAL.
Z
θ
Y
X
1.5
1.0
0.5
POTENTIAL
(1)
(2)
Analytic
simple layer potential (Smith)
Green's boundary formula (Jaswon)
SUB-AREA = 11,112
EQNS = 46
0.5
1.0
1.5
POLAR DISTANCE
(RADIANS)

Fig. 19

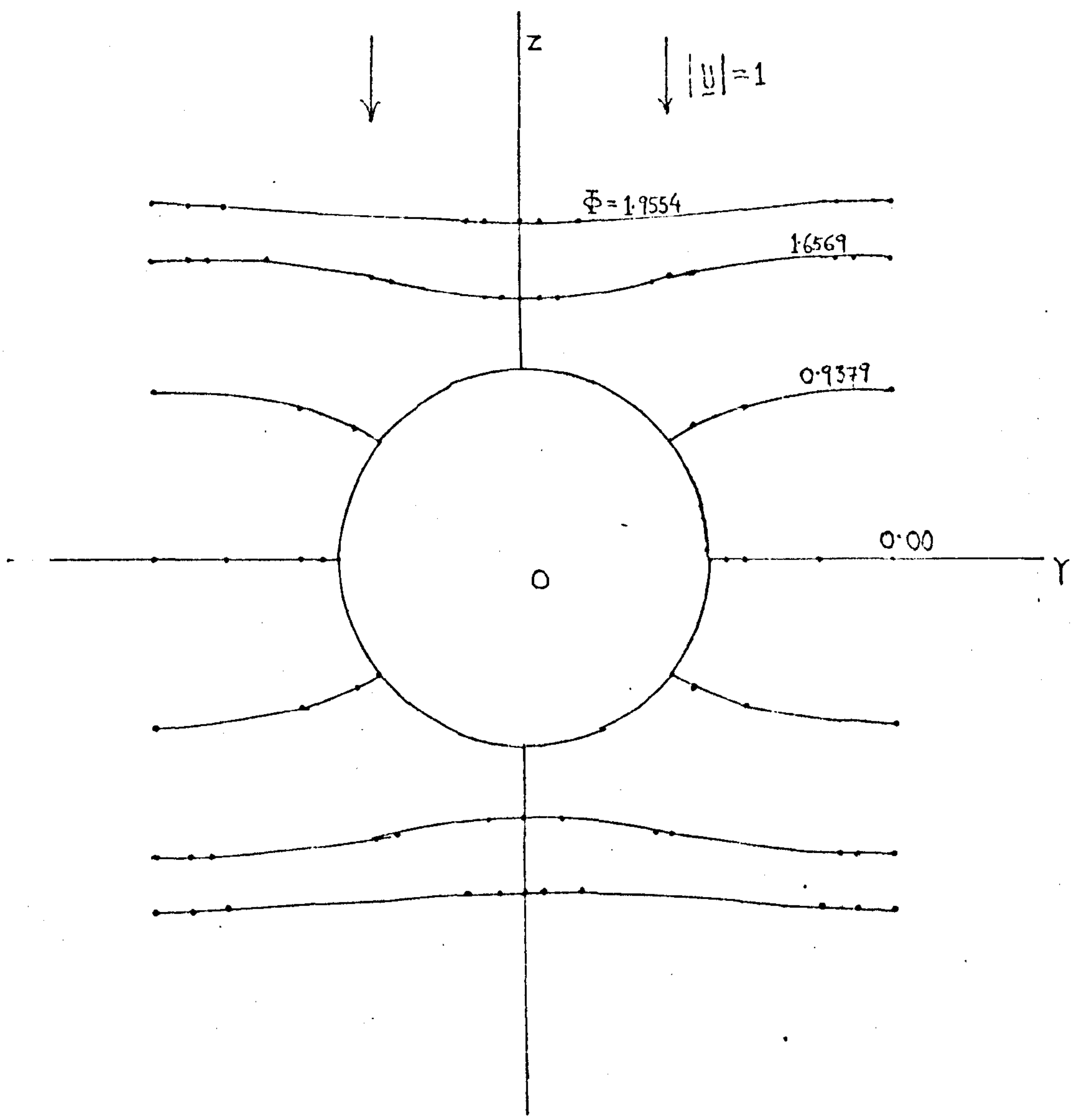

FIG.20

EQUIPOTENTIALS AROUND A FIXED SPHERE

Fluid velcoity on the surface

The analytical value of the fluid velocity at a point $\underset{\sim}{q} \in \partial B$, by (196), is

$$v_\theta(q) = \frac{3}{2} U a \sin\theta_q \tag{203}$$

where $U = 1$, $a = 1$ and θ_q represents the value of θ (Fig. 17) at the point $\underset{\sim}{q}$. The numerically computed value of the velocity at $\underset{\sim}{q}$ is found by (175), using the numerical Φ. Since the nodal points on ∂B are not equally spaced and the higher order δ is very small, the velocity component at $q \in \partial B$, in any direction S_1, is obtained by taking only the first term in (175) i.e.,

$$v_\theta(\underset{\sim}{q}) = -\frac{1}{h_1}\delta_1^1 \quad . \tag{204}$$

It has already been pointed out, that for symmetry, the flow on the surface is along the meridians on ∂B. The velocity at a point $q(= p_{j+\frac{1}{2}})$ on ∂B is determined by (204) from the numerical Φ given by (202), in which ϕ is obtained by Simple Source Formulation. Table 25 exhibits the v_θ thus obtained, for K = 46, along with the analytical v_θ at the respective points on ∂B. Similarly, v_θ is obtained from Φ in which ϕ is determined by Green's Boundary Formula under the same external condition and for the same sub-division of ∂B. The v_θ thus obtained are exhibited in Table 25. Fig.21 shows the velocity distribution on ∂B base on Table 25.

General Discussion

It is evident from Table 24 that both the formulations, i.e. Simple Source Distrubution (Smith) and Green's Boundary Formula (Jaswon), are capable of yielding a good approximation. In the case of a flow past a sphere, in this thesis, we obtained ϕ on ∂B by both the methods, in which the maximum error in ϕ at a nodal point on ∂B is $< 0{\cdot}6\%$. The error in ϕ, generated by the Simple Source Formulation is less than that in ϕ obtained by Green's Boundary Formula.

VELOCITY DISTRIBUTION ON THE SURFACE OF A UNIT SPHERE

POLAR DISTANCE IN RADIAN	ANALYTIC VELOCITY	FROM S.L.POTENTIAL (Smith)	%ERROR	FROM G.B.FORMULA (Jaswon)	%ERROR
0.684E-01	0.10257E 00	0.87146E-01	-0.150E 02	0.10291E 00	0.336E 00
0.117E 00	0.17533E 00	0.16434E 00	-0.627E 01	0.17534E 01	0.334E-02
0.159E 00	0.23724E 00	0.23233E 00	-0.207E 01	0.23823E 00	0.420E 00
0.198E 00	0.29540E 00	0.29369E 00	-0.582E 00	0.29813E 00	0.922E 00
0.236E 00	0.35060E 00	0.35025E 00	-0.101E 00	0.35401E 00	0.972E 00
0.659E 00	0.91819E 00	0.91970E 00	0.165E 00	0.91822E 00	0.331E-02
0.691E 00	0.95552E 00	0.95696E 00	0.150E 00	0.95566E 00	0.144E-01
0.723E 00	0.99195E 00	0.99333E 00	0.139E 00	0.99220E 00	0.256E-01
0.755E 00	0.10274E 01	0.10288E 01	0.131E 00	0.10278E 01	0.367E-01
0.787E 00	0.10618E 01	0.10632E 01	0.126E 00	0.10624E 01	0.477E-01
0.141E 01	0.14794E 01	0.14817E 01	0.155E 00	0.14822E 01	0.187E 00
0.144E 01	0.14868E 01	0.14891E 01	0.156E 00	0.14896E 01	0.190E 00
0.147E 01	0.14926E 01	0.14949E 01	0.157E 00	0.14954E 01	0.192E 00
0.150E 01	0.14967E 01	0.14991E 01	0.158E 00	0.14996E 01	0.194E 00
0.154E 01	0.14992E 01	0.15016E 01	0.158E 00	0.15021E 01	0.195E 00

Table 25

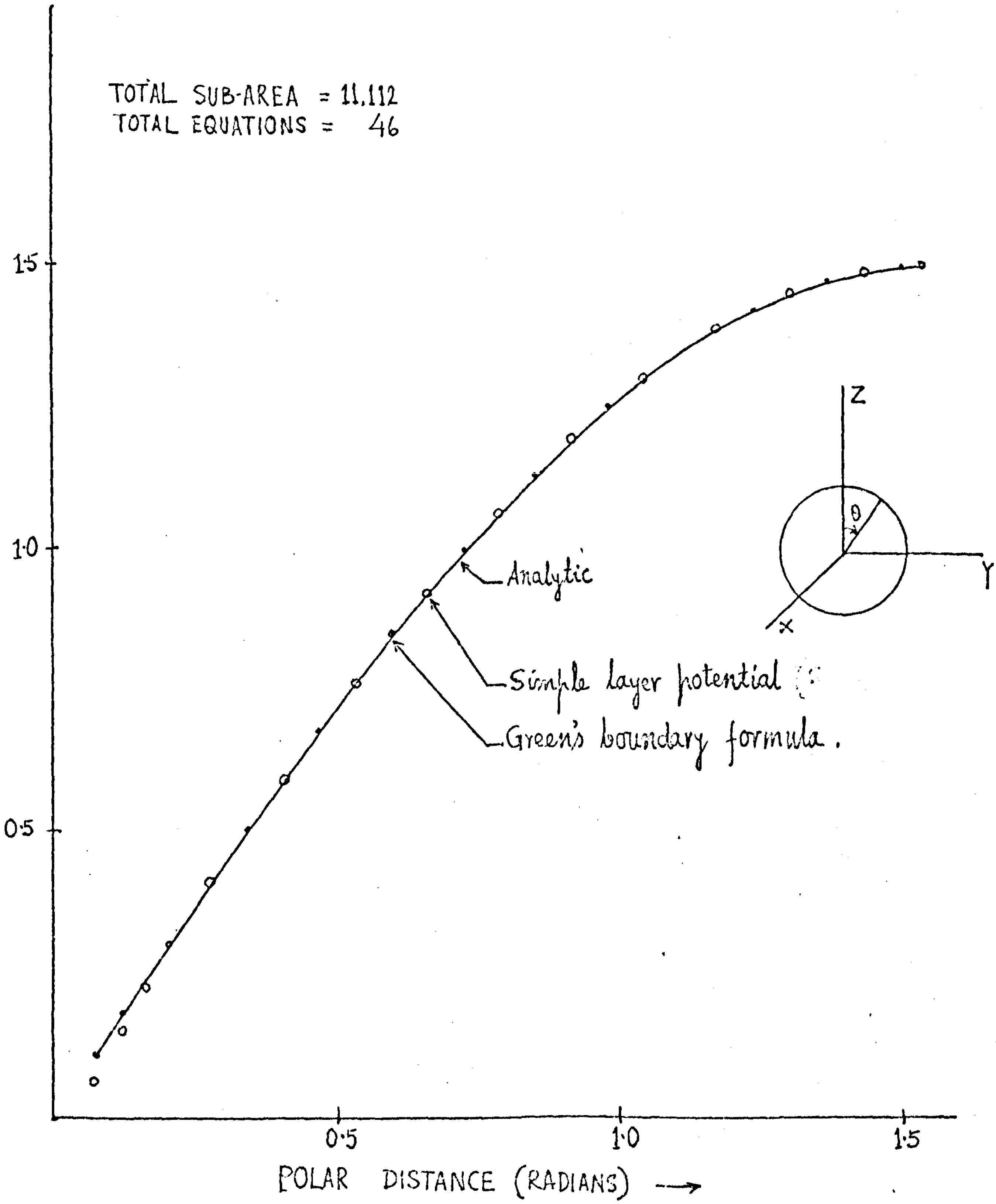

Fig. 21

VELOCITY ON THE SURFACE OF THE SPHERE

The error in ϕ, obtained by Green's Boundary Formula, is nearly uniform. As a result, the numerical velocity, near the pole on ∂B, obtained from ϕ given by Green's Boundary Formula is nearer to the analytic velocity than obtained from ϕ given by Simple Source Formulation in that region (Fig. 21).

CHAPTER 15

FLOW PAST A CYLINDER WITH HEMISPHERICAL CAPS

Introduction

Let the centroid of the cylinder define the origin of a cartesian reference frame OXYZ, the axis of Z coinciding with the axis of the cylinder (Fig.22). The cylinder is of length 2H and radius 'a', and therefore the cylindrical surface has the equation

$$x^2 + y^2 = a^2 \quad , |z| \leqslant H \quad .$$

The two hemispherical surfaces have the equations

$$x^2 + y^2 + (z \mp H)^2 = a^2 \text{ respectively, with } |z| \geqslant H.$$

The cylinder is supposed to be fixed in an infinite fluid moving with free velocity

$$\underset{\sim}{U} = (0, 0, -1) = -\nabla\psi \quad , \tag{205}$$

where ψ is the free flow potential, and by (205)

$$\psi = z \quad . \tag{206}$$

As before, the disturbance potential $\phi \to 0\,|\underset{\sim}{p}|^{-2}$ as $|\underset{\sim}{p}| \to \infty$ and satisfies

$$\nabla^2\phi(\underset{\sim}{p}) = 0 \quad ; \qquad \underset{\sim}{p} \in B_e \; , \tag{207}$$

with boundary condition

$$\phi_e' = -\nabla\psi \cdot \hat{n}_e = -(z)_e' \quad . \tag{208}$$

The integral equation formulation provides a straightforward approach to determine ϕ on the boundary. This is achieved by substituting (208) into (167) or (172) and solving the equations numerically.

Discretisation Procedures

The numerical approach demands that the surface ∂B should be divided into sub-areas. To effect the sub-division, the hemispherical part of the surface is divided into K_1 rings, similar to the surface of the sphere in Chapter 14. Hence, by (200), K_1 is given by

$$K_1 = 4\,KN + 2 \quad . \tag{209}$$

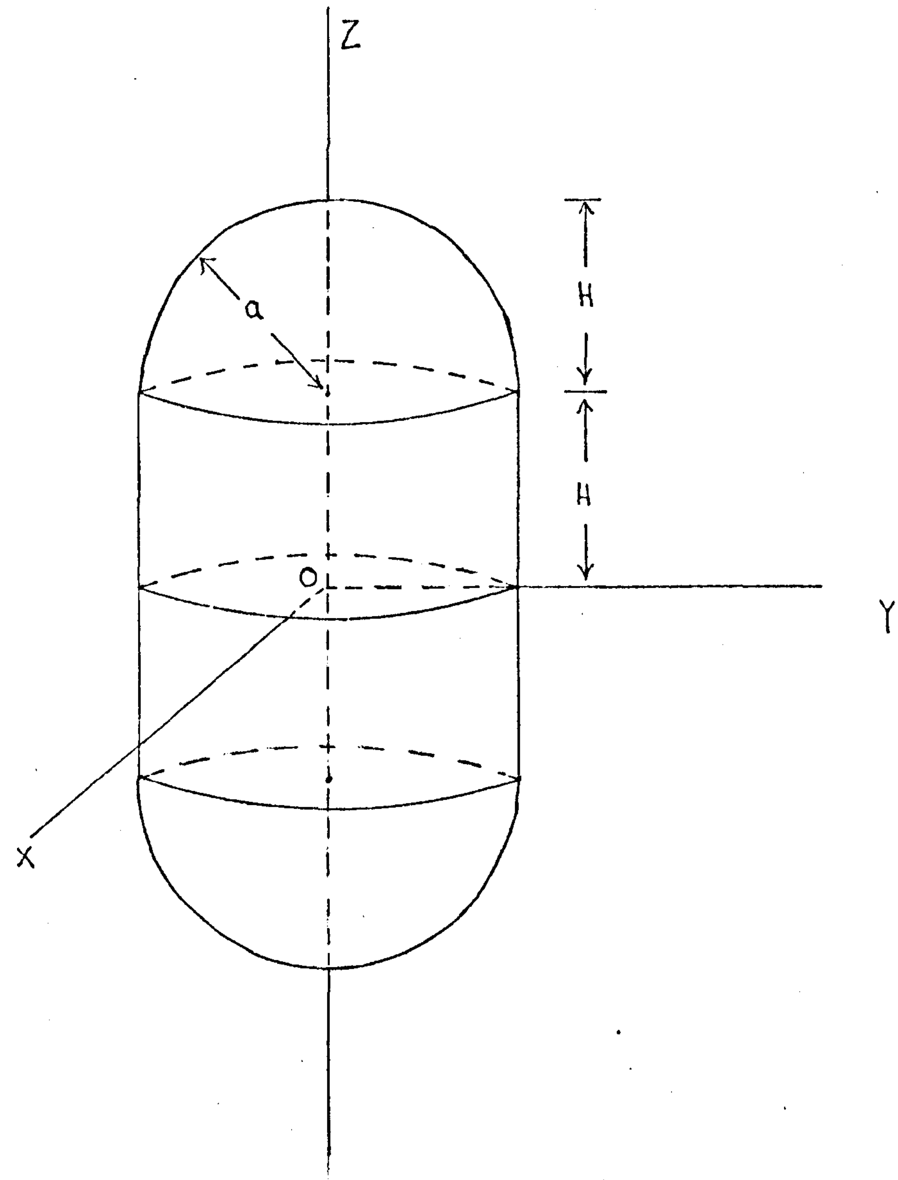

Fig. 22

CYLINDER WITH HEMISPHERICAL CAPS

By (201), the toal number of sub-areas of each of the hemispherical surfaces, is

$$N_1 = 6(7\,KN^2 + 7\,KN + 2) . \tag{210}$$

The M meridian lines which divide the K_1 th ring into M sub-areas are extended on the cylindrical surface. The cylindrical surface from z = H to z = 0 is divided into K_2 rings, such that the width of the ring at the top of the cylindrical surface nearly equals to the breadth of the sub-area in that ring, i.e.

$$\frac{H}{K_2} \simeq \frac{2\pi a}{M} ,$$

where, by Chapter 14, M = 6(1 + 2KN). When H = a = 1, from above, the approximate value of K_2 is (1 + 2KN). Since the width of the sub-area in the K_1 th ring is little less than the breadth $2\pi a/M$ (Chapter 14), the value of K_2, in this case, is taken to be

$$K_2 = 3\,KN . \tag{211}$$

Each sub-area on the cylindrical surface is of breadth b and width d, where

$$b = 2\pi a/M \quad \text{and } d = H/3KN .$$

The total number of rings on ∂B is 2K, where

$$2K = 2(K_1 + K_2) = 2(7\,KN + 2) . \tag{212}$$

The total number of sub-areas

$$\begin{aligned} N &= 2\{N_1 + K_2(M)\} \\ &= 2\left[6\{7\,KN^2 + 7\,KN + 2\} + 3\,KN + 6(1 + 2KN)\right] \\ &= 12(13\,KN^2 + 10\,KN + 2) . \end{aligned} \tag{213}$$

<u>Test function</u>

In order to test our geometrical and numerical procedures, we introduce the test function

$$h = \frac{z}{r^3} \tag{214}$$

which is a harmonic function of similar behaviour to the disturbance potential ϕ . On ∂B,

$$h'_e = \nabla h . \hat{n}_e = -\left[\frac{3zx}{r^5} , \frac{3yz}{r^5} , \frac{3z^2}{r^5} - \frac{1}{r^3}\right] . \hat{n}_e \quad . \tag{215}$$

Introducing this into the place of ϕ'_e in (167) and applying our procedures, we solve for σ and generate h at all the nodal points on the surface. The generated values are exhibited in Table 26 for comparison with the analytic values defined by (214) on the boundary. It will be seen from the Table that the error in the numerically computed values, for K = 23, is less than 1·5%.

We may compute h directly on ∂B by inserting h'_e from (215) in (172) and applying our procedures. For K = 23 the computed values of h at the nodal points are exhibited in Table 26. It will be seen from Table 26 that at no nodal point the error exceeds 1·5%. It will be noted further from the Table that the two approaches yield a comparable accuracy.

Computation of Disturbance Potential

In the actual problem ϕ'_e on ∂B is given by (208). Inserting this into (167) and applying our procedures, we solve for σ_k. Using these σ_k in (171) we generate ϕ on ∂B. For k = 23, the disturbance potential thus obtained are exhibited in Table 27. The total velocity potential is then obtained by using this ϕ , and ψ given by (206), in (53) i.e.

$$\Phi = \phi + \psi \quad . \tag{216}$$

Fig.23 shows the graphs of ϕ and Φ thus obtained for K = 23.

Similarly we insert ϕ'_e given by (208) into (172) and compute ϕ directly at the nodal points on ∂B. The ϕ_k thus obtained, for K = 23, are exhibited in Table 27. On the basis of this value of ϕ_k, Φ is calculated by (216). Fig. 23 shows the graphs of ϕ and Φ thus obtained for K = 23.

It will be seen that the two approaches yeild very similar results.

DEVELOPMENT OF TEST FUNCTION ON THE SURFACE ALONG THE PLANE y = 0

FIELD POINT (CARTESIAN CO-ORD) x	z	ANALYTICAL h	S.L.POTENTIAL (Smith)	%ERROR	G.B.FORMULA (Jaswon)	%ERROR
ON THE SPHERICAL SURFACE						
0.151	1.989	0.25072E 00	0.25355E 00	0.113E 01	0.25707E 00	0.253E 01
0.343	1.939	0.25387E 00	0.25707E 00	0.126E 01	0.25906E 00	0.204E 01
0.483	1.876	0.25816E 00	0.26159E 00	0.133E 01	0.26265E 00	0.174E 01
0.602	1.798	0.26363E 00	0.26725E 00	0.137E 01	0.26775E 00	0.156E 01
0.981	1.192	0.32382E 00	0.32854E 00	0.146E 01	0.32945E 00	0.174E 01
0.992	1.126	0.33316E 00	0.33841E 00	0.158E 01	0.33897E 00	0.175E 01
0.998	1.069	0.34192E 00	0.34781E 00	0.172E 01	0.34804E 00	0.179E 01
1.000	1.021	0.34982E 00	0.35527E 00	0.156E 01	0.35572E 00	0.169E 01
ON THE CYLINDRICAL SURFACE						
1.000	0.944	0.36291E 00	0.36734E 00	0.122E 01	0.36594E 00	0.833E 00
1.000	0.833	0.37781E 00	0.38131E 00	0.924E 00	0.38031E 00	0.662E 00
1.000	0.722	0.38478E 00	0.38777E 00	0.777E 00	0.38700E 00	0.575E 00
1.000	0.278	0.24847E 00	0.24919E 00	0.290E 00	0.24895E 00	0.192E 00
1.000	0.167	0.15996E 00	0.16030E 00	0.212E 00	0.16015E 00	0.123E 00
1.000	0.056	0.55299E-01	0.55394E-01	0.171E 00	0.55347E-01	0.857E-01

Table 26

GENERATION OF ϕ ON THE SURFACE ALONG THE PLANE $y = 0$

FIELD POINT (CARTESIAN CO-ORD) x	z	ϕ S.L.POTENTIAL (Smith)	ϕ G.B.FORMULA (Jaswon)
ON THE SPHERICAL SURFACE			
0.151	1.989	0.54115 E 00	0.54539 E 00
0.343	1.939	0.51979 E 00	0.52102 E 00
0.483	1.876	0.49051 E 00	0.49008 E 00
0.602	1.798	0.45467 E 00	0.45338 E 00
0.981	1.192	0.18835 E 00	0.18749 E 00
0.992	1.126	0.16366 E 00	0.16263 E 00
0.998	1.069	0.14374 E 00	0.14258 E 00
1.000	1.021	0.12898 E 00	0.12777 E 00
ON THE CYLINDRICAL SURFACE			
1.000	0.944	0.11006 E 00	0.10838 E 00
1.000	0.833	0.89885 E-01	0.88547 E-01
1.000	0.722	0.73556 E-01	0.72481 E-01
1.000	0.278	0.25043 E-01	0.24696 E-01
1.000	0.167	0.14847 E-01	0.14643 E-01
1.000	0.056	0.49201 E-02	0.48525 E-02

Table 27

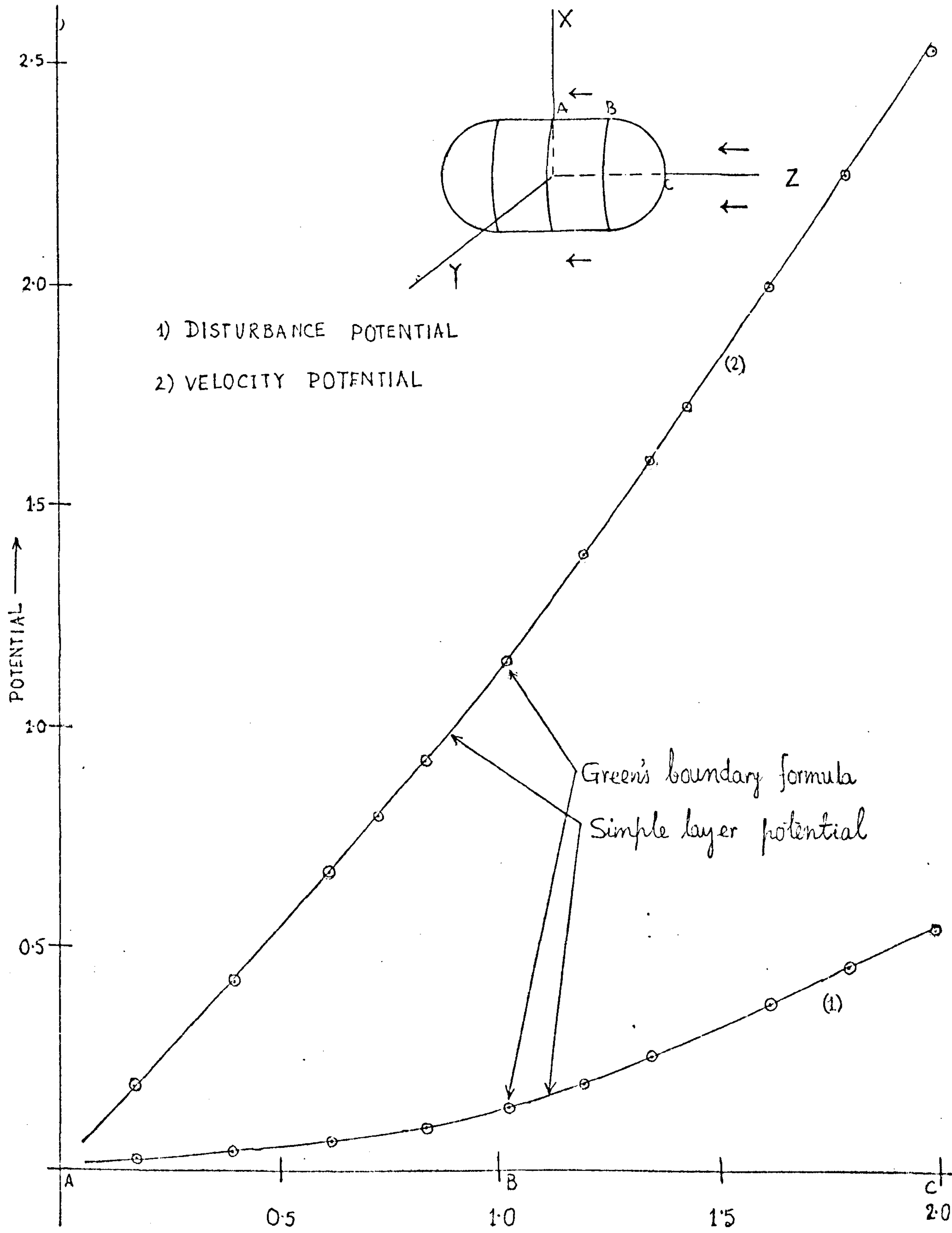

Fig. 23

POTENTIALS ON THE SURFACE OF A CYLINDER WITH HEMISPHERICAL CAPS

Tangential Velocity on the Surface

By symmetry, the tangential velocity is directed along the meridan of ∂B. The velocity at $\hat{p} \in \partial B$, neglecting the terms of higher order in (175), is

$$v_1(\underset{\sim}{p}) = v_1(\underset{\sim}{q}_{j+\frac{1}{2}}) = -\frac{1}{h_1}\delta_1^1 \quad . \tag{217}$$

The velocity thus calculated by (217), on the basis of the two formulations, are exhibited in Table 28. Fig. 24 shows the graphs of the velocities based on Table 28.

DISTRIBUTION OF VELOCITY ON THE SURFACE ALONG THE PLANE $y = 0$

FIELD POINT x	FIELD POINT z	VELOCITY FROM S.L.POTENTIAL	VELOCITY FROM G.B.FORMULA
ON THE SPHERICAL SURFACE			
0.248	1.969	0.35499 E 00	0.37014 E 00
0.414	1.910	0.60332 E 00	0.61404 E 00
0.544	1.839	0.79610 E 00	0.80217 E 00
0.654	1.757	0.96236 E 00	0.95584 E 00
0.973	1.229	0.13580 E 01	0.13608 E 01
0.987	1.159	0.13569 E 01	0.13596 E 01
0.995	1.098	0.13430 E 01	0.13451 E 01
0.999	1.045	0.13076 E 01	0.13087 E 01
ON THE CYLINDRICAL SURFACE			
1.000	0.889	0.11816 E 01	0.11785 E 01
1.000	0.778	0.11470 E 01	0.11446 E 01
1.000	0.667	0.11260 E 01	0.11240 E 01
1.000	0.333	0.10960 E 01	0.10947 E 01
1.000	0.222	0.10918 E 01	0.10905 E 01
1.000	0.111	0.10893 E 01	0.10881 E 01

Table 28

DISTRIBUTION OF VELOCITY

ON THE SURFACE

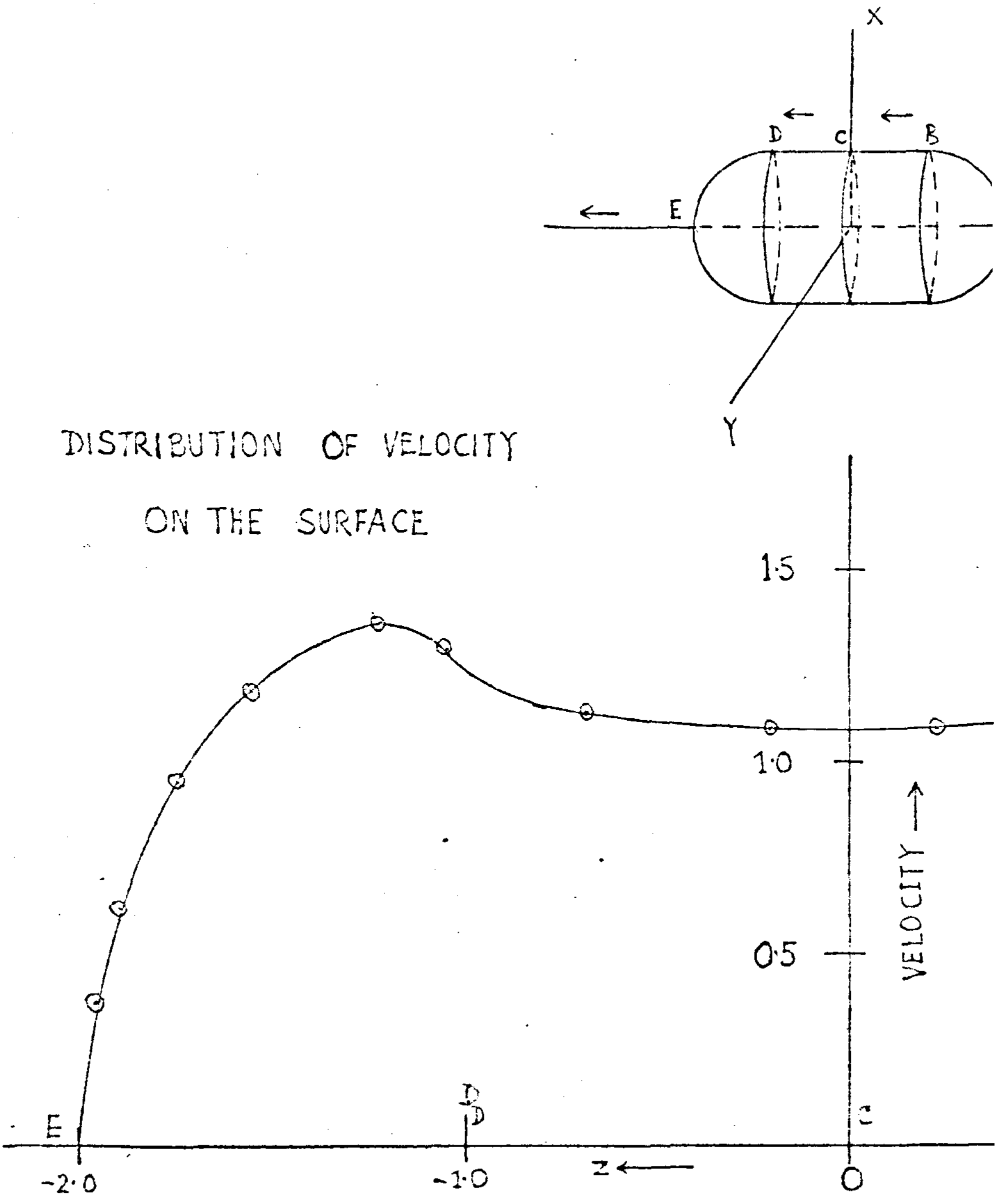

Fig 24

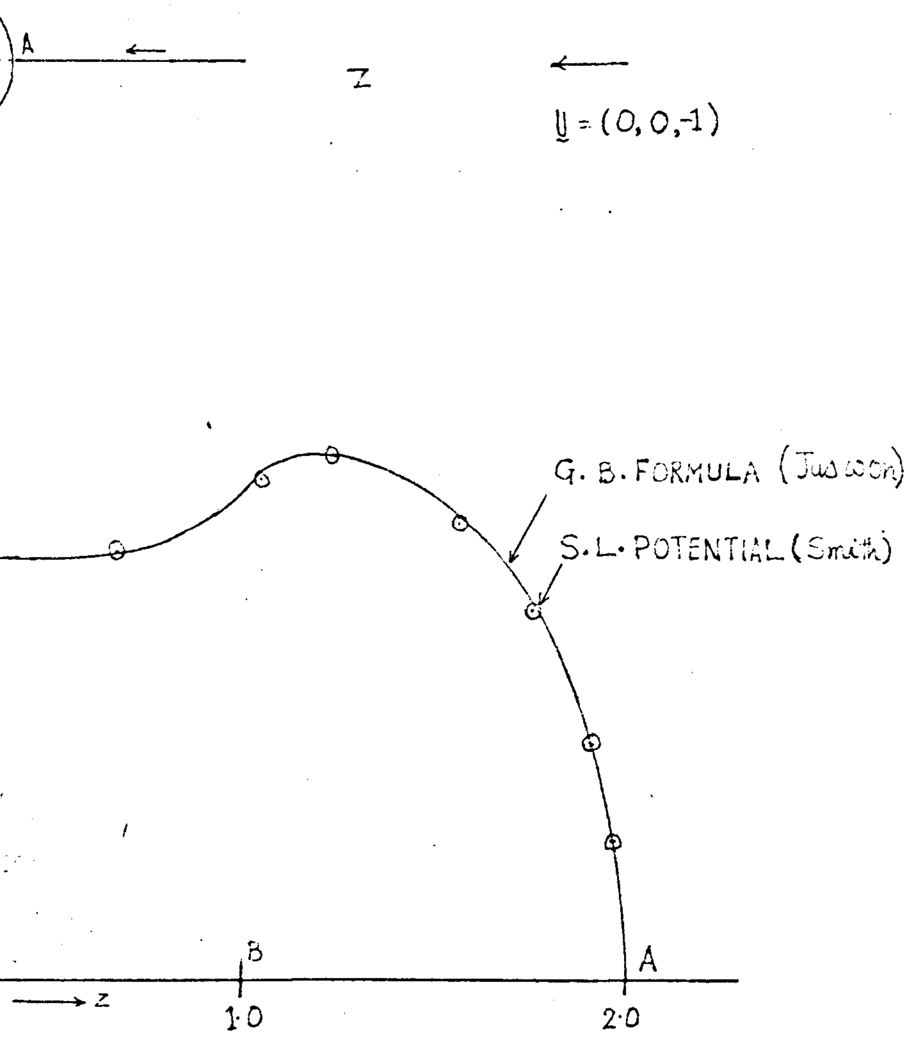
A
Z
$\underset{\sim}{U} = (0,0,-1)$
G. B. FORMULA (Jaswon)
S. L. POTENTIAL (Smith)
B
A
z
1·0
2·0

CHAPTER 16

FLOW PAST A CYLINDER WITH CONICAL CAPS

Introduction

Let the centroid of the cylinder define the origin of a cartesian reference frame OXYZ, the axis of the cylinder coinciding with the Z - axis (Fig.25). The cylindrical surface is of height 2H, and has the equation

$$x^2 + y^2 = a^2 \quad , |z| \leqslant H \quad .$$

If the vertical height of the cone be H_1, the conical surfaces have the equations

$$x^2 + y^2 = \left[\pm(H + H_1) - z\right]^2 \tan^2\alpha ; \; (H + H_1) \geqslant |z| \geqslant H \quad \text{, respectively,}$$

where α is the semivertical angle of the cone.

For a potential fluid motion past the cylinder with free flow velocity $\underline{U} = (0, 0, -1) = -\nabla\psi$, the disturbance potential ϕ satisfies

$$\nabla^2\phi(\underset{\sim}{p}) = 0 \quad ; \quad \underset{\sim}{p} \in B_e \quad ,$$

with boundary condition

$$\phi_e' = -\nabla\psi\cdot\hat{n}_e = -(z)_e' \quad (\because \psi = z) . \tag{218}$$

As before, the integral equation formulation provides a straightforward approach to determine ϕ on the boundary. This is achieved by substituting (218) into (167) or (172) and solving the equations numerically.

Subdivision of Boundary

The numerical method of solution requires that the surface should be divided into smaller sub-areas. For this purpose let us consider a definite boundary by choosing $a = 1$, $\alpha = 45^o$ and $H = 1$. Hence $H_1 = a \cot\alpha = 1$.

The cylindrical surface of radius $a = 1$ is divided into M vertical approximate rectangular slices each of length 2H and breadth $2\pi a/M$, where

$$M = 6\left\{ 1 + (KN - 1)\,2 \right\} \; ; \; KN = 2,4,6, \ldots\ldots 2m \; .$$

Following Chapter 15, each of the vertical slices from $z = 0$ to $z = H$, is divided into 3 KN rectangular sub-areas.

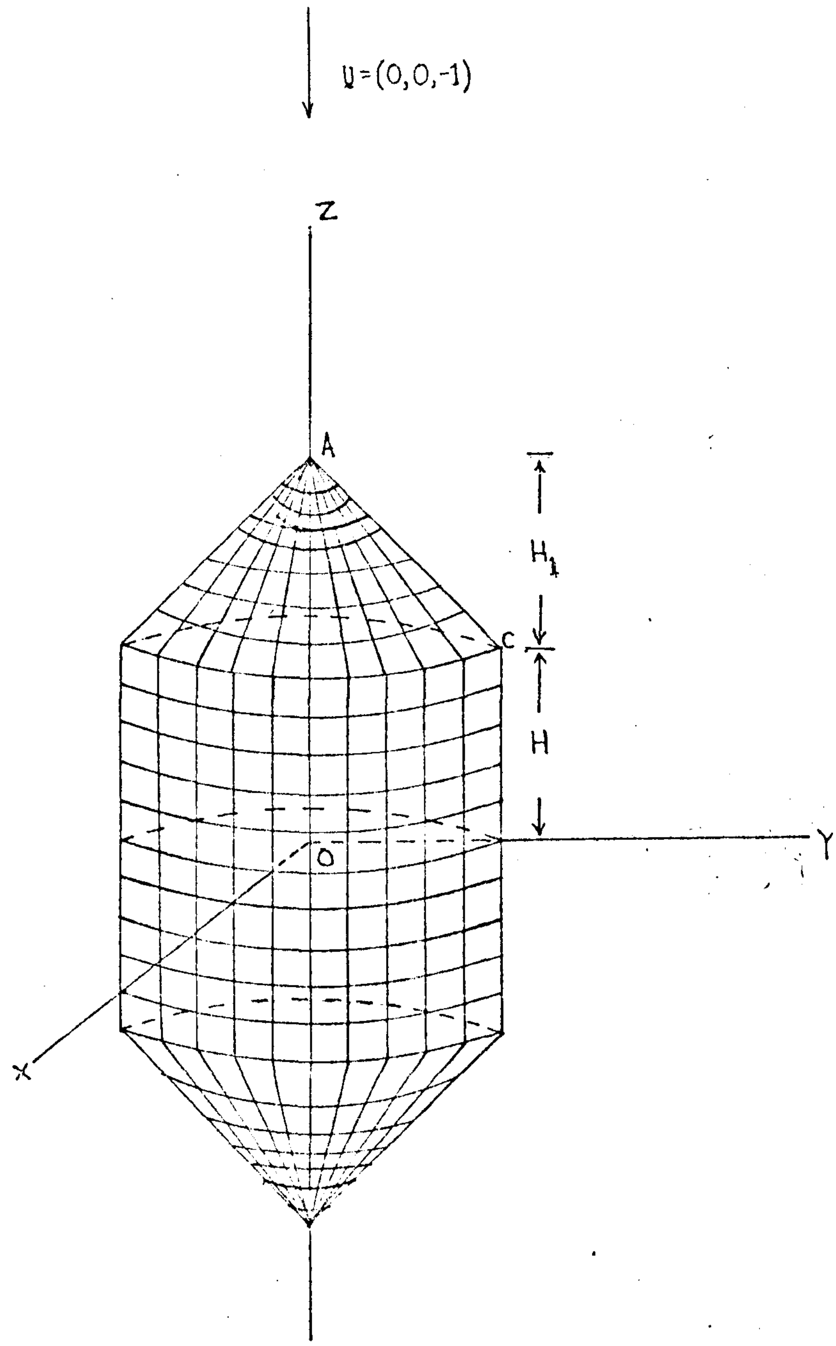

SUB-AREAS ON THE SURFACE OF A CYLINDER WITH CONICAL CAPS

Fig. 25

The conical surface is divided into M approximate triangular slices (Fig. 25). Each slice in turn is divided into n sub-areas, all of which are approximately trapezoidal in form except the one adjacent to the apex which is triangular in form. The trapezoidal sub-areas are so constructed that in every sub-area the length of the arm is equal to the average breadth of the sub-area [Fig.25 (a)].

The total number of horizontal rings on the surface is

$$2N^{*} = 2 \quad (n + 3KN) \quad . \tag{219}$$

Smoothing Procedures on Boundary

It has already been stated in Chapter 6 that, in general, we can not expect a good accuracy near a sharp edge or a corner by the numerical methods used in this thesis. In our sub-division, the sub-areas adjacent to the tip become very thin and, hence, the results obtained will be untrustworthy. To overcome this difficulty, the sharp tip is replaced by a spherical cap of a radius of curvature ρ_1 and, though it is not essential, the corner at C (Fig.26) is replaced by an arc of revolution of radius of curvature ρ_2 such that, as the number of sub-areas increases, both ρ_1 and ρ_2 tend to zero.

The cap at the top is so placed that the pole of the cap lies on the axis of z and it touches the slant line AC and A_1 where $AA_1 = h_1$ (Fig.26). Hence

$$\rho_1 = A_1O_1 = h_1 \tan\alpha . \tag{220}$$

and the angle $AO_1A_1 = \theta = 90^{\circ} - \alpha$.

The arc of revolution is so fitted that it touches AC at the point A_{n-1} and CE at C_1 (Fig.26), where

$$A_{n-1}C = h_n - h_{n-1} = CC_1 \quad .$$

The radius of curvature ρ_2, from Fig.26, is

$$\rho_2 = (CC_1) \text{ Cot } (\alpha/2) . \tag{221}$$

The distance AP_1, i.e. the gap between the tip A and the pole P_1 of the cap, is given by

$$AP_1 = AO_1 - \rho_1 = \rho_1 \text{ Cosec}\alpha - \rho_1 = \rho_1(\text{Cosec}\alpha - 1) . \tag{222}$$

The distance CP_2 i.e. the perpendicular distance between the arc $A_{n-1}P_2C_1$ and C, is given by

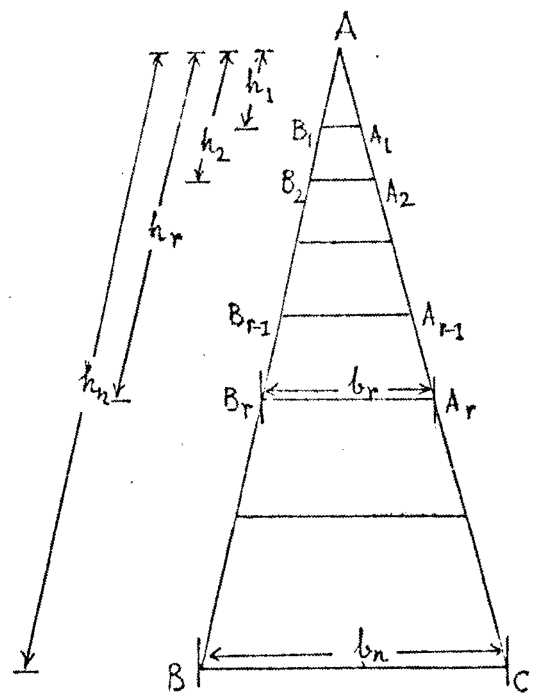

Fig. 25 (a)

$$\frac{b_r+b_{r-1}}{2} = h_r - h_{r-1} \quad . \qquad (1)$$

Now $\dfrac{b_r}{b_{r-1}} = \dfrac{h_r}{h_{r-1}}$ or $\dfrac{b_r-b_{r-1}}{b_r} = \dfrac{h_r-h_{r-1}}{h_r}$,

or $\dfrac{b_r-b_{r-1}}{b_r} = \dfrac{b_r+b_{r-1}}{2h_r}$, or $\dfrac{b_r+b_{r-1}}{b_r-b_{r-1}} = \dfrac{2h_r}{b_r} = \dfrac{2\,AB}{BC}$,

or $\dfrac{b_{r-1}}{b_r} = \dfrac{2AB-BC}{2AB+BC} = \dfrac{h_{r-1}}{h_r}$. $\qquad$ (2)

From (2), $h_{r-1} = \beta\, h_r$, where $\beta = \dfrac{2AB-BC}{2AB+BC}$ = a constant.

Hence , $h_k = \beta^{n-k} h_n$; $k = 1, 2, \cdots n$. $\qquad$ (3)

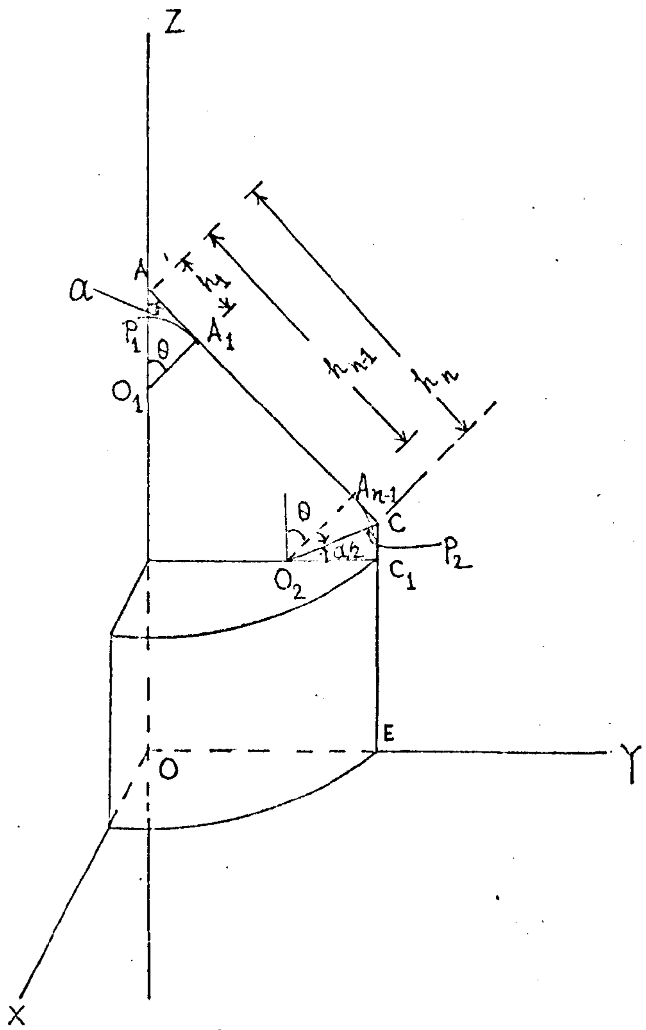

FIG. 26

(ARCS A_1P_1, $A_{n-1}P_2C_1$ rotate about the axis OZ)

SMOOTHENING OF THE CONICAL TIPS AND THE ANGULAR EDGES OF THE SURFACE

$$CP_2 = \rho_2 (\mathrm{Sec}(\alpha/2) - 1) \quad . \tag{223}$$

Table 29 and Fig.27 exhibit the relation between the total number of sub-areas N, radii of curvatures ρ_1, ρ_2 and the gaps AP_1 and CP_2 as N increases.

The cap at the top, which is a part of a sphere of radius ρ_1, can be divided into sub-areas as was done in Chapter 14. To simplify, the angle Θ which the arc A_1P_1 subtend at O_1, is divided into KN parts such that

$$\theta_j = \theta_{j-1} + d\theta + T(KN - j + 1) \; ; \quad j = 2, 3, \cdots KN$$

where,

$$d\theta = \Theta/(KN + KN/2), \; T = \{d\theta\,(KN)/2\}/\{KN(KN+1)/2\} \quad .$$

and

$$\theta_1 = d\theta + T\,(KN) \quad .$$

The top cap is thus divided into KN rings of which the j th ring is of width

$$dl_j = \rho_1 \; d\theta_j \quad ; \quad j = 1, 2, \cdots KN \; .$$

As before, the j th ring is divided into IK_j sub-areas given by

$$IK_j = 6\{1 + (j-1)2\} \; ; \quad j = 1, 2, \cdots KN \; .$$

The curved surface, formed by the arc of revolution $A_{n-1}P_2C_1$ of radius of curvature ρ_2 is divided into KN rings each is of width

$$d\Delta_1 = \rho_2 (\alpha/KN)$$

and each ring in its turn is divided into 2M sub-areas.

Because of the rounding off, the number of sub-areas in each of the M triangular slices reduces by 2. Hence the number of rings on the slant curved conical surface reduces to (n - 2).

The curved cylindrical surface, of height $(H - CC_1)$ above the plane $z = 0$, is divided into K_1 rings each of width

$$d\Delta_2 = (H - CC_1)/K_1$$

where, following Chapter 15, $K_1 = 3\,(KN - 1)$.

Now the total number of rings on the upper half of the cylinder is

$$K = KN + (n - 2) + KN + 3(KN - 1) = 5\,(KN - 1) + n \quad . \tag{224}$$

The toal number of sub-areas on the surface is

$$N = 2\left[\frac{6KN}{2}\left\{2*1 + (KN-1)2\right\} + (n-2)\,6\left\{1 + (KN-1)\,2\right\}\right.$$

ROUNDING OFF OF THE NODE AND THE EDGE OF THE CYLINDER WITH CONICAL CAPS

TOTAL SUBAREA N	NO. OF RINGS 2K	ρ_1	AP_1	ρ_2	CP_2
6372	90	0.39340	0.16295	0.22235	0.01840
14268	150	0.20617	0.08540	0.16448	0.01355
24140	210	0.14183	0.05875	0.13052	0.01075

Table 29

(This should be read in conjunction with fig.26 and fig.27.)

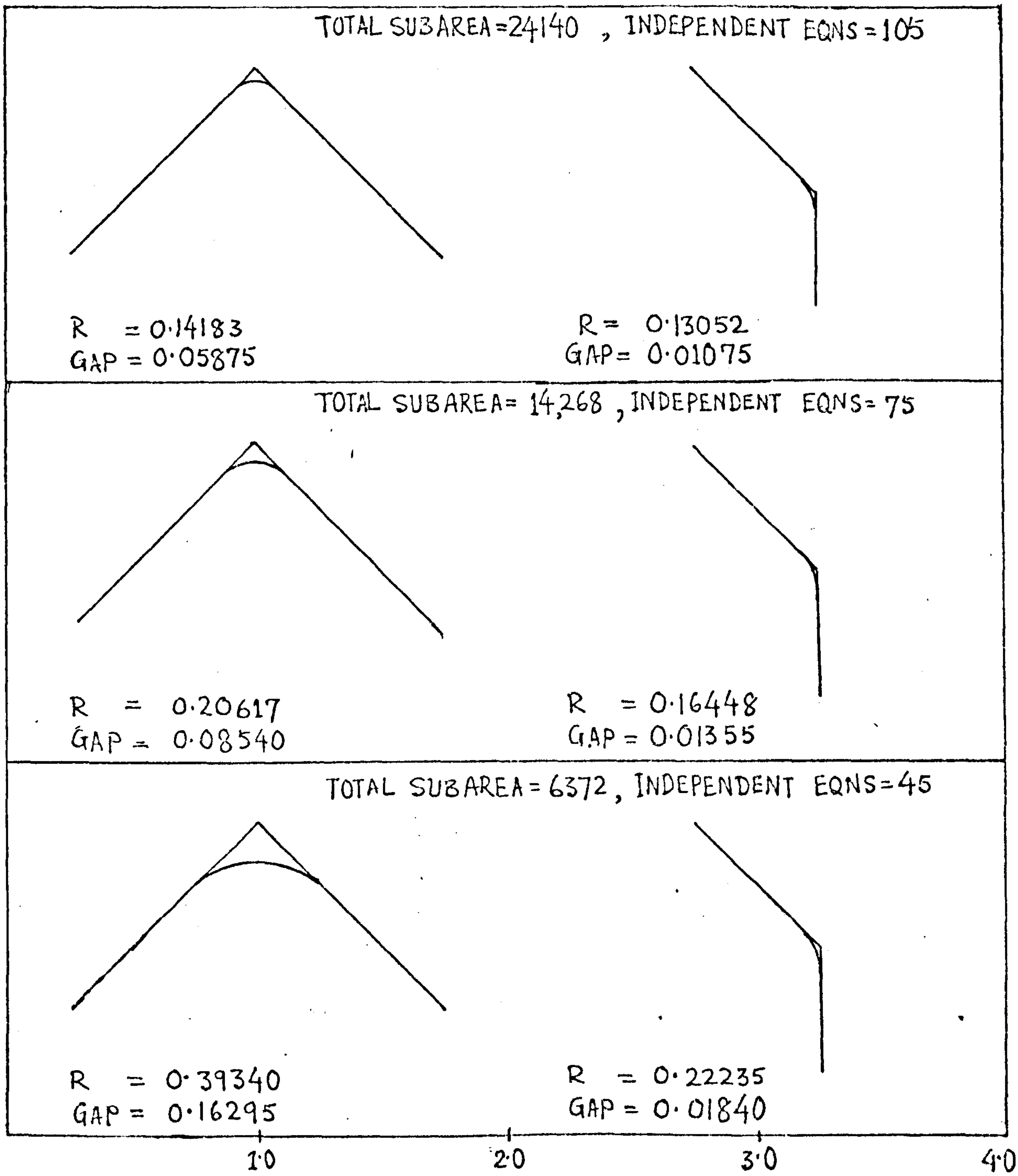

SUCCESSIVE STAGES OF APPROXIMATIONS OF THE CONE AT THE TOP AND THE CORNER AT THE EDGE.

R = RADIUS OF CURVATURE

Fig. 27

$$+2* \; 6KN\left\{1 + (KN-1)\;2\right\} + 3(KN-1)6\left\{1 + (KN-1)2\right\}\Big],$$

$$= \; 12\left[KN^2 + 5(2KN-1)\;(KN-1) + n\right] \quad . \qquad (225)$$

Test Function

The test function in this case, by (189) of Chapter 13, is

$$h = \frac{z}{r3} \quad .$$

On the surface ∂B, by (215),

$$h'_e = -\left[\frac{3zx}{r5}, \; \frac{3yz}{r5}, \; (\frac{3z^2}{r5} - \frac{1}{r3})\right]\cdot\hat{n}_q \qquad (226)$$

Introducing this into the place of ϕ'_e in (167) and applying our procedures, we solve for σ and generate h at all nodal points on the surface. The generated values are exhibited in Table 30 for comparison with the analytic values defined by (214) i.e. h = $z/r3$ on the boundary. It will be seen that the error in the numerically computed values, for K = 45, is less than 1·0%.

As before, we compute h directly on ∂B by inserting h'_e from (226) in (172) and applying our procedures. For K = 45, the computed values of h at the nodal points are exhibited in Table 30. It will be seen from the Table that the maximum error in the computed h occurs at a nodal point either at the rounded off tip or corner of ∂B and the maximum error does not exceed 2·5%. Further, in this case also, the Simple Source Distribution formulation generates h at the nodal points of ∂B which are nearer to the analytic values of h than those generated by Green's Boundary Formula. It will be noted from the Table that the two approaches yield a comparable accuracy.

Computation of Disturbance Potential

In the actual problem, ϕ'_e on ∂B is given by (218). Inserting this into (167) and applying our procedures, we solve for σ_j. Using these σ_j in (169) we generate the ϕ_k on ∂B. For K = 105, the ϕ_k thus obtained are exhibited in Table 31. The total velocity potential is then given by

$$\Phi = \phi + \psi$$

where ψ is given by (218). Fig. 28 exhibits the ϕ and Φ thus obtained for K = 105.

Similarly we insert ϕ'_e given by (218) into (172) and compute ϕ directly. The ϕ thus obtained for K = 105 are exhibited in Table 31. Fig 28 exhibits the computed ϕ and Φ thus obtained for K = 105.

DEVELOPMENT OF TEST FUNCTION ALONG A MERIDIAN

y = 0 ON THE SURFACE

FIELD POINT (CARTESIAN CO-ORD) x	z	ANALYTICAL h	G.B.FORMULA (Jaswon)	%ERROR	S.L.POTENTIAL (Smith)	%ERROR
ON THE ROUNDED SPHERICAL NOSE						
0.037	1.835	0.29670	0.30291	2.090	0.29863	0.652
0.095	1.825	0.29889	0.30544	2.190	0.30103	0.717
0.232	1.761	0.31415	0.31972	1.770	0.31641	0.719
0.264	1.735	0.32095	0.32664	1.680	0.32323	0.710
ON THE CONICAL SURFACE						
0.288	1.712	0.32720	0.32768	0.146	0.32936	0.659
0.304	1.692	0.33265	0.33344	0.237	0.33484	0.658
0.494	1.506	0.37817	0.37939	0.324	0.38030	0.564
0.528	1.472	0.38489	0.38606	0.304	0.38698	0.543
0.846	1.154	0.39391	0.39410	0.047	0.39585	0.491
0.905	1.095	0.38199	038212	0.034	0.38460	0.684
ON THE ROUNDED OFF CORNER						
0.945	1.054	0.37151	0.37919	2.070	0.37404	0.681
0.963	1.031	0.36732	0.37472	2.010	0.37019	0.780
0.996	0.951	0.36426	0.37164	2.030	0.36731	0.836
1.000	0.922	0.36661	0.37570	2.480	0.36983	0.877
ON THE CYLINDRICAL SURFACE						
1.00	0.878	0.37262	0.37424	0.435	0.37539	0.744
1.00	0.817	0.37942	0.38160	0.576	0.38191	0.657
1.00	0.757	0.38371	0.38586	0.560	0.38603	0.604
1.00	0.151	0.14626	0.14672	0.311	0.14672	0.311
1.00	0.091	0.08968	0.08995	0.300	0.08995	0.300
1.00	0.030	0.03022	0.03031	0.295	0.03031	0.295

Table 30

GENERATION OF DISTURBANCE POTENTIAL ALONG MERIDIAN $y = 0$ ON THE SURFACE

FIELD POINT (CARTESIAN CO-ORD) x	z	ϕ S.L.POTENTIAL	ϕ G.B.FORMULA
ON THE ROUNDED SPHERICAL NOSE			
0.008	1.941	0.37332	0.37717
0.021	1.940	0.37380	0.37763
0.091	1.908	0.38023	0.38264
0.097	1.902	0.38185	0.38419
ON THE CONICAL SURFACE			
0.102	1.898	0.38336	0.38234
0.106	1.894	0.38476	0.38391
0.215	1.785	0.41595	0.41576
0.468	1.532	0.44412	0.44401
0.907	1.093	0.32913	0.32903
0.944	1.056	0.30000	0.29978
ON THE ROUNDED-OFF CORNER			
0.965	1.035	0.27493	0.27744
0.972	1.027	0.26577	0.26706
0.999	0.961	0.19524	0.19603
1.00	0.951	0.18687	0.18869
ON THE CYLINDRICAL SURFACE			
1.00	0.928	0.17262	0.17285
1.00	0.893	0.15608	0.15646
1.00	0.543	0.07127	0.07148
1.00	0.053	0.00619	0.00621
1.00	0.018	0.00206	0.00207

Table 31

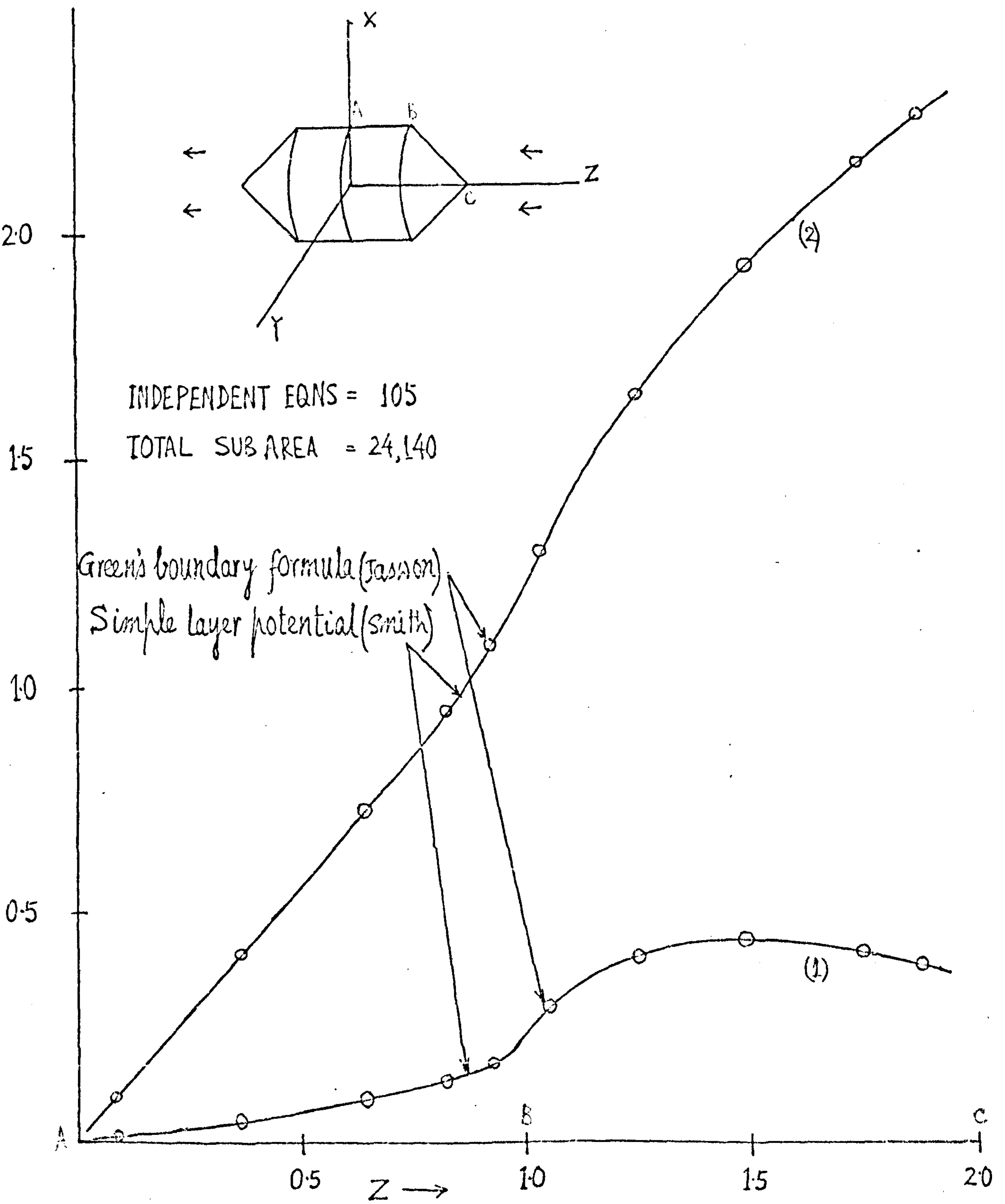

1) DISTURBANCE POTENTIAL

2) VELOCITY POTENTIAL

Fig. 28

It will be seen that the two approaches yield similar result.

Tangential Velocity on the Surface

By symmetry, the tangential velocity is directed along the meridians of ∂B. The velocity at $\underset{\sim}{p} \in \partial B$, by (175), neglecting the higher order terms, is given by

$$v_1(\underset{\sim}{p}) = v_1(\underset{\sim}{q}_{j+\frac{1}{2}}) = -\frac{1}{h_1}\delta_1^1 \ .$$

The velocities thus calculated, on the basis of the two formulations, are exhibited in Table 32 and graphed in Fig. 29.

We know from theory of potential flow that the velocity becomes infinite[14] in the neigh-bourhood of a sharp edge or a corner. Fig. 30 shows the numerically computed velocity in the neighbourhood of a corner C, smoothed out by an arc of a circle of contact of radius ρ_2 (Fig. 26). It is interesting to note that the velocity at the corner rises indefinitely as the radius of curvature of the circle of contact decreases.

VELOCITY ON THE SURFACE ALONG A MERIDIAN $y = 0$

FIELD POINT (CARTESIAN CO-ORD) x	z	VELOCITY ON THE SURFACE S.L.POTENTIAL	G.B.FORMULA
ON THE ROUNDED SPHERICAL NOSE			
0.0148	1.9405	0.06868	0.07038
0.0278	1.9385	0.16228	0.18352
0.0876	1.9110	0.45915	0.47560
0.0943	1.9053	0.47237	0.48111
ON THE CONICAL SURFACE			
0.1043	1.8957	0.46295	0.43375
0.1085	1.8915	0.46450	0.44424
0.2104	1.7896	0.54209	0.54118
0.4413	1.5587	0.69142	0.69139
0.8901	1.1099	1.15854	1.15852
0.9255	1.0745	1.27812	1.28048
ON THE ROUNDED-OFF CORNER			
0.9687	1.0307	1.65374	1.77310
0.9751	1.0226	1.79843	1.81988
0.9984	0.9663	1.88886	1.87750
0.9996	0.9562	1.81258	1.71292
ON THE CYLINDRICAL SURFACE			
1.00	0.9109	1.47207	1.46797
1.00	0.8759	1.37907	1.37996
1.00	0.5956	1.17657	1.17695
1.00	0.0701	1.11817	1.11856
1.00	0.0350	1.11773	1.11812

Table 32

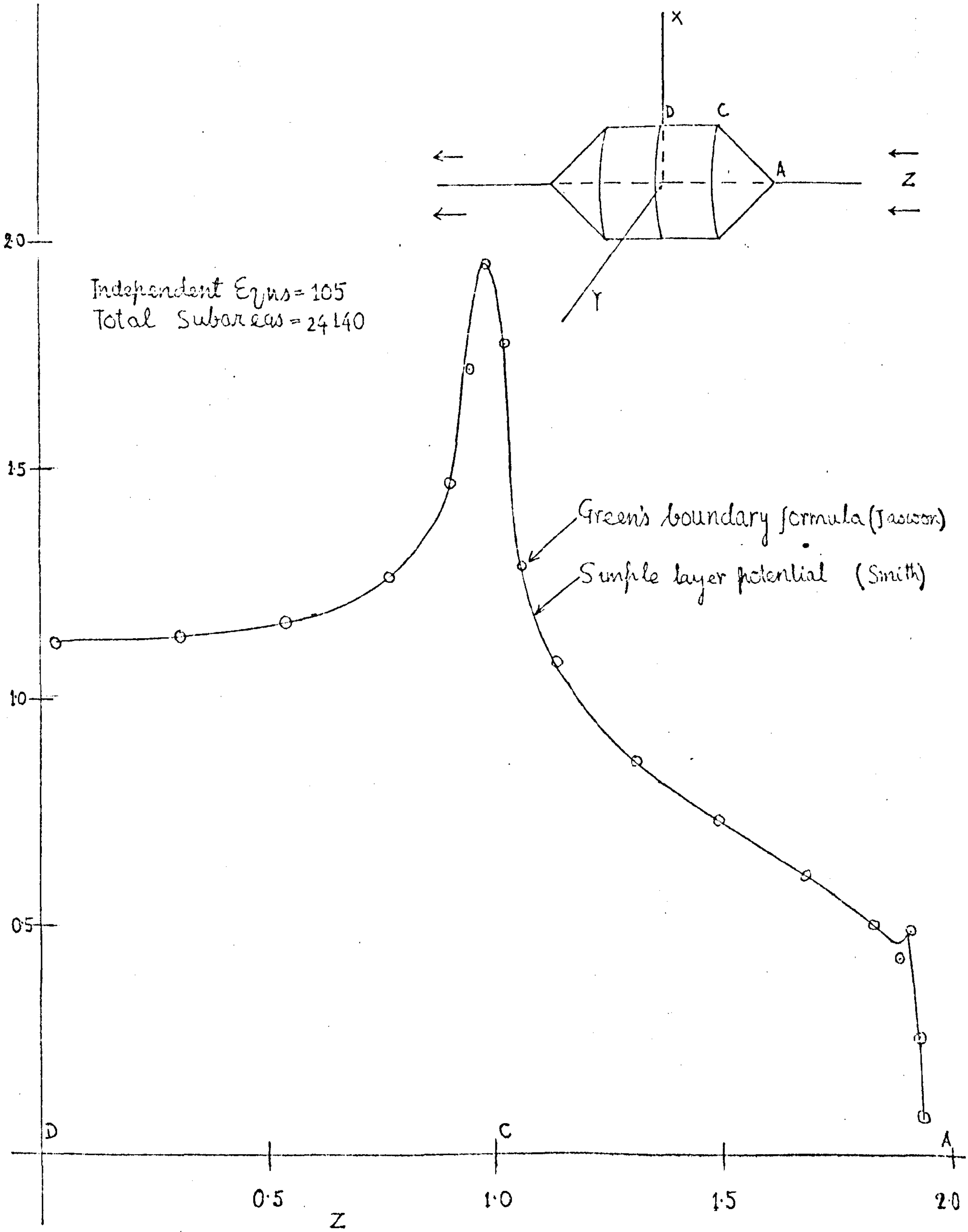

Fig. 29

VELOCITY DISTRIBUTION ON THE SURFACE

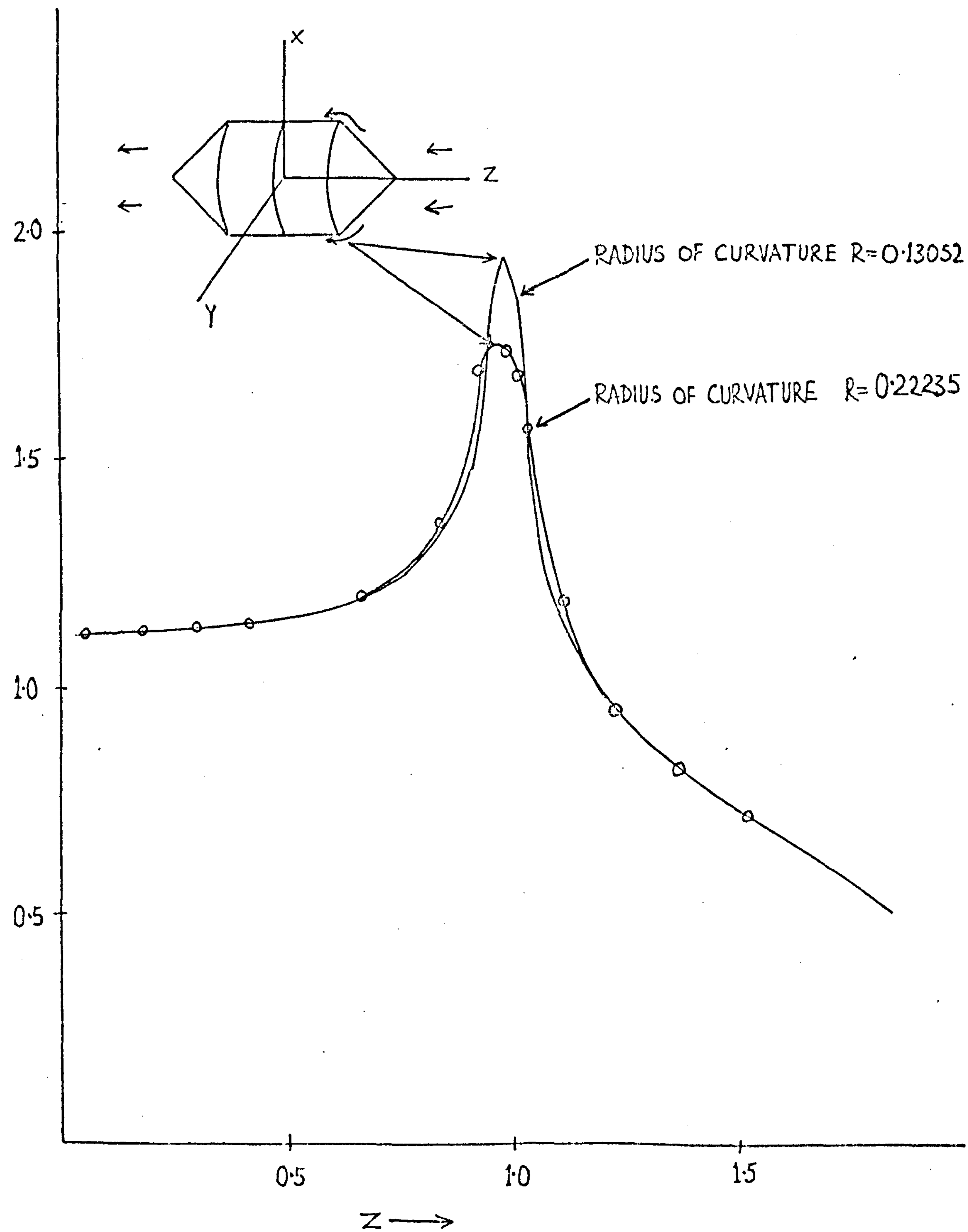

FLUID VELOCITY AT SHARP EDGE ON SUCCESSIVE APPROXIMATIONS

Fig. 30

CHAPTER 17

POTENTIAL FLOW PAST A THICK DELTA WING

Introduction

A thick isosceles triangular plate of semi-apex angle 60°, perturbs an otherwise uniform free flow directed approximately parallel to the plane of the plate. The centroid O of the plate defines the origin of a cartesian reference frame OXYZ [Fig.31(a)], where OZ is perpendicular to the plane of the plate. Relative to the co-ordinates axes, the triangular faces define the planes $z = \pm H$ [Fig. 31(b)] .

The free flow is approximately parallel to the XOY plane in the negative Y-direction. If velocity vector $\underset{\sim}{U}$ makes an angle $-\theta$ with OY [Fig. 31(c)] , it follows that

$$\underset{\sim}{U} = -\nabla\psi = U(0,\ -\cos\theta,\ \sin\theta) \ . \tag{227}$$

Therefore, taking U = 1 ,

$$\psi = (0,\ \cos\theta,\ -\sin\theta)\cdot(x,y,z) \ . \tag{228}$$

For a small angle ($=\theta$) of attack, the flow remains potential.[14,15] The disturbance potential $\phi \to O|\underset{\sim}{r}|^{-2}$ as $|\underset{\sim}{r}| \to \infty$, and satisfies Laplace's equation

$$\nabla^2\phi(\underset{\sim}{r}) = 0 \quad ; \quad \underset{\sim}{r} \in B_e \quad ,$$

with boundary condition (168), i.e.

$$\phi_e' = -\psi_e' = (0,-\cos\theta,\sin\theta)\cdot\hat{n}_e \ . \tag{229}$$

The integral equation formulation provides a straight forward approach to determine ϕ on the boundary. This is achieved by substituting (229) into equations (167) or (172) and solving them numerically.

Subdivision of Boundary

To solve the integral equation numerically, we divide ∂B into sub-areas. In this case, we shall not be forced, as in the previous case, to deal with thin sub-areas, and hence the rounding-off of the corner is not necessary. Of course, rounding-off of the sharp edge and corner improves the solution at the

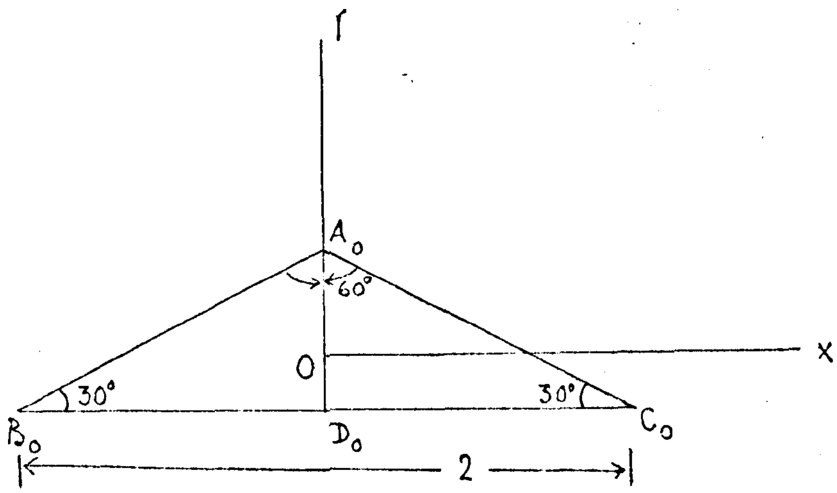

Fig. 31(a)

Plane section through the centroid O, parallel to the triangular surfaces of the plate, exhibiting orientation of axes and apex A_0. The Z-axis passes through O and is perpendicular to this plane.

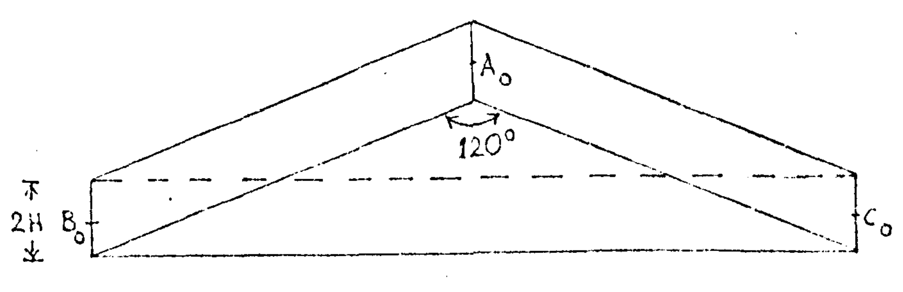

Fig. 31(b)

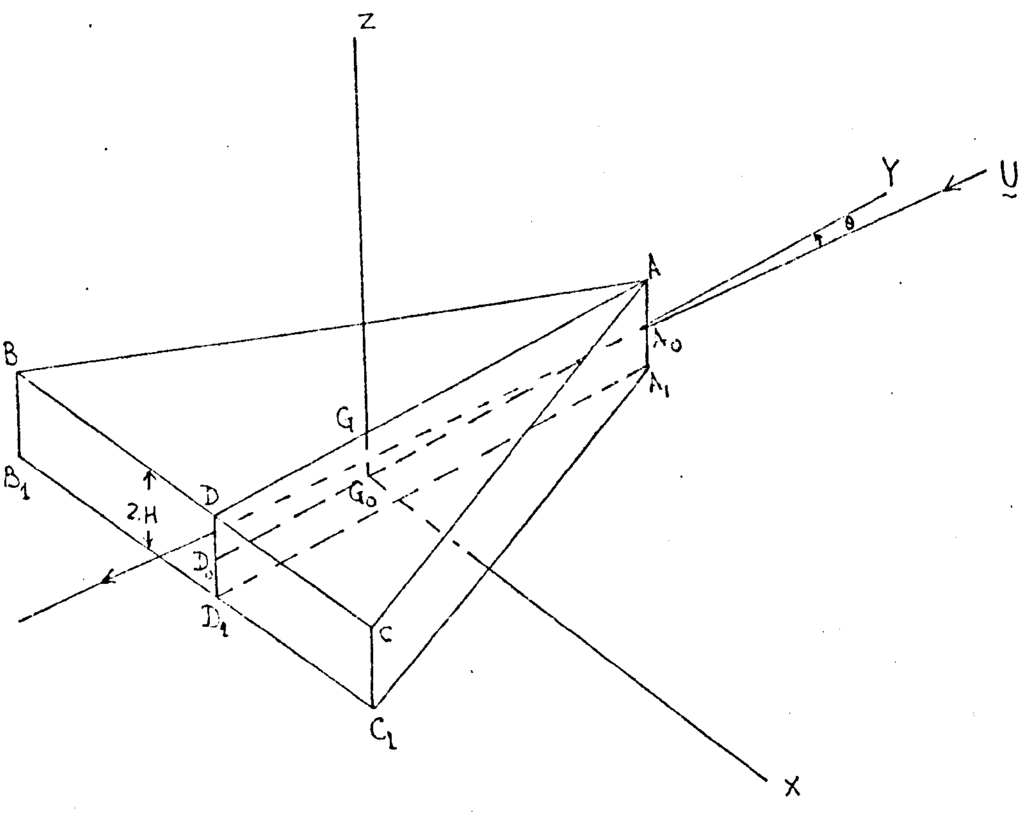

FLOW PAST A THICK DELTA WING

Fig. 31(c)

expense of greater complications.

From symmetry, the sub-areas on the plane $z = -H$ are made exactly similar to those on the plane $z = H$. Further, for a sub-area to the right of the plane $x = 0$, there is a corresponding sub-area on the left.

From the Fig. 32, the number of sub-areas in the zone

$(A\,\bar{A}\,\bar{F}\,F \quad + \quad \bar{F}\,F\,C\,E\,\bar{E})$ is

$$N_1 = (2NT - 1)\,7 + 10; \quad NT = 3, 6 \; . \; . \; . \quad 3 + (n-1)3 \; . \tag{230}$$

The number of sub-areas in the region $(D\,\bar{D}\,\bar{E}\,E \quad + \quad \bar{D}\,E\,\bar{F}\,\bar{A}\,G)$ is

$$N_2 = \frac{NT-3}{2}\left\{2 * 4 + \left(\overline{NT-3} - 1\right)\right\} * 2 + 6 \; . \tag{231}$$

The half thickness H of the plate is determined by

$$H = AA_0 = \left(\frac{AC}{4NT}\right) KN \; ; \quad KN = 2, 3, \cdots m \; . \tag{232}$$

The number of sub-areas in the region DD_oC_oC [Fig. 32 (a)] is

$$N_3 = 2NT * KN, \tag{233}$$

and that on the region $F\,C\,C_oF_o$ [(Fig.32(b)] is

$$N_4 = (4NT - 2) * KN \; . \tag{234}$$

If N_5 is the number of sub-areas on AFF_oA_o [Fig.32(b)], then

$$N_5 = 2 * 2 * 2\,KN = 8KN \; .$$

Hence, the total number of sub-areas N on ∂B is

$$N = 4\sum_{j=1}^{5} N_j \quad \left(= 4N^* \text{ say}\right),$$

$$= 4\left[14\,NT + (NT-3)\,(NT + 4) + 6KN\,(NT + 1) + 9\right] \; . \tag{236}$$

There are 11 different sub-areas on ∂B [Fig. 32, Fig. 32(a), Fig. 32 (b)] . An analysis of these for $NT = 6$, $KN = 2$ are given in Table 33.

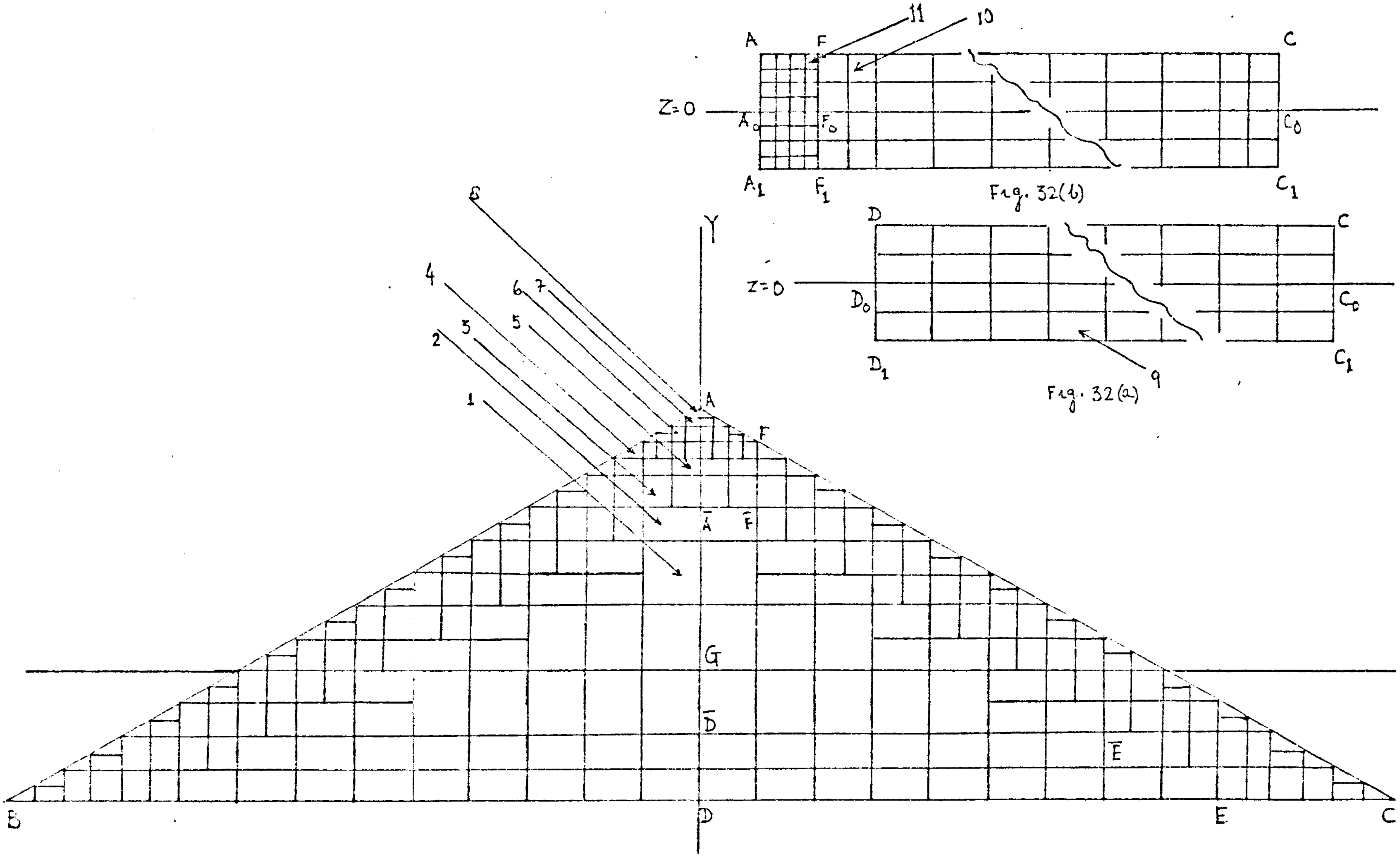

Fig. 32(b)

Fig. 32(a)

Fig. 32

DIVISION OF THE TRIANGULAR PLANE FACE INTO SUB-AREAS

ANALYSIS OF SUB-AREA ON THE SURFACE FOR KN=2 and NT=6

REGION	FORM	BASE	HEIGHT	AREA
$A\bar{A}\bar{F}F$	TRIANGULAR (7)	0.02083	0.01203	0.00013
	RECTANGULAR (6)	0.02083	0.01203	0.00025
	" (5)	0.02083	0.02405	0.00050
	" (4)	0.04167	0.02405	0.00100
	" (3)	0.04167	0.04810	0.00201
$F\bar{F}\bar{E}EC$	RECTANGULAR (4)	0.04167	0.02405	0.00100
	" (3)	0.04167	0.04810	0.00201
	TRIANGULAR (8)	0.04167	0.02405	0.00050
$\bar{A}\bar{F}\bar{E}ED$	RECTANGULAR (1)	0.08333	0.09623	0.00802
	" (2)	0.08333	0.04811	0.00401
DCC_oD_o	RECTANGULAR (9)	0.08333	0.04811	0.00401
CC_oF_oF	RECTANGULAR (10)	0.04812	0.04812	0.00232
	" (11)	0.02406	0.02406	0.00058

Table 33

(This should be read in conjunction with Fig.32)

Test Function

We now introduce the test function

$$h = \frac{y}{r^3} \tag{237}$$

which behaves in a comparable way to the disturbance potential ϕ on ∂B,

$$h_e' = -\left[\frac{3xy}{r^5}, \frac{3y^2}{r^5} - \frac{1}{r^3}, \frac{3yz}{r^5}\right] \cdot \hat{n}_e \quad . \tag{238}$$

Introducing this in place of ϕ_e' in (167) and applying our procedures, we solve for σ and generate h at the nodal points on the surface. The values of h generated for KN = 2, NT = 6 i.e. N^* = 207, are exhibited in Table 34 for comparison with the analytic values defined by (237) on ∂B.

Alternatively we find h directly on ∂B by inserting (238) into (172) and applying our procedures. A few of the values of h at the nodal points in the neighbourhood of the apex of the delta, thus determined, for $N^* = 207$, are exhibited in Table 34.

It is evident from Table 34 that, for the same sub-division of ∂B the Simple Layer potential method (Smith) generates an h which is nearer to analytic value than that obtained by Green's Boundary Formula (Jaswon).

The percentage error in the computed value of h obtained by Green's Boundary Formula increases, as expected, when it is generated at a nodal point adjacent to the apex or the leading edge of the delta. This error falls rapidly as we move away from the edge.

Computation of Disturbance Potential

In the actual case, ϕ_e' is given by (229). Substituting this in (167) and applying our procedures we solve for σ_j. Using these σ_j in (170) we generate ϕ on ∂B. For NT = 12, KN = 2 and $\theta = 1^\circ$, the disturbance potential ϕ is generated at the nodal points on ∂B and some of these values are exhibited in Table 35. The total velocity potential Φ is then obtained by (53) viz.

$$\Phi = \phi + \psi$$

where ψ is given by (228).

Similarly, we insert ϕ_e', given by (229) into (172) and compute ϕ directly on ∂B. ϕ thus computed for NT = 12, KN = 2 and $\theta = 1^\circ$ are exhibited in Table 35.

DEVELOPMENT OF TEST FUNCTION h ON THE PLANE z=0.096

FIELD POINT (CARTESIAN CO-ORD) x	y	ANALYTICAL h	S.L.POTENTIAL (Smith)	%ERROR	G.B.FORMULA (Jaswon)	%ERROR
0.007	0.377	6.4009	6.4597	0.918	8.2628	29.149
0.028	0.365	6.7365	6.8004	0.947	8.5138	26.383
0.049	0.365	7.0264	7.0958	0.988	8,9163	26.897
0.069	0.341	7.2520	7.3252	1.009	9.1888	26.708
0.010	0.367	6.7169	6.7816	0.964	7.2132	7.388
0.031	0.349	7.2810	7.3552	1.020	7.5911	4.259
0.052	0.343	7.3572	7.4328	1.028	7.9761	8.412
0.073	0.325	7.8081	7.8928	1.084	8.4657	8.466
0.010	0.349	7.3534	7.4289	1.027	7.4734	1.631
0.031	0.325	8.2516	8.3402	1.074	8.4150	1.981
0.052	0.325	8.0693	8.1566	1.082	8.3040	2.909
0.021	0.301	9.4926	9.5875	0.999	9.5222	1.366
0.010	0.325	8.3453	8.4335	1.056	8.4806	1.621
0.062	0.301	9.0193	9.1162	1.075	9.1889	1.880
0.046	0.217	15.5520	15.5900	0.244	15.5510	-0.008
0.042	0.144	25.4190	24.5260	3.513	24.4960	-3.630
0.042	0.048	31.3320	32.7570	4.549	32.6920	4.342
0.042	-0.048	-31.3320	-34.0760	8.761	-34.2140	-9.201
0.042	-0.120	-29.6030	-29.2020	1.356	-29.3520	0.846

Table 34

GENERATION OF ϕ ON THE PLANE SURFACE z=0.0484

FIELD POINT		DISTURBANCE POTENTIAL	
x	y	S.L.POTENTIAL (Smith)	G.B.FORMULA (Jaswon)
0.0052	0.3759	0.03367	0.03720
0.0156	0.3669	0.03185	0.03422
0.0260	0.3669	0.03287	0.03714
0.0365	0.3548	0.03139	0.03592
0.0052	0.3669	0.03057	0.03180
0.0156	0.3548	0.02833	0.02978
0.0260	0.3548	0.02943	0.03138
0.0104	0.3428	0.02574	0.02684
0.0052	0.3548	0.02774	0.02903
0.0312	0.3428	0.02719	0.02842
0.0208	0.3007	0.01948	0.02032
0.0208	0.2646	0.01502	0.01581
0.0208	0.2165	0.01014	0.01076
0.0208	0.1684	0.00583	0.00629
0.0208	0.1203	0.00180	0.00202
0.0208	0.0722	-0.00212	-0.00197
0.0208	0.0241	-0.00610	-0.00612
0.0208	-0.0241	-0.01035	-0.01056
0.0208	-0.0722	-0.01518	-0.01562
0.0208	-0.1203	-0.02130	-0.02204
0.0208	-0.1564	-0.02752	-0.02868

Table 35

Tangential velocity Component on the Surface

The downward tangential velocity component of the fluid on the surface is calculated, as in Chapter 14, by taking only the 1st term in (175). For KN = 2, NT = 12 i.e. $2N^* = 954$ and $\theta = 1^o$, the velocity thus obtained along a line x = constant, is exhibited in Table 36. Fig 33 shows the velocity component along x = constant, on the planes $z = \pm H$, based on Table 36. Table 37 exhibits the downward velocity component distributed along the lines y = constant, adjacent to the upper and lower edges CD and C_1D_1 [Fig. 31(c)] on the planes $z = \pm H$. Fig. 34 shows the graphs of the above velocities based on Table 37.

Effect of Thickness Variation

To keep the error due to the approximations made in the evaluation of the integrals below 1%, the distance between the two triangular planes i.e. the thickness 2H, must satisfy (102) of Chapter 7, i.e.

$$2H \geqslant 2L \quad , \tag{239}$$

where L is the diagonal of the biggest sub-area on ∂B.
From Fig. 32,

$$L = 2\left(\frac{AC}{4NT}\right)$$

and, by (232),

$$2H = 2\left(\frac{AC}{4NT}\right) KN = L^* \, KN \quad .$$

Hence, by (239), the minimum value of KN is 2. For a particular AC, keeping KN fixed if NT is increased the thickness decreases satisfying (239) at every stage. Alternately, keeping NT fixed if KN is increased thickness increases keeping the subdivisions on the triangular planes unchanged.

To find the effect of thickness on ϕ, following our procedures, ϕ is calculated for $\theta = 0$ taking KN = 2, NT = 9 and again for $\theta = 0$ taking KN = 3, NT = 9. The ϕ_k thus computed on ∂B, along a line x = constant, are exhibited in Fig. 35.

Discussion

It is evident from Table 35 that the two values of ϕ obtained by the two methods at the nodal points on ∂B approximately agree with one another axcept, as expected, at those points adjacent to the sharp edge and to the corner.

VELOCITY ON THE SURFACES $z = \pm 0.0481$ ALONG THE INTERSECTION OF THE PLANE $x = 0.0208$

FIELD POINT y	DOWNWARD VELOCITY ON SURFACE	
	ON UPPER PLANE z=0.0481	ON LOWER PLANE z=-0.0481
0.2827	1.12321	1.09748
0.2406	1.10146	1.08326
0.1925	1.08943	1.07649
0.1443	1.08343	1.07501
0.0962	1.08136	1.07733
0.0481	1.08267	1.08314
0.000	1.08806	1.09345
-0.0481	1.10019	1.11138
-0.0962	1.12709	1.14558
-0.1383	1.17239	1.20533
-0.1684	1.34726	1.39694

Table 36

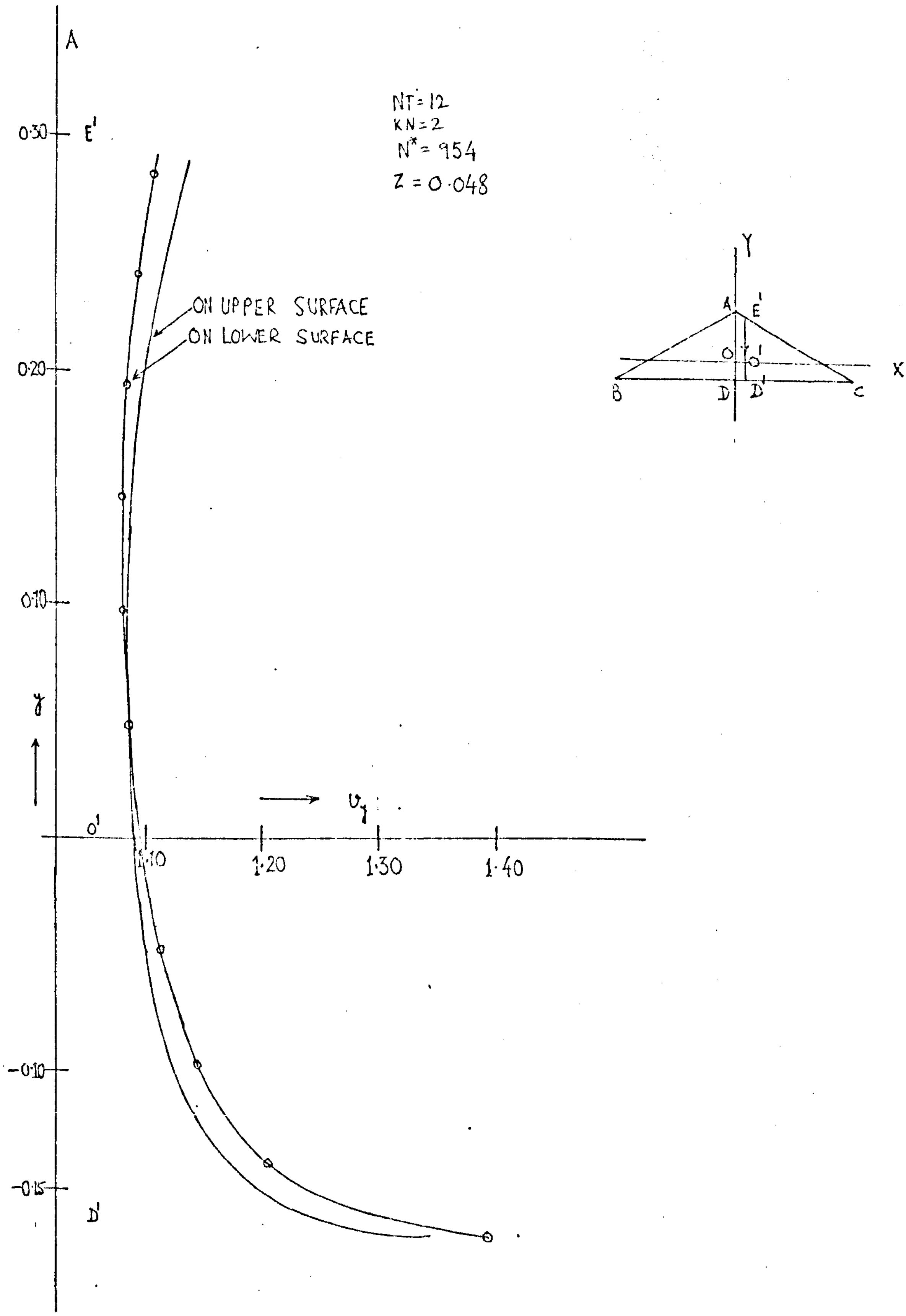

Fig. 33

DOWNWARD VELOCITY COMPONENT ON THE UPPER AND ON THE LOWER SURFACES ALONG A LINE x = CONSTANT (0·0208) PASSING THROUGH E'O'D'.

DOWNWASH ON THE LINE y = -0.1684 ON THE SURFACES z = ±0.0481

FIELD POINT x	DOWN WASH VELOCITY ON UPPER PLANE z=0.0481	DOWN WASH VELOCITY ON LOWER PLANE z=-0.0481
0.0208	1.34726	1.39694
0.0625	1.34759	1.39713
0.1042	1.34824	1.39750
0.1458	1.34921	1.39806
0.1875	1.35050	1.39880
0.2292	1.35211	1.39972
0.2708	1.35406	1.40084
0.3125	1.35634	1.40216
0.3542	1.35898	1.40370
0.3958	1.36200	1.40550
0.4375	1.36547	1.40759
0.4792	1.36944	1.41004
0.5208	1.37402	1.41295
0.5625	1.37937	1.41644
0.6042	1.38572	1.42078
0.6458	1.39341	1.42625
0.6875	1.40376	1.43400
0.7292	1.42276	1.45227

Table 37

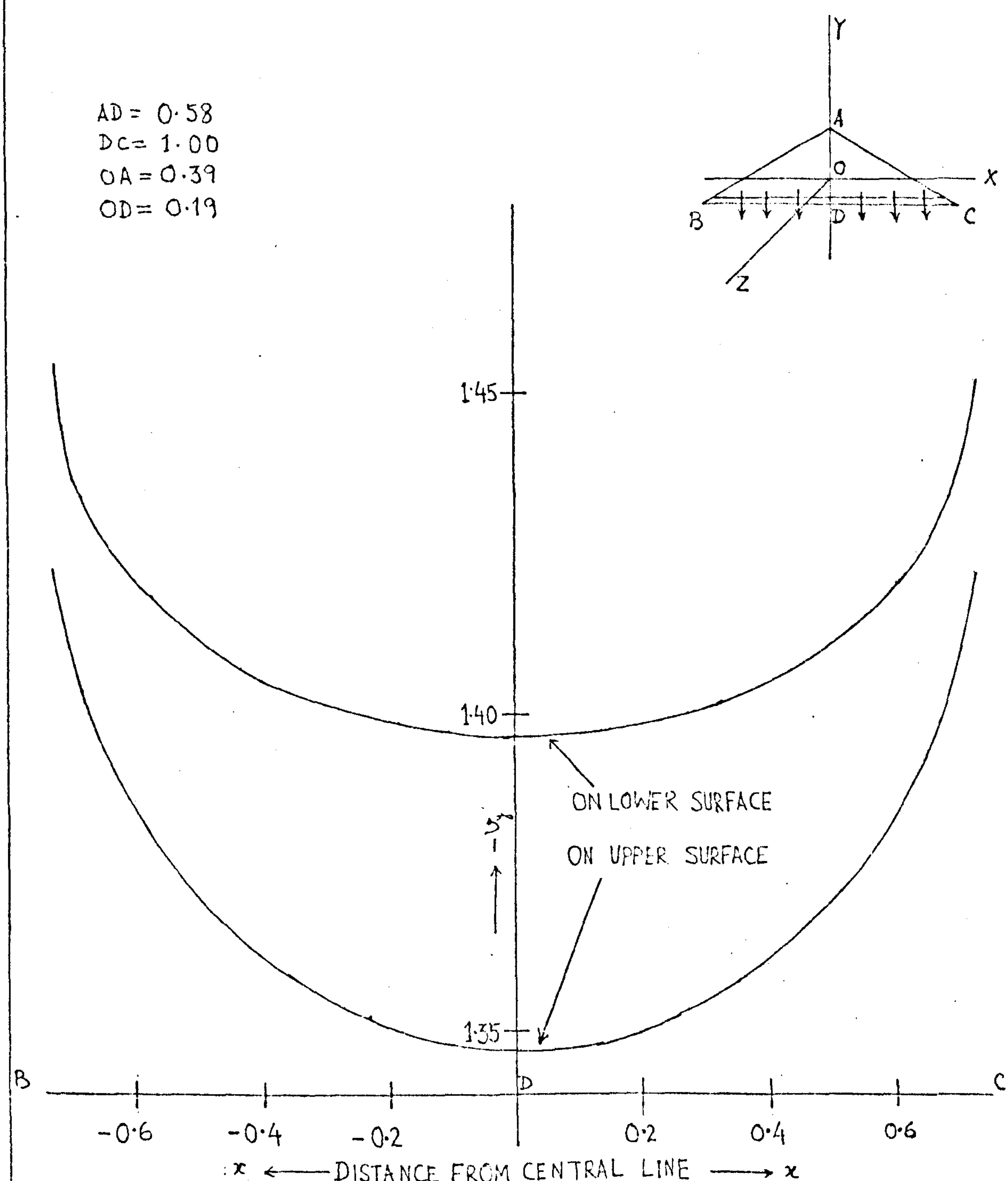

Fig. 34

DOWNWARD VELOCITY COMPONENT ON THE UPPER AND ON THE LOWER SURFACES OVER THE LINES y = CONSTANT (-0·17).

(v_y stands for velocity component in y-direction)

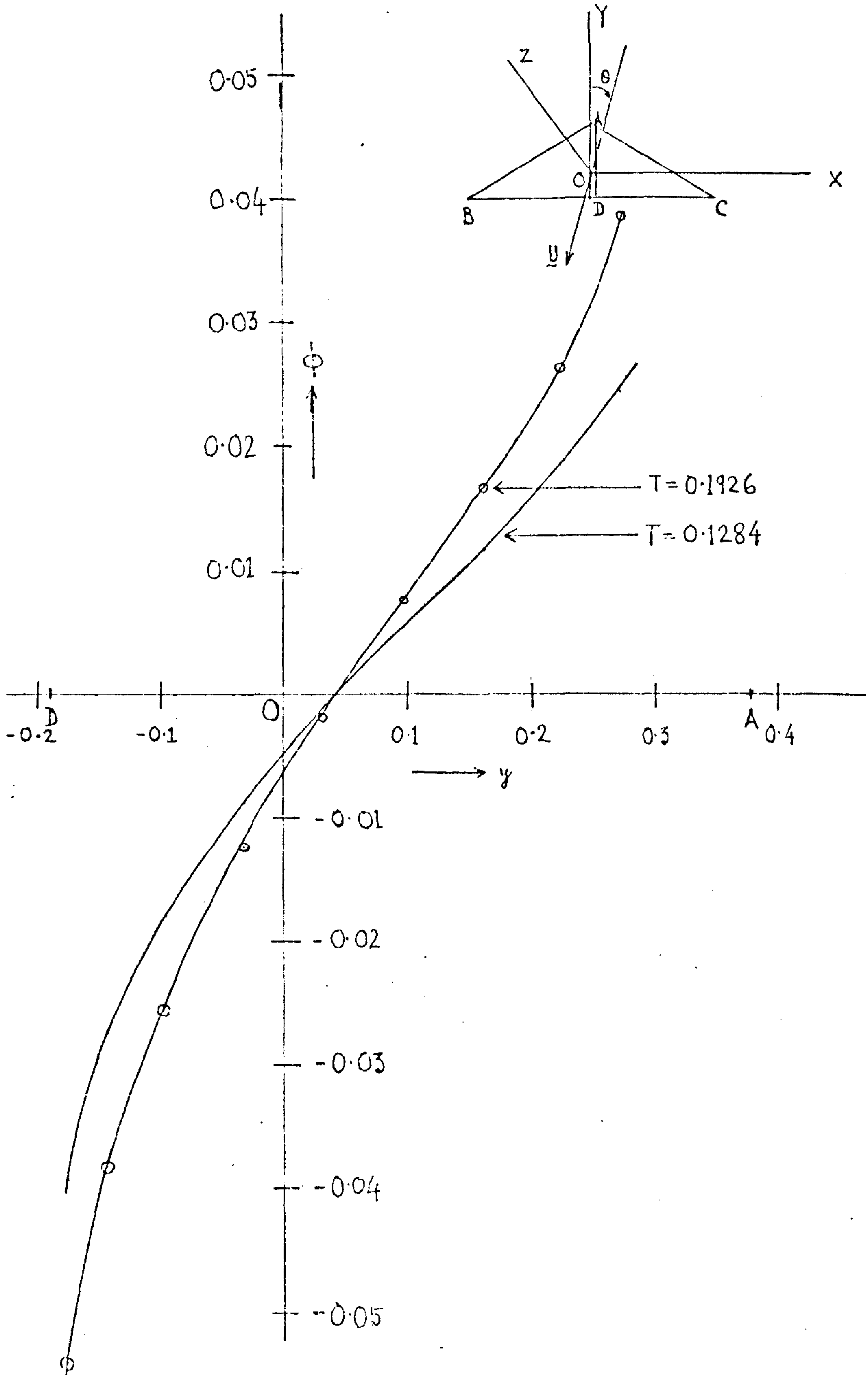

Fig. 35

EFFECT OF THICKNESS ON THE DISTURBANCE POTENTIAL

(T Stands for thickness)

It is evident from Fig. 33 and Fig. 34 that, near the trailing edge, the downward velocity on the upper surface is less than that at the corresponding point on the lower surface. This clearly indicates that a vortex sheet will be formed behind the delta wing in the case of a real fluid.

Fig. 35 demonstrates that the disturbance, due to the thickness alone, gradually dies out as the thickness diminishes to zero.

CHAPTER 18

FLOW PAST A THIN DELTA WING

Introduction

For symmetric flow past a thick plate the disturbance potential ϕ is, in general, the superposition of two function ϕ_s and ϕ_a, i.e.

$$\phi = \phi_s + \phi_a \quad , \tag{240}$$

where ϕ_s is symmetric and ϕ_a is antisymmetric about the plane of the plate. The former arises from thethickness of the plate and the later arises because of the inclination of the plate to the direction of flow. Thus if 2H (thickness) $\neq 0$ and θ (angle of attck) $= 0$, $\phi = \phi_s$. If $2H = 0$ and $\theta \neq 0$, $\phi = \phi_a$.

The formulation (169) and (171) are only valid when the volume enclosed by ∂B differs from zero. Hence they do not apply to a thin delta wing. We may compute ϕ as a limit when the volume enclosed by ∂B tends to zero. To proceed directly with this plan, keeping the numerical error within a tolerable range, 2H should be determined by (239) of Chapter 17. As a result, to attain a reasonably small value of H, the number of independent equations becomes very large and this in turn demands a huge matrix for storage in the computer. For example, when NT = 15 , for KN = 2 2H = 0·07698 and the corresponding number of equations, by (236), becomes 1278. Hence because of the storage capacity alone, leaving aside the attainment of a sufficient degree of accuracy in solving such a huge number of equations, we can not proceed beyond a certain limit.

15

A way out of the difficulty is to separate the symmetric and antisymmetric components of ϕ for any thickness t = 2H. If ϕ_a^+ , ϕ_a^- represent ϕ_a , and if ϕ_s^+ , ϕ_s^- represent ϕ_s respectively on the upper and on the lower surfaces of ∂B, we have

$$\phi_+ = \phi_a^+ + \phi_s^+ \quad , \tag{241}$$

$$\phi_- = \phi_a^- + \phi_s^- \quad , \tag{242}$$

where ϕ_+ , ϕ_- represent the values of ϕ on the upper and on the lower surfaces respectively. Since

$$\phi_a^+ = -\phi_a^- \qquad \text{and} \qquad \phi_s^+ = \phi_s^- ,$$

we find

$$\phi_s^+ = \phi_s^- = \frac{\phi_+ + \phi_-}{2} , \tag{243}$$

$$\phi_a^+ = -\phi_a^- = \frac{\phi_+ - \phi_-}{2} . \tag{244}$$

The relations (243), (244) yield ϕ_s and ϕ_a of (240). We expect this ϕ_a to approximate the value of ϕ for a thin plate inclined at a small angle of attack $\theta \neq 0$.

An useful check on ϕ_s is to compute ϕ for a thick plate parallel to the stream (i.e. $\theta = 0$). This computation can be compared with the ϕ_s previously determined on the basis of (243). It will be seen from Table 38 that the two results compare very closely. The same applies to the computation of ϕ_a.

Polynomial Interpolation

After computation of ϕ on ∂B by the methods stated in Chapter 17, ϕ_a at the discrete points on ∂B can be found by (244). If we wish to know the value of ϕ_a at any point in the neighbourhood of any discrete point, we shall have to fit a polynomial through the function values at these points, which should represent the function to a certain degree of accuracy. It has been pointed out, in Chapter 6, that this can be done as accurately as we please, by fitting a polynomial of sufficiently high degree to the data.

Let $\phi(\underset{\sim}{q}_1)$, $\phi(\underset{\sim}{q}_2)$, $\phi(\underset{\sim}{q}_3)$, ... $\phi(\underset{\sim}{q}_L)$ represent the values of ϕ at the discrete points $\underset{\sim}{q}_1$, $\underset{\sim}{q}_2$ . . . $\underset{\sim}{q}_L$ on ∂B. A suitable polynominal p(x,y,z) of degree m is given by

$$P = \sum_{j=0}^{m} C_j P_j \quad ; \quad m \leq L , \tag{245}$$

VERIFICATION OF THE SEPARATION OF THE SYMMETRIC AND ANTISYMMETRIC PART OF THE DISTURBANCE POTENTIAL

DISTURBANCE POTENTIAL ON THE PLANE SURFACE z=0.0962 IN THE NEIGHBOURHOOD OF THE TIP

x	y	ANGLE OF INCIDENCE $\theta=1°$			INCIDENCE $\theta=0°$
		ϕ^+	ϕ^-	$\phi_s=\frac{\phi^++\phi^-}{2}$	ϕ_s
0.0069	0.3769	0.05767	0.06059	0.05913	0.05914
0.0278	0.3649	0.05747	0.06068	0.05907	0.05908
0.0104	0.3669	0.05360	0.05707	0.05533	0.05534
0.0104	0.3488	0.04707	0.05139	0.04923	0.04924
0.0313	0.3488	0.04965	0.05375	0.05170	0.05171
0.0104	0.3248	0.04098	0.04614	0.04356	0.04357
0.0313	0.3248	0.04215	0.04721	0.04468	0.04469
0.0486	0.3528	0.05631	0.05980	0.05805	0.05806
0.0694	0.3408	0.05690	0.06049	0.05869	0.05870
0.0521	0.3428	0.05160	0.05560	0.05360	0.05361
0.0521	0.3248	0.04436	0.04920	0.04678	0.04679
0.0729	0.3248	0.04832	0.05280	0.05056	0.05056
0.0208	0.3007	0.03650	0.04229	0.03940	0.03940
0.0625	0.3007	0.03942	0.04492	0.04217	0.04218

Table 38

where P_j is a homogeneous polynomial of degree j and C_j is the coefficient of P_j. If we wish to approximate ϕ by P to a certain degree of accuracy, defined by a pre-assigned small quantity ϵ (>0), starting from m = 2 we increase m by a step of 1 and at every stage the C_j are determined by the least squares method until a stage comes when

$$|\phi(\underset{\sim}{q}_k)-P(\underset{\sim}{q}_k)| \leq \epsilon \quad ; \quad k=1,2,\cdots L . \tag{246}$$

In this case, ϕ is a harmonic function symmetric with respect to x and antisymmetric with respect to z. Hence the P_j are to be so chosen that they must satisfy

$$\begin{aligned} \nabla^2 P_j &= 0 \quad , \\ P_j(x,y,z) &= P_j(-x,y,z) \\ \text{and } \frac{\partial}{\partial z}P_j(x,y,z) &= -\frac{\partial}{\partial z}P_j(x,y,-z) \quad . \end{aligned} \tag{247}$$

Under the above conditions the polynomials P_j may be chosen as

$$\begin{aligned}
P_0 &= 1 \\
P_1 &= y + z \\
P_2 &= x^2 + y^2 + yz \\
P_3 &= y^3 + z^3 - 3x^2y + x^2z - 4y^2z \\
P_4 &= x^4 + y^4 - 6x^2y^2 + 6x^2yz - yz^3 - zy^3 \\
P_5 &= y^5 + z^5 + x^4z + y^4z + 5x^4y - 10x^2y^3 - 5x^2z^3 + 5y^2z^3 + 9x^2y^2z \\
P_6 &= x^6 - y^6 - 15x^4y^2 - x^4yz + 15x^2y^4 + x^2y^3z + x^2yz^3 - y^5z + 3y^3z^3 - yz^5 \\
P_7 &= y^7 - 2z^7 - 7yx^6 + 4x^6z + 35x^4y^3 - 25x^4y^3 - 21x^2y^5 + 21x^2z^5 \\
&\quad + 4y^6z - 25y^4z^3 + 21y^2z^5 + 15x^4y^2z + 15x^2y^4z - 60x^2y^2z^3
\end{aligned}$$

and so on.

Computed Results

It has already been pointed out that the Simple Layer Formulation yields a tolerably accurate ϕ, particularly near the edges and the apex. Hence to obtain information about ϕ near the apex of the delta, we consider the values of ϕ obtained by the Simple Layer potential method only. Further, since values of ϕ at the nodal points, adjacent to the tip and the leading edge, are not so reliable, these values are not taken into consideration.

Table 39 exhibits the values of ϕ_a^+ near the tip of the delta for t = 2H = 0·07698. Leaving the 4 values which are at the nodal points adjacent to the leading edge, the polynomial P, given by (245), is fitted

INTERPOLATION OF POLYNOMIAL THROUGH THE COMPUTED VALUE OF ϕ_a^+ NEAR THE TIP

TOTAL SUB-AREAS = 2556

EQUATIONS = 1278

x	y	Z=0.03849 ϕ^+	Z=-0.03849 ϕ^-	ϕ_a^+	FITTED ϕ_a^+
0.0028	0.03817	0.302867E-01	0.321257E-01	-0.18390E-02	
0.0111	0.3769	0.302825E-01	0.322881E-01	-0.20056E-02	
0.0194	0.3721	0.299089E-01	0.320787E-01	-0.21698E-02	
0.0278	0.3673	0.302348E-01	0.324788E-01	-0.22440E-02	
0.0042	0.3777	0.288050E-01	0.309338E-01	-0.10644E-02	-0.10625E-02
0.0125	0.3705	0.273680E-01	0.298600E-01	-0.12460E-02	-0.14493E-02
0.0208	0.3681	0.281888E-01	0.306419E-01	-0.12265E-02	-0.12245E-02
0.0292	0.3608	0.270332E-01	0.297689E-01	-0.13679E-02	-0.13795E-02
0.0042	0.3705	0.263423E-01	0.289474E-01	-0.13025E-02	-0.13121E-02
0.0125	0.3608	0.245812E-01	0.276223E-01	-0.15205E-02	-0.14432E-02
0.0208	0.3608	0.254590E-01	0.283889E-01	-0.14649E-02	-0.14059E-02
0.0250	0.3512	0.237079E-01	0.270389E-01	-0.16655E-02	-0.16627E-02
0.0042	0.3608	0.241135E-01	0.272119E-01	-0.15492E-02	-0.14678E-02
0.0083	0.3512	0.225456E-01	0.260311E-01	-0.17427E-02	-0.17427E-02

Table 39

through these values in the least-squares sense, taking $\epsilon = 0{\cdot}0001$. The condition (246) is satisfied at every point $\underset{\sim}{q}_1, \underset{\sim}{q}_2 \ldots \underset{\sim}{q}_{10}$ when m = 7, and at this stage the co efficients are found to be

$$C_0 = -5{\cdot}25287, C_1 = 32{\cdot}82636, C_2 = 92{\cdot}36869$$

$$C_3 = 218{\cdot}21335, C_4 = -390{\cdot}53000, C_5 = 595{\cdot}55897$$

$$C_6 = 501{\cdot}92655 \text{ and } C_7 = 103{\cdot}60649.$$

The fitted values of ϕ_a^+ thus found are exhibited in Table 39.

Fluid velocity near the Apex of the Delta Wing

To find the nature of the flow near the tip of the thin delta, a polynomial P, given by (245) is fitted through the values of ϕ_a^+ in the neighbourhood of the tip. If the tip O of the delta OAB defines the origin of a cylindrical polar frame $O\, r\, \eta\, z$ [Fig. 36(a)], the simplest formula for the velocity component on OB in the η increasing direction is given by

$$v(\underset{\sim}{q}_{k+\frac{1}{2}}) = -\left\{\phi_a(\underset{\sim}{q}_{k+1}) - \phi_a(\underset{\sim}{q}_k)\right\}/d \quad , \tag{248}$$

where $\underset{\sim}{q}_k = (r, \eta, z)$, $\underset{\sim}{q}_{k+1} = (r, \eta + d\eta, z)$; $\underset{\sim}{q}_{k+\frac{1}{2}} = (\underset{\sim}{q}_{k+1} - \underset{\sim}{q}_k)/2$

and $d = r d\eta$. For numerical calculation d was taken to be 0·001 radians. Table 40 exhibits the tangential velocity component on the plane $z = H$ for different values of r . It is evident from Table 40 that, on the upper surface, the tangential velocity component is maximum near the leading edge and it gradually falls to zero on the central line OD [fig. 36] .

Since $\phi_a^- = -\phi_a^+$, the tangential component of the velocity at any point $(r,\eta,-z)$ will be of the same magnitude, but of the opposite sign to that at the point (r, η, z). Hence on the lower surface, near the tip, the fluid is coming away from the central line OD towards the leading edges. Table 40 exhibits the above property of the flow near the apex of the delta. Fig.36 gives the graphs of the velocity component near the tip based on Table 40.

NATURE OF THE FLOW NEAR THE TIP ON THE SURFACE Z=±0.0385

FIELD POINT			
r	η in degree	Z =0.03849	Z=-0.03849
0.0099	30	0.62974E-01	-0.62974E-01
"	45	0.44458E-01	-0.44458E-01
"	60	0.27776E-01	-0.27776E-01
"	75	0.13229E-01	-0.13229E-01
"	90	0.0	0.0
0.0199	30	0.53943E-01	-0.53943E-01
"	45	0.30463E-01	-0.30463E-01
"	60	0.15891E-01	-0.15891E-01
"	75	0.68995E-01	-0.68995E-02
"	90	0.0	0.0

Table 40

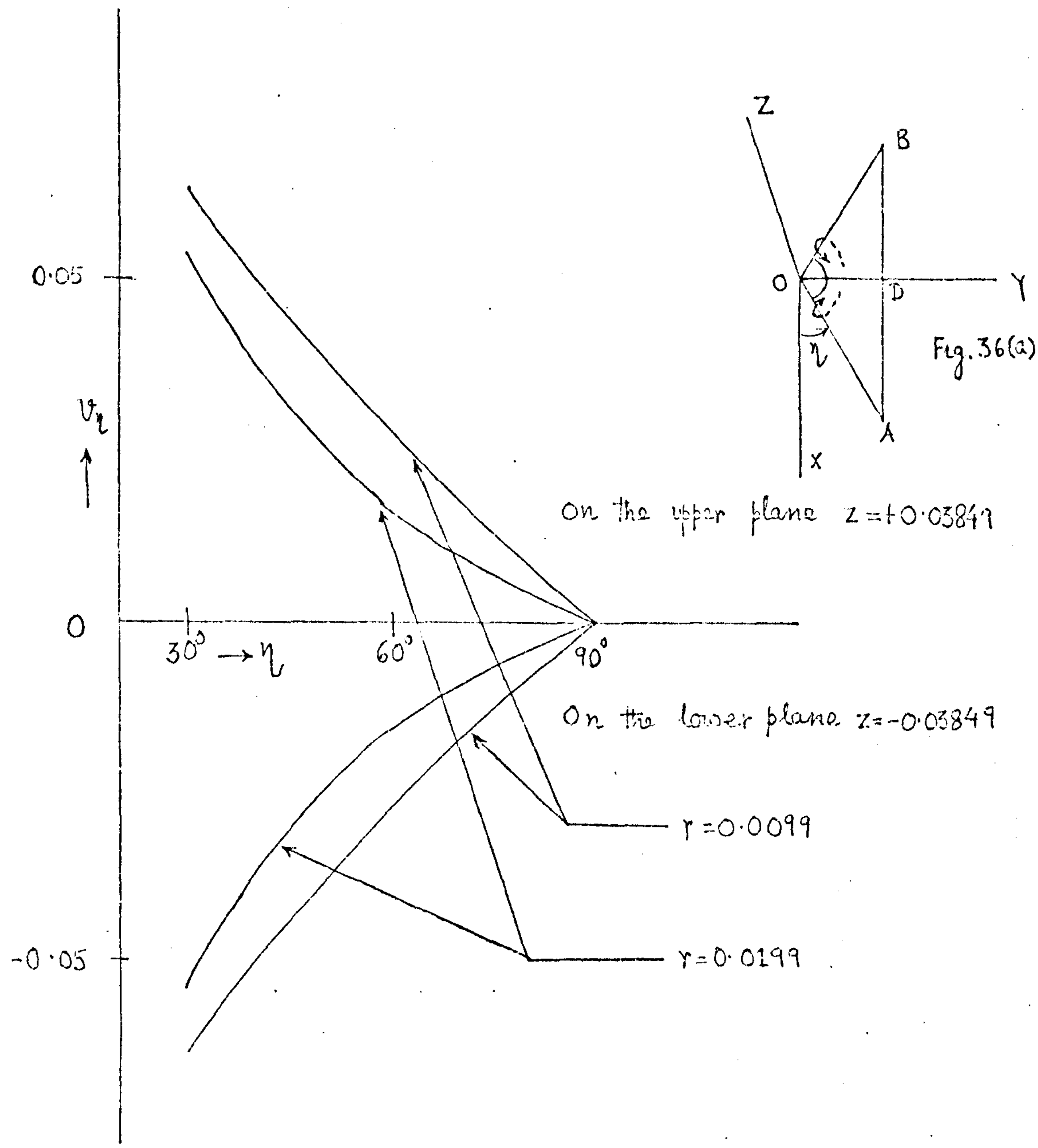

Fig. 36

TANGENTIAL COMPONENT OF VELOCITY ALONG THE CIRCULAR ARCS ON THE SURFACES Z = ± H NEAR THE TIP OF THE DELTA.

CHAPTER 19

BEHAVIOUR OF ϕ NEAR THE TIP OF A DELTA

Introduction

In the case of flow past a thin delta wing with small angle of attack, the flow remains potential. The disturbance potential ϕ is antisymmetric in character and singular at the tip. According to Brown and Stewartson[16] and to Arscott and Taylor[17], for points sufficiently near the apex, in spherical polar co-ordinates (r, ξ, η) with the origin at the tip (Fig.37),

$$\phi = r^{\nu} V(\xi, \eta) \quad , \tag{249}$$

where V is some function of the angular co-ordinates ξ and η. The angular sector lies in the plane $\xi = 90^{\circ}$ between the lines $\eta = 90^{\circ} - \alpha$ and $\eta = 90^{\circ} + \alpha$, where α is the semi-apex angle of the sector. $V(\xi, \eta)$ is a constant along any radius vector and hence we may write for points along a radius vector,

$$\phi = c\, r^{\nu} \;.. \tag{250}$$

The exponent ν, which determines the order of the singularity, has an infinite set of possible values of which the smallest positive value is of greatest interest for practical purposes. For semi-apex angle $\alpha = 60^{\circ}$, $\nu = 0{\cdot}69$.

Computed Values of ϕ

Following our procedures, we compute for each choice of H, a set of values of ϕ_a^+. Omitting the values of ϕ_a^+ at the nodal points adjacent to the leading edge and the apex, the polynomial (245) is fitted for $\epsilon = 0{\cdot}0001$ through the ϕ_a^+ in the neighbourhood of the apex. In each case, we have $L = 10$ and the condition (246) was satisfied for $m = 7$. The coefficients C_j of P, thus found for 4 different values of 2H i.e. thickness, are given in Table 41.

For a given H the line ξ, η = constant intersects the plane $z = H$ at a point $\underset{\sim}{p}$ (x,y,z) [The origin of the cartesian frame is at the centroid

NT	KN	EQUATIONS 2N*	HALF THICKNESS Z	CO-EFFICIENTS C_0	C_1	C_2	C_3	C_4	C_5	C_6	C_7
15	2	1278	0.03849	-5.25287	32.82636	92.36869	218.21335	-390.53000	595.55897	501.92655	103.60649
12	2	954	0.04311	-0.70087	4.13993	-3.47074	168.50832	-836.79922	1202.47260	103.44603	-706.67361
9	2	666	0.06415	-0.56808	3.07722	2.43991	45.87133	-226.61312	336.51414	33.57290	-206.33711
12	3	1010	0.07217	-2.24340	11.42473	6.99570	147.13780	-744.44676	1068.63150	58.78167	-665.38939

Table 41

of the thin plate (Fig. 37)]. This is not necessarily a nodal point. At this point

$$r = z \quad \mathrm{Sec}\xi \ , \tag{251}$$

which determines γ . Now at (r, ξ, η) ϕ is determined by

$$\phi \simeq P(x,y,z) \quad , \tag{252}$$

where P is the approximate polynomial defined in Chapter 18. For different values of z the corresponding values of γ and ϕ thus obtained for a given set of ξ and η are given in Table 42.

Numerical Determination of ν

Taking log of both sides of (250), we have

$$\log \phi = \log C + \nu \log \gamma \quad . \tag{253}$$

This relation is fitted, in the least square sence, through the set of values of ϕ obtained from (252) for given values of r along a radial line through the tip. The ϕ_a^+ (= ϕ in the case of a thin delta wing) thus fitted along different radial lines are given in Table 43. The ν thus found for different radial lines, in the neighbourhood of the tip, are given in Table 44. The perpendicular OD of the triangular sector (Fig. 37), in the case under consideration, is 0·5774. To consider the values of ϕ sufficiently near the tip, the values of γ , in this case, is not exceeded beyond 0·065 which is nearly the 10% of OD.

It is evident from Table 44 that the computed ν , for the set of computed ϕ_a^+ nearest to the tip, closely approximates the theoretically expected value $\nu = 0{\cdot}69$. The average value of ν , from the Table, is 0·71.

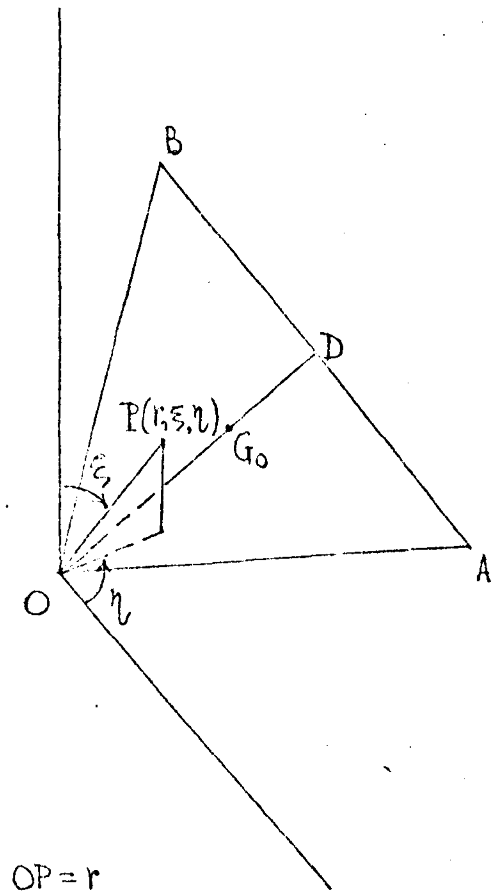

Fig. 37

SPHERICAL POLAR FRAME DEFINED AT THE APEX OF A THIN DELTA WING OAB

COMPUTED VALUES OF ϕ_a^+ NEAR THE TIP OF THE DELTA

r	ξ	ϕ_a^+		
		$\eta=30°$	$\eta=60°$	$\eta=90°$
0.039	5°	-0.721E-03	-0.820E-03	-0.854E-03
0.048	5°	-0.901E-03	-0.105E-02	-0.107E-02
0.064	5°	-0.114E-02	-0.121E-02	-0.124E-02
0.039	10°	-0.821E-03	-0.998E-03	-0.106E-02
0.049	10°	-0.103E-02	-0.103E-02	-0.120E-02
0.065	10°	-0.119E-02	-0.134E-02	-0.140E-02

Table 42

THE FITTED VALUE OF ϕ_a^+ ALONG A RADIUS VECTOR

r	ξ	η	ϕ_a^+ READING	ϕ_a^+ FITTED VALUE
0.038	5°	60°	-0.8196E-03	-0.84215E-03
0.048	"	"	-0.1045E-02	-0.99609E-03
0.064	"	"	-0.1211E-02	-0.12368E-02
0.038	"	90°	-0.8540E-03	-0.87333E-03
0.048	"	"	-0.1066E-02	-0.10244E-02
0.064	"	"	-0.1236E-02	-0.12583E-02

Table 43

DETERMINATION OF ν FOR THE ANGULAR SECTOR OF SEMIAPEX ANGLE 60°

r	ξ	η	ν
0.038	5°	30°	0.88
0.048	"	60°	0.75
0.064	"	90°	0.72
0.039	10°	30°	0.72
0.049	"	60°	0.58
0.065	"	90°	0.55

Table 44

CHAPTER 20

SOLUTION BY SUCCESSIVE APPROXIMATION

Introduction

In the case of potential flow past a fixed boundary the disturbance potential ϕ is zero at infinity and remains generally small compared with the free flow potential ψ ($= -\underset{\sim}{U}.\underset{\sim}{r}$; $|\underset{\sim}{U}| = 1$) on ∂B. Hence we take $\phi = 0$ as the zeroth approximation to ϕ in the right hand side of Green's boundary formula

$$\phi(\underset{\sim}{p}) = \frac{1}{2\pi}\int_{\partial B} \frac{\phi(\underset{\sim}{q})}{|\underset{\sim}{p}-\underset{\sim}{q}|'_e}\,dq - \frac{1}{2\pi}\int_{\partial B}\frac{\phi'_e(\underset{\sim}{q})}{|\underset{\sim}{p}-\underset{\sim}{q}|}\,dq \quad ; \ \underset{\sim}{p}, \underset{\sim}{q} \in \partial B \ , \tag{254}$$

and so define a better approximation to ϕ given by

$$\phi_1(\underset{\sim}{p}) = -\frac{1}{2\pi}\int_{\partial B}\frac{\phi'_e(\underset{\sim}{q})}{|\underset{\sim}{p}-\underset{\sim}{q}|}\,dq \quad ; \ \underset{\sim}{p}, \underset{\sim}{q} \in \partial B \ . \tag{255}$$

Insertion of this ϕ_1 into (254) yields ϕ_2, given by

$$\phi_2(\underset{\sim}{p}) = -\frac{1}{2\pi}\int_{\partial B}\frac{\phi_1(\underset{\sim}{q})}{|\underset{\sim}{p}-\underset{\sim}{q}|}\,dq + \phi_1(\underset{\sim}{p}) \quad ; \ \underset{\sim}{p}, \underset{\sim}{q} \in \partial B \ . \tag{256}$$

So proceeding, we compute successive approximate $\phi_1, \phi_2, \ldots \phi_n$ to ϕ, of which the convergence can be examined.

The integral can be computed numerically as before. On discretisation

$$\phi_1(\underset{\sim}{q}_k) \simeq \frac{1}{2\pi}\sum_{j=1}^{N}\phi'_e(\underset{\sim}{q}_j)\int_j \frac{dq}{|\underset{\sim}{q}_k - \underset{\sim}{q}|} \quad ; \quad k = 1, 2, \cdots N \ , \tag{257}$$

$$\cdot\cdot \qquad \cdot\cdot \qquad \cdot\cdot \qquad \cdot\cdot$$

$$\phi_n(\underset{\sim}{q}_k) \simeq -\frac{1}{2\pi}\sum_{j=1}^{N}\phi_{n-1}(\underset{\sim}{q}_j)\int_j \frac{dq}{|\underset{\sim}{q}_k - \underset{\sim}{q}|} + \phi_1(\underset{\sim}{q}_k) \ ; \ k = 1, 2, \cdots N \ . \tag{258}$$

This procedure yields a set of approximation to ϕ at the pivotal points $\underset{\sim}{q}_1, \underset{\sim}{q}_2, \ldots \underset{\sim}{q}_N$. The approximation to ϕ at the point $\underset{\sim}{q}_m$ after the r th iteration is written as

$$\phi^{r}(\underset{\sim}{q}_m) \; ; \quad r = 1, 2, \cdots n \, . \tag{259}$$

For a pre-assigned small positive quantity ϵ , if there exists an M such that

$$\left| \phi^{M}(\underset{\sim}{q}_k) - \phi^{M-1}(\underset{\sim}{q}_k) \right|_{max} = B^{M} \leq \epsilon \; ; \quad k = 1, 2, \cdots N \, , \tag{260}$$

then ϕ^M is said to be the approximate solution of (254).

Flow past a sphere

Applying the above approach to the case of flow past a sphere, it appears that the approximation converges to the expected solution (Table 45). Referring to (260) , for KN = 4 , i.e. N = 2544 [see (201)] and for ϵ = 0·0001, the approximation converges for M = 9 with B^1 = 0·69493 and B^9 = 0·00006.

The computed value of ϕ obtained by the successive approximation method has the worst behaviour at the point $\underset{\sim}{q}$ (0·998, 0·000, 0·070) and it is exhibited in Fig. 38.

Flow past a thick delta wing

In the case of flow past a thick delta wing, given in Chapter 17, the solution obtained by the successive approximation method does not converge. Fig. 39 exhibits the non-convergence of the computed ϕ , obtained by the above method, for a plate of thickness t = 0·0962 with a number of sub-areas N = 1908. Fig. 40 exhibits the behaviour of computed ϕ at a point $\underset{\sim}{q}$(0·005, 0·376, 0·048) [See Fig. 31(c), Chapter 17] at which the value of ϕ , determined by the integral equation method, is 0·0372.

Table 46 exhibits the approximate ϕ obtained at some representative points on the surface of the wing of thickness 0·0962 for r = 38 [see (259)] compared with the ϕ obtained by the integral equation method.

COMPARISON OF SOLUTIONS OBTAINED BY DIFFERENT METHODS IN THE CASE OF FLOW PAST A UNIT SPHERE

DISTURBANCE POTENTIAL ALONG A MERIDIAN

FIELD POINT		ϕ		
x	z	ANALYTICAL	INTEGRAL EQN.	SUCCESSIVE APPROX.
0.091	0.996	0.49795	0.50339	0.50340
0.209	0.978	0.48899	0.49421	0.49423
0.230	0.954	0.47703	0.48206	0.48208
0.382	0.924	0.46214	0.46687	0.46688
0.457	0.890	0.44483	0.44905	0.44906
0.526	0.851	0.42533	0.42932	0.42933
0.590	0.808	0.40376	0.40761	0.40762
0.649	0.761	0.38042	0.38414	0.38415
0.999	0.023	0.01140	0.01154	0.01154

Table 45

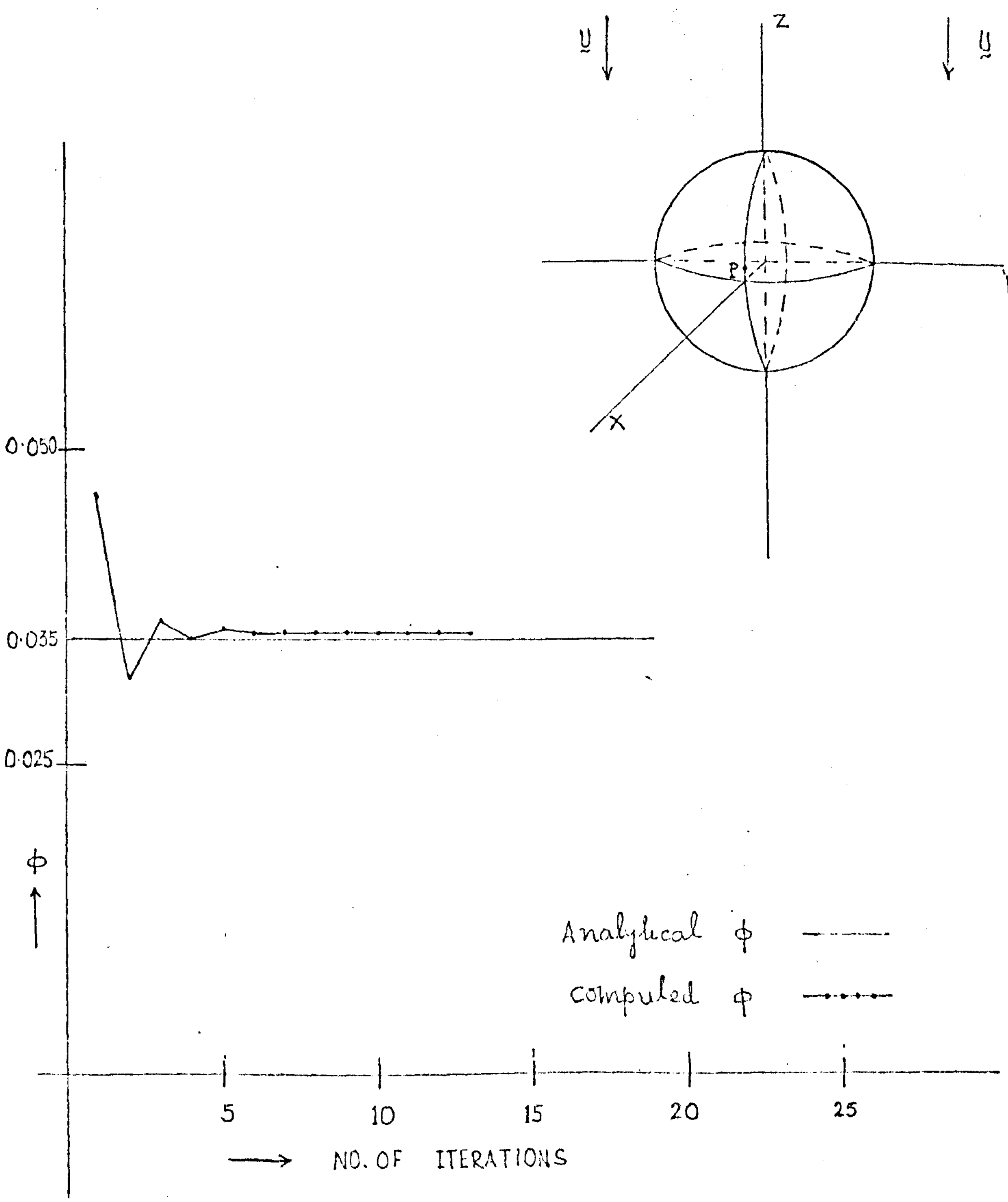

Fig. 38

BEHAVIOUR OF THE SOLUTION AT A FIXED POINT

ON SUCCESSIVE ITERATIONS

(The computed value of φ has the worst behaviour at P)

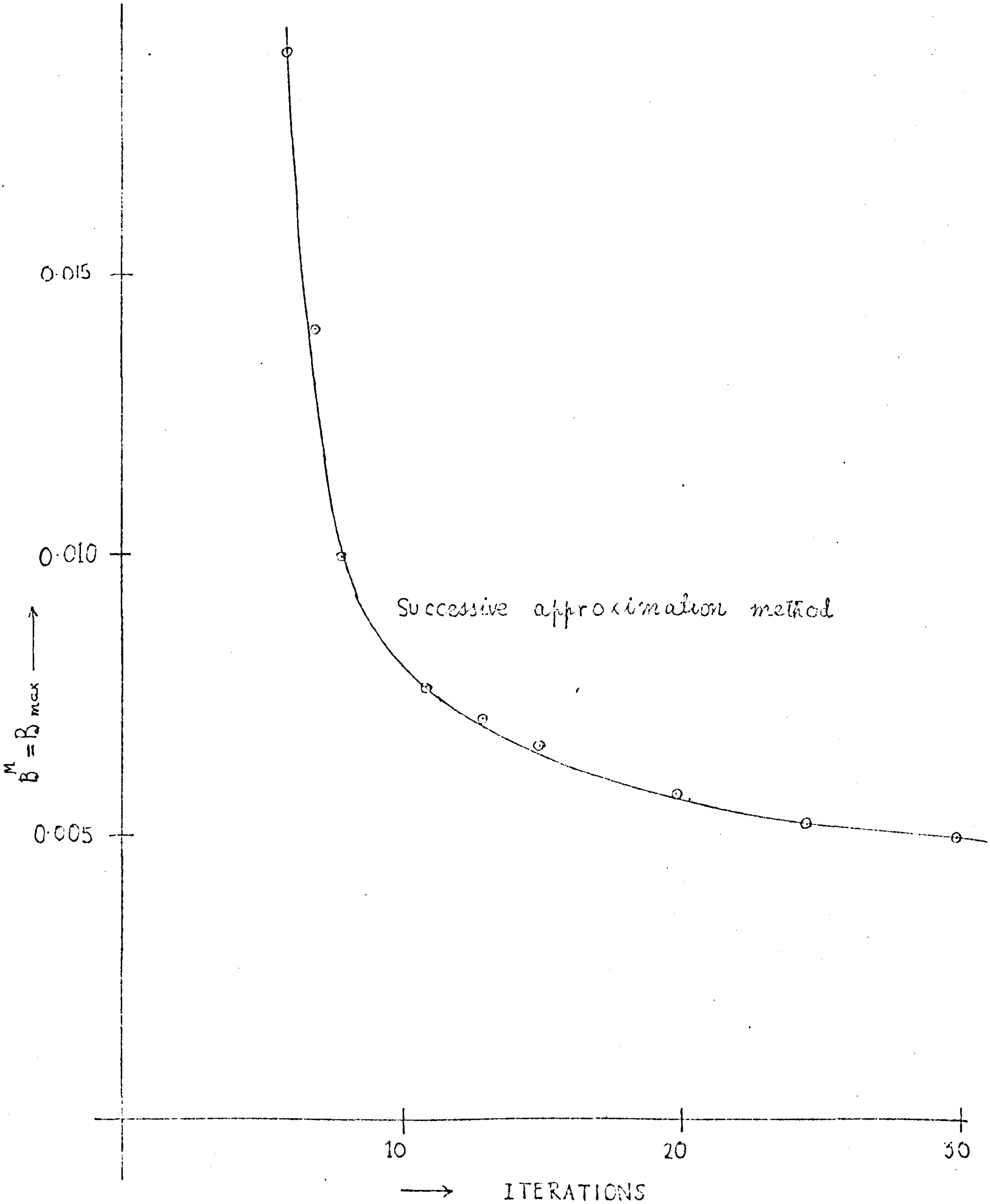

Fig. 39

BEHAVIOUR OF THE SOLUTION ON SUCCESSIVE ITERATIONS

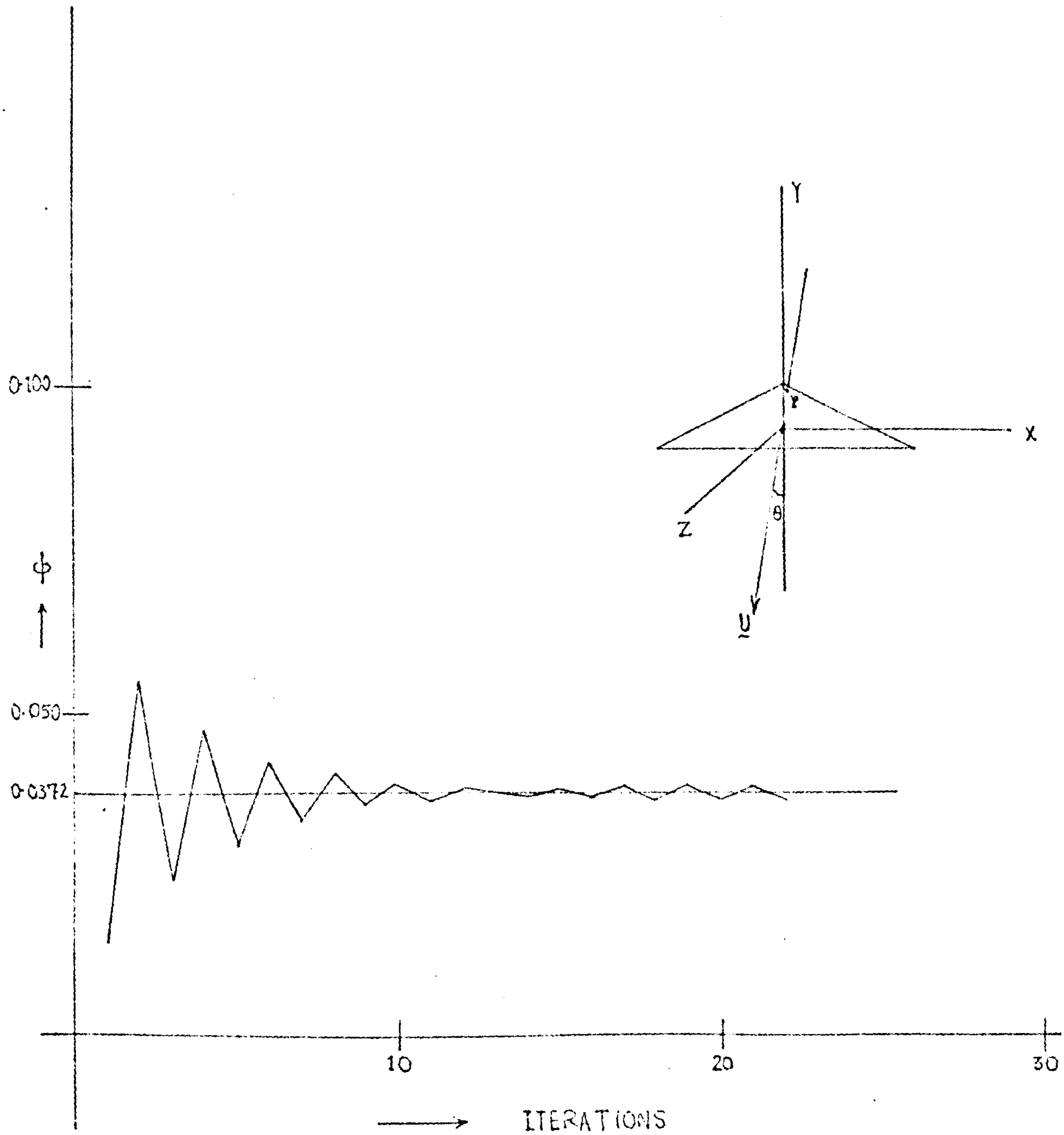

Fig. 40

BEHAVIOUR OF THE SOLUTION AT A FIXED POINT P ON SUCCESSIVE ITERATIONS. VALUE OF φ AT P IS 0·0372 (INTEGRAL EQUATION METHOD).

COMPARISON OF SOLUTIONS OBTAINED BY DIFFERENT METHODS IN CASE OF FLOW PAST A THICK DELTA WING

DISTURBANCE POTENTIAL ON THE SURFACE NEAR THE TIP

FIELD POINT		ϕ	
x	y	INTEGRAL EQN.	SUCCESSIVE APPROX.
0.005	0.376	0.03720	0.03886
0.005	0.367	0.03180	0.03359
0.016	0.367	0.03473	0.03597
0.006	0.355	0.02903	0.03083
0.016	0.355	0.02979	0.03158
0.026	0.364	0.03714	0.03882
0.026	0.355	0.03139	0.03317
0.037	0.355	0.03692	0.03759
0.010	0.343	0.02684	0.02865
0.031	0.343	0.02842	0.03023

Table 46

APPENDIX I

Evaluation of

$$S = \int_{\partial B} \frac{dq}{|\underset{\sim}{p} - \underset{\sim}{q}|} \qquad (1)$$

when ∂B is a plane rectangular area.

Let ∂B define a rectangular area, in the plane Z = 0 with sides 2a and 2b, of which the centroid O defines the origin of a reference frame OXYZ Fig.41(a) . Let the co-ordinates of $\underset{\sim}{p}$ be (X,Y,Z) and those of $\underset{\sim}{q}$, since $\underset{\sim}{q} \in \partial B$, are (x,y,O).

$$\therefore\ S = \int_{-b}^{b} dy \int_{-a}^{a} \frac{dx}{\sqrt{(X-x)^2+(Y-y)^2+Z^2}} ,$$

$$= \int_{-b}^{b} \left[\int_{X-a}^{X+a} \frac{d\alpha}{\sqrt{\alpha^2+(Y-y)^2+Z^2}} \right] dy \quad ; \quad \alpha = X-x ,$$

$$= \int_{-b}^{b} \left[\log\left\{(X+a)+\sqrt{(X+a)^2+Z^2+(Y-y)^2}\right\} - \log\left\{(X-a)+\sqrt{(X-a)^2+Z^2+(Y-y)^2}\right\}\right] dy ,$$

$$= S_1 - S_2 \quad \text{(Say), Where}$$

$$S_1 = \int_{-b}^{b} \log\left\{(X+a)+\sqrt{(X+a)^2+Z^2+(Y-y)^2}\right\} dy ,$$

$$= \int_{k=Y-b}^{k=Y+b} \log\left\{C+\sqrt{D^2+k^2}\right\} dk \quad ; \quad C = X+a ,\ D^2 = C^2+Z^2 ,\ k = Y-y ,$$

$$= \left[k \log\left(C + \sqrt{D^2 + k^2}\right) - \int \frac{\frac{1}{2} \cdot 2 \cdot k \cdot k}{\left(C + \sqrt{D^2 + k^2}\right)} dk \right]_{k = Y - b}^{k = Y + b} ,$$

$$= \left[k \log\left(C + \sqrt{D^2 + k^2}\right) - \int \frac{D^2 + k^2 - C^2 + (C^2 - D^2)}{\left(C + \sqrt{D^2 + k^2}\right)\sqrt{D^2 + k^2}} dk \right]_{k = Y - b}^{k = Y + b} ,$$

$$= \left[\log\left\{ \left(C + \sqrt{k^2 + D^2}\right)^k \left(k + \sqrt{k^2 + D^2}\right)^C \right\} - k \right]_{k = Y - b}^{k = Y + b} + Z^2 \int_{k = Y - b}^{Y + b} \frac{dk}{\left(C + \sqrt{k^2 + D^2}\right)\sqrt{k^2 + D^2}} ,$$

$$= \left[\log\left\{ \left(C + \sqrt{k^2 + D^2}\right)^k \left(k + \sqrt{k^2 + D^2}\right)^C - k - Z \sin^{-1} \frac{D^2 + C\sqrt{k^2 + D^2}}{D\left(C + \sqrt{k^2 + D^2}\right)} \right] \right]_{k = Y - b}^{k = Y + b} .$$

Similarly putting $E = X - a$, $F^2 = E^2 + Z^2$

$$S_2 = \left[\log\left\{ \left(E + \sqrt{k^2 + F^2}\right)^k \left(k + \sqrt{k^2 + F^2}\right)^E \right\} - k - Z \sin^{-1} \frac{F^2 + E\sqrt{k^2 + F^2}}{F\left(E + \sqrt{k^2 + F^2}\right)} \right]_{k = Y - b}^{k = Y + b} .$$

Now $S = S_1 - S_2$,

$$= \left[\log\left\{ \left(\frac{C + \sqrt{k^2 + D^2}}{E + \sqrt{k^2 + F^2}} \right)^k \frac{\left(k + \sqrt{k^2 + D^2}\right)^C}{\left(k + \sqrt{k^2 + F^2}\right)^E} \right\} + Z\left\{ \sin^{-1}\left(\frac{F^2 + E\sqrt{k^2 + F^2}}{F\left(E + \sqrt{k^2 + F^2}\right)} \right) - \sin^{-1}\left(\frac{D^2 + C\sqrt{k^2 + D^2}}{D\left(C + \sqrt{k^2 + D^2}\right)} \right) \right\} \right]_{k = Y - b}^{k = Y + b} . \qquad (2)$$

When ∂B is a square of edge length h and $\underset{\sim}{p}$ coincides with the centroid of ∂B, we have

$$X = Y = Z = 0$$

and $a = b = \frac{1}{2}h$

Hence,

$$S = 4h \log (1 + \sqrt{2}) \tag{3}$$

2. Evaluation of S over a triangular area when $\underset{\sim}{p}$ concides with a vertex of the triangle.

Let the triangular area ABC, bounded by arms r_1 , r_2 and r_3, lie in the plane Z = 0 [Fig. 41 (b)]. The vertex C defines the origin of a cylindrical polar reference frame with CA as the initial line. In this frame, the arm CB is given by

$$\theta = \theta_1 \quad ,$$

p coincides with C and the co-ordinates of q are $(r, \theta, 0)$.

Now

$$S = \int_{\partial B} \frac{dq}{|\underset{\sim}{p} - \underset{\sim}{q}|}$$

$$= \int_{\theta=0}^{\theta_1} \left[\int_{r=0}^{f(\theta)} \frac{1}{r}\, r\, dr \right] d\theta = \int_{\theta=0}^{\theta_1} f(\theta) d\theta \quad .$$

Let the equation of AB in a cartesian frame OXYZ, with the origin at C and Z-axis coinciding with the initial line CA, be

$$y = mx + C \;,$$

with conditions

$$y = 0 \qquad \text{when} \qquad x = r_2$$

$$\text{and } y = r_1 \sin \theta_1 \quad \text{when} \qquad x = r_1 \cos \theta_1$$

Hence, $C = - mr_2$ and $m = r_1 \sin \theta_1/(r_1\cos \theta_1 - r_2)$.

In terms of r and θ ,$f(\theta)$ stands as

$$f(\theta) \equiv r = \frac{r_1 r_2 \sin \theta_1}{(r_2 - r_1 \cos \theta_1) \sin \theta + r_1 \sin \theta_1 \cos \theta}$$

If $a = r_2 - r_1 \cos \theta_1$ and $b = r_1 \sin \theta_1$, we have

$$a^2 + b^2 = r_1^2 + r_2^2 - 2r_1r_2 \cos \theta_1 = r_3^2$$

and $f(\theta) = \dfrac{r_1 r_2 \sin\theta_1}{a \sin\theta + b \cos\theta}$.

Using these in (4)

$$S = r_1 r_2 \sin\theta_1 \int_{\theta=0}^{\theta_1} \frac{d\theta}{a \sin\theta + b \cos\theta} ,$$

$$= \frac{r_1 r_2 \sin\theta_1}{\sqrt{a^2+b^2}} \left[\log\left(\frac{b \sin\theta - a\cos\theta + \sqrt{a^2+b^2}}{b\cos\theta + a \sin\theta} \right) \right]_{\theta=0}^{\theta_1} ,$$

$$= \frac{2\Delta}{r_3} \left[\log\left(\frac{r_1 \sin\theta_1 \sin\theta - (r_2 - r_1 \cos\theta_1)\cos\theta + r_3}{r_1 \sin\theta_1 \cos\theta + (r_2 - r_1\cos\theta_1)\sin\theta} \right) \right]_{\theta=0}^{\theta_1} ,$$

$$= \frac{2\Delta}{r_3} \log\left(\frac{r_1 - r_2\cos\theta_1 + r_3}{r_2 \sin\theta_1} \cdot \frac{r_1 \sin\theta_1}{r_3 - r_2 + r_1\cos\theta_1} \right) ,$$

$$= \frac{2\Delta}{r_3} \log\left(\frac{r_1^2 + r_1 r_3 - r_1 r_2 \cos\theta_1}{r_2 r_3 - r_2^2 + r_1 r_2 \cos\theta_1} \right) ,$$

$$= \frac{2\Delta}{r_3} \log\left(\frac{r_1 + r_2 + r_3}{r_1 + r_2 - r_3} \right) , \qquad (4)$$

where Δ is the area of the triangle ABC .

APPENDIX II

Evaluation of

$$S^{1} = \int_{\partial B} \frac{dq}{|\underset{\sim}{p}-\underset{\sim}{q}|} \quad ; \quad \underset{\sim}{p}, \underset{\sim}{q} \in \partial B .$$

Let ∂B be the part of a sphere of radius 'a'. The centre of the sphere defines the origin of a spherical polar co-ordinates, in which the co-ordinates of $\underset{\sim}{p}$ are (a,0,0) and those of $\underset{\sim}{q}$ are (a, θ, η).

Now $$\frac{1}{|\underset{\sim}{p}-\underset{\sim}{q}|} = \frac{1}{|\underset{\sim}{q}_k-\underset{\sim}{q}|} ,$$ (replacing $\underset{\sim}{p}$ by $\underset{\sim}{q}_k$)

$$= \frac{(\underset{\sim}{q}_k-\underset{\sim}{q})\cdot \hat{n}_e(\underset{\sim}{q}_k)}{|\underset{\sim}{q}_k-\underset{\sim}{q}|^3} = \frac{2a\,\mathrm{Sin}(\theta/2)\cdot\mathrm{Sin}(\theta/2)}{8a^3\,\mathrm{Sin}^3(\theta/2)} ,$$

$$= \frac{1}{4a^2\,\mathrm{Sin}(\theta/2)} ,$$

where $n_e(\underset{\sim}{q}_k)$ denotes the unit vector normal to ∂B at the point $\underset{\sim}{q}_k$.

$$\therefore \quad S^{1} = \int_{\eta=0}^{2\pi} \int_{\theta=0}^{\Theta} \frac{a\,\mathrm{Sin}\,\theta \; d\eta \; a\,d\theta}{4a^2\,\mathrm{Sin}(\theta/2)}$$

$$= 2\pi \int_{\theta=0}^{\Theta} \frac{2a^2\,\mathrm{Sin}(\theta/2)\,\mathrm{Cos}(\theta/2)\,d\theta}{4a^2\,\mathrm{Sin}(\theta/2)}$$

$$= 2\pi \Big[\mathrm{Sin}(\theta/2)\Big]_{\theta=0}^{\Theta} = 2\pi\,\mathrm{Sin}(\Theta/2) ,$$

where 2Θ is the solid angle, subtended by ∂B, at the centre of the sphere [Fig. 41(c)].

If APB be the rim of the circular cap ∂B with its centre at $\underset{\sim}{q}_k$ and if $q_k A = h_k$,

$$S' = \frac{\pi \ 2a \ \sin(\theta/2)}{a} = \frac{\pi \ h_k}{a} \quad . \tag{5}$$

For a flat surface ∂B,

$$(\underset{\sim}{q}_k - \underset{\sim}{q}) \cdot \hat{n}(\underset{\sim}{q}_k) = 0 = (\underset{\sim}{q} - \underset{\sim}{q}_k) \cdot \hat{n}(\underset{\sim}{q})$$

$$\therefore \int_{\partial B} \frac{dq}{'|\underset{\sim}{p} - \underset{\sim}{q}|} = \int_{\partial B} \frac{dq}{|\underset{\sim}{p} - \underset{\sim}{q}|'} = 0 \quad . \tag{6}$$

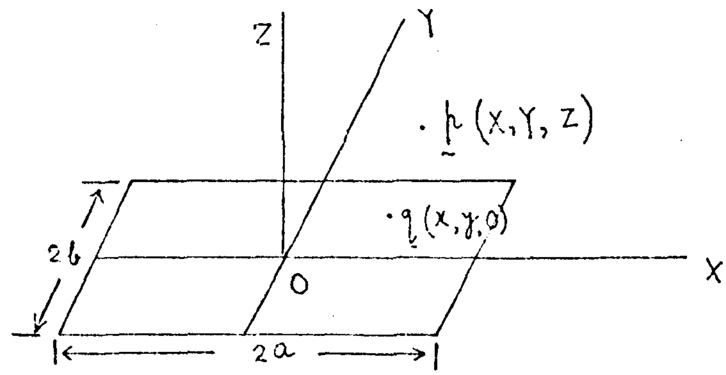

Fig. 41(a)

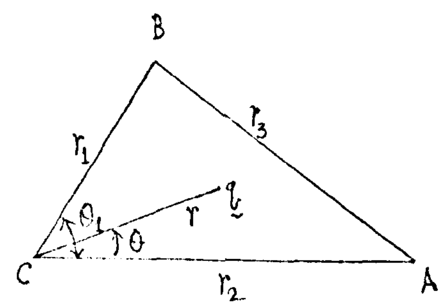

Fig. 41(b)

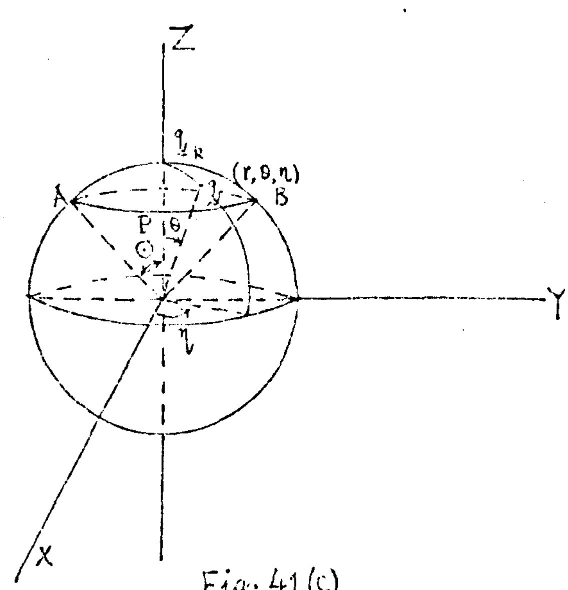

Fig. 41(c)

APPENDIX III

Nature of the solution of a system of 2k linear algebraic equations represented by

$$[A]\,[X] = [B] \,, \tag{7}$$

where $[A]$ is a square matrix of order 2k x 2k with $|A| \neq 0$; the elements of $[A]$ and $[B]$ satisfy

$$a_{ij} = a_{2k-i+1 \;\; 2k-j+1}$$

and $b_i = -b_{2k-i+1}$ respectively.

On the above conditions, the expanded form of (7) is given by

$$\begin{bmatrix} a_{11} & a_{12} & \cdots & a_{1\,k} & a_{1\,k+1} & \cdots & a_{1\,2k} \\ a_{21} & a_{22} & \cdots & a_{2\,k} & a_{2\,k+1} & \cdots & a_{2\,2k} \\ .. & .. & & .. & .. & & .. \\ .. & .. & & .. & .. & & .. \\ a_{k1} & a_{k2} & \cdots & a_{kk} & a_{k\,k+1} & \cdots & a_{k\,2k} \\ a_{k\,2k} & a_{k\,2k-1} & \cdots & a_{k\,k-1} & a_{kk} & \cdots & a_{k\,1} \\ .. & .. & & .. & .. & & .. \\ .. & .. & & .. & .. & & .. \\ .. & .. & & .. & .. & & .. \\ a_{1\,2k} & a_{1\,2k-1} & & a_{1\,k-1} & a_{1k} & & a_{11} \end{bmatrix} \begin{bmatrix} X_1 \\ X_2 \\ \\ \\ X_k \\ X_{k+1} \\ \\ \\ \\ X_{2k} \end{bmatrix} = \begin{bmatrix} b_1 \\ b_2 \\ \\ \\ b_k \\ -b_k \\ \\ \\ \\ -b_1 \end{bmatrix} .$$

Since the determinant of $|A| \neq 0$, i.e.

$$D = |A| \equiv |a_{11} \; a_{22} \cdots a_{kk} \cdots \cdots a_{11}| \neq 0$$

by Cramer's rule ,

$$X_r = \frac{|a_{11} \; a_{22} \cdots b_r \;\; a_{r+1\;\,r+1} \cdots a_{kk} \cdots a_{11}|}{|A|} , \quad r < k \, .$$

Simiarly,

$$X_{2k-r+1} = \frac{|a_{11} \quad a_{22} \cdots a_{kk} \cdots -b_r \quad a_{r-1\ r-1} \cdots a_{11}|}{|A|},$$

$$= \frac{-|a_{11} \quad a_{22} \cdots a_{kk} \cdots b_r \quad a_{r-1\ r-1} \cdots a_{11}|}{|A|},$$

$$= \frac{-|a_{11} \quad a_{22} \cdots b_r \quad a_{r+1\ r+1} \cdots a_{kk} \cdots a_{11}|}{|A|},$$

$$= - X_r \quad ,$$

i.e. $X_r = - X_{2k-r+1}$.

The above relation holds good for $r = 1, \ldots k$.

REFERENCES

1. Kellogg,O. D., 1929 Foundations of Potential Theory, P.152, 162, 168, 223, 237, 277, 287. Ungar: New York .

2. Jaswon,M. A., 1963 Proc. Roy. Soc. A, 275 .

3. Lamb,H., 1953 Hydrodynamics. Cambridge University Press .

4. Simmons,G. F., 1963 Introduction to Topology and Modern Analysis. McGraw Hill .

5. Froberg,C. E., 1964 Introduction to Numerical Analysis. World Student Series: Addison-Wesley.

6. Polya,G. and Szego,G., 1951 Isoperimetric Inequalities in Mathematical Physis. Princeton University Press .

7. Tranter,C. J., 1966 Integral Transforms in Mathematical Physics. Methuen's Monographs .

8. Watson,G. N., 1952, A Treatise on the Theory of Bessel Functions. Cambridge University Press .

9. Hayes,J. G., 1970 Numerical Approximation to Functions and Data. The Athlone Press: London .

10. Hess,J. L. and Smith,A. M. O., 1967 Calculation of Potential Flow about Arbitrary Bodies. Progress in Aeronautical Sciences. Vol. 8 . Pergamon Press .

11. Jaswon,M. A. and Ponter,A. R., 1963 Proc. Roy. Soc. A, 273 .

12. Jaswon,M. A. and Maiti,M. and Symm,G. T., 1967 Numerical Biharmonic Analysis and Some Applications. Int. J. Solid Structures .

13. Redish,K. A., 1966 An Introduction to Computational Methods. The English University Press .

14. Landau,L. D. and Lifshitz,E. M., 1966 Fluid Mechanics. Pergamon Press .

15. Robinson,A. and Laurmann,J. A., 1956 Wing Theory. Cambridge University Press .

16. Brown,S. N. and Stewartson,K., 1969 Flow Near the Apex of a Plane Delta Wing. J. Inst. Maths Applics. 5 .

17. Taylor,R. S., 1971 A New Approach to the Delta Wing Problem. J. Inst. Maths Applics. 7 .